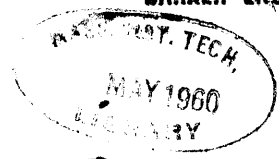


Eng'g  
36.  
TC171  
• M4/  
• H99  
no. 36.

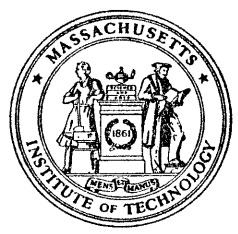
BARKER ENGINEERING LIBRARY



MASSACHUSETTS INSTITUTE OF TECHNOLOGY

# HYDRODYNAMICS LABORATORY

DEPARTMENT OF CIVIL AND SANITARY ENGINEERING



TECHNICAL REPORT NO. 36

## THE HYDROELASTIC BEHAVIOR OF FLAT PLATES AS INFLUENCED BY TRAILING EDGE GEOMETRY

BY

A. T. IPPEN, G. H. TOEBES AND P. S. EAGLESON

APRIL 1960

PREPARED UNDER  
CONTRACT NO. Nonr-1841(21)  
BUREAU OF SHIPS  
FUNDAMENTAL HYDROMECHANICS RESEARCH PROGRAM  
PROJECT NS 715-102  
ADMINISTERED BY THE  
DAVID TAYLOR MODEL BASIN  
U. S. DEPARTMENT OF THE NAVY  
WASHINGTON, D. C.

HYDRODYNAMICS LABORATORY  
Department of Civil and Sanitary Engineering  
Massachusetts Institute of Technology

THE HYDROELASTIC BEHAVIOR OF FLAT PLATES  
AS INFLUENCED BY TRAILING EDGE GEOMETRY

by

A. T. Ippen, G. H. Toebes and P. S. Eagleson

April, 1960

Technical Report No. 36

Prepared Under  
Contract No. Nonr-1841(21)  
Bureau of Ships Fundamental Hydromechanics Research Program  
Project NS 715-102  
Administered by the  
David Taylor Model Basin  
U. S. Department of the Navy  
Washington, D. C.

(Reproduction of this report in whole or in part  
is permitted for any purpose of the United States Government)

## ABSTRACT

This report presents the results of a theoretical review and an experimental investigation of the hydroelastic vibration of thin flat plates suspended at zero mean angle of attack in a fluid stream.

The review indicated that recognized experimental facts such as the influence of trailing edge geometry and the three-dimensional wake structure were inadequately related to theoretical considerations about the vibration phenomenon.

The experimental investigation consisted of a detailed determination of the amplitude and frequency spectra of the vibration on a number of flat test plates which were mounted in the test section of a water tunnel at zero mean angle of attack.

The effects on the vibrational behavior of trailing edge geometry, geometric and elastic properties of the plate support, free stream velocity and ambient pressure have been explored experimentally.

An equation of motion has been written for the test plate - torsion spring system employed. Results of a qualitative analysis of this non-linear equation are compared with the experimental results obtained.

## ACKNOWLEDGEMENTS

The investigation reported herein was made possible by the sponsorship of the David Taylor Model Basin, U.S. Department of the Navy, under Contract No. Nonr-1841(21). Contract administration was provided by the M.I.T. Division of Sponsored Research under D.S.R. 7579.

The work was performed in the Hydrodynamics Laboratory of the Department of Civil and Sanitary Engineering at the Massachusetts Institute of Technology.

The investigation was under the general direction of Dr. Arthur T. Ippen, Professor of Hydraulics and under the technical supervision of Dr. Peter S. Eagleson, Assistant Professor of Hydraulic Engineering.

Dr. Eric Mollo-Christensen, Associate Professor of Aeronautical Engineering provided valuable advice concerning the mathematical formulation of the problem.

Particular credit is due Mr. Frank E. Perkins, Research Engineer, who contributed greatly to all phases of the investigation.

## TABLE OF CONTENTS

	<u>Page</u>
I. INTRODUCTION	
A. General Statement of the Problem	1
B. Scope of the Investigation	2
II. REVIEW OF PREVIOUS WORK	
A. Vortex Induced Vibrations	2
B. Structure and Periodicity of Wake Flow	
1. Experimental Findings	4
2. Theoretical Work	8
C. Wake Dynamics and Trailing Edge Geometry	
1. Trailing Edge Geometry	11
2. Location of the Separation Points	12
3. Distance Between the Shear Layers	12
4. History of the Shear Layers	12
D. Summary	14
III. EXPERIMENTAL EQUIPMENT AND PROCEDURES	
A. General Description of Water Tunnel	15
B. Test Plate Assembly	
1. Selected Test Plates	17
2. Mounting of the Test Plates	17
3. Spring Constants and Viscous Damping	19
C. Electronic Equipment and Data Procurement	
1. Equipment and Procedures for the 1/8"-Thick Plates	22
2. Equipment and Procedures for the 1/4"-Thick Plates	22
IV. THEORETICAL CONSIDERATIONS	
A. The Common Model of Vortex Induced Vibrations	
1. Theoretical Determination of Periodic Lift Forces	25
2. Structural Response to a Periodic Lift Force	29
3. The Common Model of Vortex Induced Vibrations	31
B. Shortcomings of the Notion of "von Karman Vortex Vibrations"	
1. Inadequate Formulation of the Forcing Moment	31
2. Neglect of the Trailing Edge Geometry	32
3. Disregard of the Relation between Wake Structure and Reynolds Number	32
4. The Occurrence of Instabilities in Vibrational Amplitude	33



	<u>Page</u>
C. Test Plate Vibrations of Hydroelastic Origin	
1. Hydroelastic Characteristics of the Test Plate Vibrations	34
2. Formulation of a Hydrodynamic Forcing Function	34
3. Formulation of the Reduced Equation of Motion	40
4. The Reduced Amplitude Response Curves	41
V. PRESENTATION AND DISCUSSION OF RESULTS	
A. Some Exploratory Tests with 1/8"-Thick Test Plates	
1. Amplitude and Frequency of Plate Vibration	44
2. Discussion of Results and Conclusions	45
3. Apparent Mass Forces	48
4. Modification of Equipment	48
B. Vibrational Frequency vs. Free Stream Velocity (1/4"-Plates)	
1. "Strouhal Graphs"	49
2. Sub- and Ultra Harmonics	53
3. Natural Frequency and Apparent Mass Determinations	55
C. Vibrational Amplitude vs. Free Stream Velocity	
1. Presentation and Discussion of the Amplitude Records	55
2. Amplitude Response Curves	58
D. Reproducibility of Experimental Observations	
1. Reproducibility of Vibrational Frequency and Amplitude	63
2. Effect of Ambient Pressure	66
3. Influence of Tunnel Vibrations	66
4. Summary	66
E. Stability of Vibrational Amplitude and Frequency	
1. Comparison of Wave Analyzer and Voltmeter Signals	68
2. Stability of Vibrational Amplitude	68
3. Stability of Vibrational Frequency	69
4. Discussion of the Stability of Vibration Graphs	69
F. Maximum Vibrational Amplitudes	
1. Comparison of the Maximum Vibrational Amplitudes	72
2. Maximum Vibrational Amplitudes as a Function of Restraint	73
3. Influence of the Location of the Axis of Plate Rotation	75
4. Self-excitation of the Plate Vibration	78
G. Reduced Amplitude Response Curves	
1. Amplitude Response Curves as Function of Velocity	78
2. Reduction of the Amplitude Response Curves	79
3. Similarity of the Reduced Amplitude Response Curves	79

VI. CONCLUSIONS AND RECOMMENDATIONS	<u>Page</u>
A. Summary and Conclusions	83
B. Recommendations for Practical Application	84
C. Recommendations for Future Experiments	84
VII. BIBLIOGRAPHY	85
VIII. APPENDICES	
A. Hydraulic Characteristics of the Water Tunnel	89
B. Wave Analyzer, Leaf Spring and Accelerometer Calibrations	97
C. Natural Frequency and Apparent Mass Determination	99
D. Conversion Factor Transducer Output-Amplitude of Vibration	104
E. Comparison of some Voltmeter Readings and Micrometer Measurements	105

LIST OF FIGURES

<u>No.</u>		<u>Page</u>
1.	Wake Flows - Amplitude of Vibrations	13
2.	Water Tunnel, Pressure Circuit and Circulation Pumps	16
3.	Overall View of Water Tunnel and Instrumentation	18
4.	Test Section with mounted 1/4"-Test Plate	18
5.	Test Plate Assembly for 1/8"-Plates	20
6.	Test Plate Assembly for 1/4"-Plates	21
7.	Samples of Wave Analyzer Records	23
8.	Block Diagram of Instrumentation	24
9.	The Common Model of Vortex Induced Vibrations	26
10.	Expected Amplitude Responses	42
11.	Strouhal Graph for 1/8"-Test Plates	47
12.	Strouhal Graph for Plate #11 - Pivot Leading Edge	50
13.	Strouhal Graph for Plate #11 - Pivot 1/4-chord	51
14.	Strouhal Graph for Plate #12 - Pivot 1/4-chord	51
15.	Strouhal Graph for Plate #15 - Pivot Leading Edge	52
16.	Strouhal Graph for Plate #16 - Pivot Leading Edge	52
17.	Characteristics of Torsion Spindle	57
18.	Amplitude Response Curve for Plate #11 - Pivot 1/4-chord	59
19.	Amplitude Response Curve for Plate #12 - Pivot 1/4-chord	60
20.	Amplitude Response Curve for Plate #15 - Pivot Leading Edge	61
21.	Amplitude Response Curve for Plate #16 - Pivot Leading Edge	62
22.	Reproducibility of Test Results for Plate #1	64
23.	Reproducibility of Test Results for Plate #11	65
24.	Influence of Ambient Pressure	67
25.	Stability Graph for Plate #11	70
26.	Stability Graph for Plate #12	70
27.	Stability Graph for Plate #15	71
28.	Stability Graph for Plate #16	71
29.	Maximum Amplitude as Function of Restraint	74
30.	Reduced Amplitude Response Curve for Plate #11	80
31.	Reduced Amplitude Response Curve for Plate #12	80
32.	Reduced Amplitude Response Curve for Plate #15	81
33.	Reduced Amplitude Response Curve for Plate #16	81

<u>No.</u>		<u>Page</u>
A-1.	Calibration Curves of Water Tunnel Contraction	90
A-2.	Contraction Calibration Constant	91
A-3.	Velocity Profiles in Horizontal Plane of Test Section	93
A-4.	Velocity Profiles in Horizontal Plane of Test Section	94
A-5.	Operating Characteristics of Water Tunnel	95
B-1.	Wave Analyzer Calibration Curves	97
B-2.	Calibration of Leaf Spring and Accelerometer	98

#### LIST OF TABLES

<u>No.</u>		<u>Page</u>
1.	Assumptions Regarding the Forcing Function	35
2.	Trailing Edge Shapes of 1/8"-Test Plates	46
3.	Experimental Results for 1/8"-Test Plates	46
4.	Comparison of Strouhal Numbers	53
5.	Ultra-harmonics at Resonance	54
6.	Secondary Resonant Frequencies	56
7.	Comparison of Results for Plate #11 of Test Series #1 and #2	63
8.	Reproducibility of Transitional Velocity and Vibrational Amplitude for Plate #11, Clamp Position No. 5	67
9.	Comparison of Stability Graphs	69
10.	Vibration Characteristics of 1/4"-Plates at Resonance	76
C-1.	Determination of Moment of Inertia Ratios	102
C-2.	Determination of Apparent Mass Moment of Inertia	103
E-1.	Micrometer Measurements	105
E-2.	Comparison of Micrometer and Voltmeter Measurements	105

### LIST OF NOTATIONS

a	= longitudinal spacing of vortices; inch.
$a_m$	= dimensional constants; m = integer.
$a_o$	= amplitude of vibration of accelerometer; inch.
$a_{ot}$	= amplitude of vibration of trailing edge; inch.
$a_s$	= constant associated with net lift force acting on a steady plate.
2b	= length of test plate in the direction of flow; inch.
c	= coefficient of damping; lbs-in-sec.
$c_c$	= critical damping; lbs-in-sec.
d	= a transverse body dimension; inch.
$d'$	= distance between horizontal portions of free shear layers; inch.
e	= 2.7182.....
f	= frequency; cps.
$f_n$	= natural frequency; cps.
$f_p$	= frequency of plate vibration; cps.
$f_{pr}$	= predominant frequency; cps.
$f_r$	= frequency at resonance; cps.
$f_s$	= Strouhal frequency; cps.
g	= gravitational acceleration, 32.2 ft/sec <sup>2</sup> .
h	= transverse spacing of vortices; inch.
i	= $\sqrt{-1}$
k	= spring constant; lbs-in.
$\bar{k}$	= $U_1/U$ = correction factor for velocity at the free streamline; fps.
$k$	= $\frac{\omega b}{U}$ reduced frequency.
m	= magnification factor for static loads.
$m_i$	= dimensional constants; i = integer.
$p_b$	= base pressure; psi.
$p_o$	= ambient pressure; psi.
$p_v$	= vapor pressure; psi.
t	= time; seconds.
$t'$	= test plate thickness; inch.
$u', v'$	= fluctuating velocity components; fps.
$u_s$	= velocity of vortices relative to U; fps.

$w$  = downwash; fps.  
 $x, y$  = cartesian coordinates.  
 $z$  =  $x + iy$  = complex coordinate.  
 $\alpha$  = geometric angle of attack, radians.  
 $\beta$  =  $K/K_1$  = measure of annihilation of vorticity at the trailing edge; radians.  
 $\beta'$  = instantaneous angle of attack, radians.  
 $\delta$  = logarithmic decrement.  
 $\delta_t$  = boundary layer thickness at trailing edge; inch.  
 $\Sigma$  = (Wave Analyzer reading) / (Mean Voltmeter reading).  
 $\rho$  = strength of a single vortex;  $\text{ft}^2/\text{sec}$ .  
 $\lambda$  =  $K/U^2$  = proportionality factor.  
 $\nu$  = kinematic viscosity of fluid;  $\text{ft}^2/\text{sec}$ .  
 $\pi$  = 3.1415.....  
 $\rho$  = mass density of fluid; slug/ $\text{ft}^3$ .  
 $\sigma$  =  $2(p_0 - p_v) / \rho U^2$  = cavitation index.  
 $\phi_n$  = phase angle;  $n$  = integer.  
 $\phi(t)$  = Wagner's function.  
 $\omega$  = frequency; radians/sec.  
 $\omega_n$  = natural frequency; radians/sec.  
 $\omega_s$  = Strouhal frequency; radians/sec.  
 $A$  = amplitude of vibration; inch.  
 $A_n$  = dimensionless coefficients;  $n$  = integer.  
 $B_n$  = dimensional coefficients;  $n$  = integer.  
 $C_D$  =  $2D/U^2$  = drag coefficient.  
 $D$  = drag force; lbsf.  
 $F'$  = real part of Theodorsen's function.  
 $F_L$  = lift force; lbsf.  
 $G$  = dimensionless factor indicative of a moving trailing edge geometry's ability to enhance 2-dimensional wake conditions.  
 $G'$  = imaginary part of Theodorsen's function.  
 $H$  = length of test plate perpendicular to the direction of flow; inch.  
 $I$  = polar mass moment of inertia; lbs-in- $\text{sec}^2$ .  
 $I'$  = apparent mass moment of inertia.

$2K$  = rate at which discrete vorticity diffuses into the wake;  
 $\text{ft}^2/\text{sec}^2$ .

$K_1$  = rate of vorticity discharge per side of an object;  $\text{ft}^2/\text{sec}^2$ .

$L', L'_V$  = lift force due to vortex shedding;  $\text{lbs}_f$ .

$L'_C$  = lift force associated with circulatory potential flow;  $\text{lbs}_f$ .

$L'_{n.c.}$  = lift force associated with non-circulatory potential flow;  $\text{lbs}_f$ .

$M$  = magnification factor for  $L'_V$ .

$M'_V$  = moment due to  $L'_V$ ;  $\text{lbs}_f\text{-in.}$

$M'_C$  = moment due to  $L'_C$ ;  $\text{lbs}_f\text{-in.}$

$M'_{n.c.}$  = moment due to  $L'_{n.c.}$ ;  $\text{lbs}_f\text{-in.}$

$Q$  =  $1 - \bar{k}^2$  = base pressure coefficient.

$R$  = Reynolds number; in case of test plates:  $R = U \cdot t' / \nu$ .

$S$  = Strouhal number; in case of test plates:  $S = f \cdot t' / U$ .

$U, U_0$  = free stream velocity;  $\text{fps.}$

$U_1$  = free stream line velocity;  $\text{fps.}$

$U_r$  = free stream velocity at resonance;  $\text{fps.}$

$W$  = complex velocity potential.

$X_b$  = distance in semi-chords between resultant lift force and leading edge of test plate;  $\text{inch.}$

## I. INTRODUCTION

### A. General Statement of the Problem

Operational difficulties such as the singing of ship propellers, of turbine and pump blades and the vibration of other moving vanes, cylinders and struts are commonly associated with the formation of a periodic wake. The need for a satisfactory definition of these phenomena is being felt in the design of components for increasingly powerful and faster Naval vessels. As a contribution in elucidating this question the "hydroelastic" vibration of thin flat shapes has been studied.

Any deformation of an elastic body due to a fluid flow around it can be termed a hydroelastic response. More specifically this term applies whenever the elastic deformation substantially modifies the magnitude of the hydrodynamic loading. Where in the classical theory of elasticity external forces or displacements determine stress and deformation, the external load in the aero- or hydroelastic case remains unknown, until a solution to the problem is obtained.

From a practical viewpoint and analogous to the division in the field of aeroelasticity, the field of hydroelasticity can be divided into response and stability problems.

In response problems an effort is made to obtain the absolute magnitude of stress or displacement of a structure when subjected to an external load or deformation. The formulation of such problems is in terms of boundary conditions; governing equations are non-homogeneous, their solutions non-trivial. Adequate strength of the structure is a main design objective.

In stability problems on the other hand, attention is directed toward the relation between elastic stiffness of a structure, which is independent of speed, and the hydrodynamic load, which may grow exponentially with increasing speed. Possibly there then exists a critical speed at which the structural deformations become excessive. This sometimes suddenly reached limit of structural stability is associated mathematically with the trivial solution of a set of homogeneous equations. Usually these equations are linear ones since near the limit of stability the amplitudes of elastic deformation may still be regarded as very small. In design the objective is to avoid the region of possible instability by giving special attention to rigidity, damping characteristics and hydrodynamic shape.

Response problems are encountered with rudder systems of ships and the buffeting of hydrofoils as well as with cavitation on vibrating surfaces.

Stability problems may be illustrated by the flutter of hydrofoils, the vibration of cylindrical objects such as submarine periscopes and submerged towing cables. An example which has been known for more than 50 years and is not yet completely understood is the singing of hydraulic



turbine and propeller blades.

In the field of aerodynamics, where streamlined shapes are the rule, many stability problems are solved satisfactorily via linearization of the pertinent, classical aerodynamic equations. For understreamlined objects, such as cylindrical bodies, where the shedding of discrete vortices clearly plays a decisive role, this approach does not suffice since in general the flow field near the trailing edge is not amenable to theoretical treatment.

Both the downstream diffusion of vorticity and the fluctuating forces on a structural component depend upon the wake dynamics at the trailing edge. A better understanding of how the early wake is related to the body which produces it is a prerequisite to a more rational formulation of the frequency of vortex shedding and the associated lift forces.

## B. Scope of the Investigation

The description of the wake structure near the trailing edge is a problem involving many variables. Besides trailing edge geometry, general body shape and free stream velocity, the magnitude of motion exhibited by the body is of prime importance. Boundary layer thickness and character at the trailing edge, spanwise periodicities in the wake and free stream turbulence constitute further influences which yet lack a proper formulation.

In order to reduce the variables associated with the overall body shape it was decided to employ flat plates of reasonable aspect ratio as the fundamental structural shape. Further, the mean angle of incidence was limited to zero degrees. Opportunity for classical flutter was greatly reduced by allowing the test plates but one degree of freedom at a time. The plates were suspended in the test section of a water tunnel for which the free stream velocity could be selected over a fairly wide range. Thus the investigation could be directed toward the remaining variables which were considered of primary importance. These include:

1. trailing edge configuration,
2. plate restraint and magnitude of plate motion.

The experimental program provided for measurement of the:

1. frequency spectra of plate vibration, and
2. amplitude of plate motion.

## II. REVIEW OF PREVIOUS WORK

### A. Vortex-Induced Vibrations

A large number of practical examples of vortex induced vibrations have been reported in the literature. Most frequently encountered is the

vibration of circular cylinders. A few of the recent reports are those by Den Hartog (1), Dickey (2) and Ozker (3) on the vibrations of steel stacks; by Baird (4) and Housner (5) on the vibration of suspended pipe lines. Grimmer (6) and Price (7) discuss suppression of the excitation of cylinders. Krall (8), Penzien (9) and Scruton (10) deal with the question of whether vortex induced motion of cylinders is forced or self-excited.

Not only bluff bodies such as cylinders, but also streamlined shapes are reported to be excitable by vortices shed at the trailing edge. Usually the singing of hydraulic turbine- and propeller blades is associated with this phenomenon. The remedy for these undesirable vibrations is often found in but slightly modifying the trailing edge, although results are varied and not always successful (11). In fact, it may be said that the mechanism of vortex shedding is not yet completely understood, even though it attracted attention quite early. Following is a summary of the pertinent and sometimes conflicting observations.

With the adoption of high tensile alloys some 35 years ago in the manufacture of propellers a vibration problem occurred known as "singing". The emitted noise often became so intense as to be clearly audible through the vessel. The term singing is indicative of the fact that the acoustic spectrum of a singing propeller's noise contains one or more predominant frequencies (12) in the audible range. Whereas some propellers sang over but a limited speed range, others could produce a series of notes for which the frequency increased in discrete steps with increasing speed. In some cases zones of singing were separated by quiet speed zones. In others several zones each associated with a particular note overlapped each other. For one and the same propeller a decrease in the ship's draft, or the temperature of the water, or an increase in dissolved air content of the water could materially lessen the tendency to sing. That the phenomenon is a capricious one is illustrated (13) by cases of identical propellers in which some sang and others were "silent".

The number of explanations which have been advanced is indicative of the complexity of propeller singing.

Conn (14) suggests that torsional vibrations occur due to continuously varying location of the pressure center for blades placed in the turbulent wake of a ship. Duncan (discussion of 14) proved Conn's basic assumptions to be incompatible with airfoil theory.

Shannon (15) concludes from a statistical examination, that rounded leading edges with their particular pressure distribution are the controlling factors and he advocates sharp leading edges. However, the compilation of shapes examined shows that the same conclusions follow if the trailing edges were made the subject of consideration.

Davis (16) assumes that collapsing cavitation bubbles at the leading edge form the driving mechanism and then attempts to compute the ideal non-singing shape, but the assumption was not supported by evidence.

G. Hughes (17) postulates separation at the leading edge and attempts to evolve the remedial blade design from theory based on such separation and

on statistical evidence. He too suggests adoption of sharp leading edges.

Several times Coulomb friction in stern-tube bearings has been suggested as the exciting mechanism (12).

Some investigators are convinced of the possibility of flutter, while others are equally convinced of the contrary. Gutsche (18) contends that small faults in the profile and the surface texture of propeller blades would induce singing and that wandering of the point of laminar- to turbulent boundary layer transition could sustain the singing.

Finally, vortex shedding at the trailing edge was proposed by Kito (19), Gongwer (20) and Krivtsov (21) as the exciting mechanism.

Of all the explanations offered, the vortex shedding hypothesis fits most of the practical experiences and is supported by creditable research work.

Gongwer's experiments (20) with vanes showed clearly the functional relationship that exists between singing of vanes and trailing edge thickness. Gongwer improves on Kito's empirical relation for singing frequency and trailing edge thickness by proposing that a percentage of the local turbulent boundary layer thicknesses be added to the physical trailing edge dimension. Further, from results with swept back vanes he found evidence that the significant velocity in the Strouhal parameter is the component normal to the trailing edge. This latter observation was followed up by Lankester (12) in computing  $S$  along the edge of an actual propeller. He shows near constancy of  $S$  over a reasonable length at 0.8 of the blade radius.

Perhaps the most convincing is Krivtsov's paper (21) on the hydro-elastic behavior of vanes which covers 5 years of research in the Soviet Union. More than 50 flat bronze vanes resembling propeller blades were tested in a fluid flow, for vibrational behavior. The influences of trailing edge thickness, angle of attack, ambient pressure and fluid density were investigated. G. Hughes' (17) and W. L. Hughes' (22) work on the relative damping and frequency change in air and water as well as Burril's (23) classification of vibration modes of propeller blades were confirmed and supplemented. Measurements of instantaneous pressures at the sharply cut-off trailing edge of some vanes showed unmistakably the constancy of the Strouhal number,  $S$ , for a given edge thickness. Krivtsov's final conclusion regarding the mechanism of singing is substantially the same as set forth by Gongwer: i.e., as soon as the vortex shedding frequency synchronizes with the natural frequency of one of the modes of vibration of the vane, singing occurs.

## B. Structure and Periodicity of Wake Flow

### 1. Experimental Findings

The character of the wake, in particular behind bluff bodies, demonstrates strikingly the significance of the Reynolds Number. Following Hollingdale (24)

and others the subsequent division in regimes as a function of  $R$  may be given:

a. Oseen Flows	1
b. Steady Viscous Wakes	40 - 600
c. Regularly Periodic Wakes	150 - 1300
d. Irregularly Periodic Wakes	300 - 2000
e. Turbulent Wake	300 - 2000

The noted values of  $R$  vary considerably depending on the actual shape, the surface texture and the motion of the body which produces the wake. For a circular cylinder the lower values apply. The transition between regimes is fairly smooth.

Periodic wakes are not only of immediate practical importance but also of considerable theoretical interest. The salient features of these wakes have intrigued many an investigator during the past 50 years. Yet no complete mathematical description has been advanced.

Audible manifestations of vortex shedding of a cylinder were first studied by Strouhal (25), who showed in 1878 that vibrations existed transverse to the flow and that their frequency,  $f$ , was a function of the speed of flow  $U$  and the cylinder diameter  $d$ . The functional relation could be approximated by  $6df = U$ .

Thirty years later Benard (26) detected a row of vortices in the flow behind cylinders and correlated this "vortex street" with the particular sound generation studied by Strouhal. For a circular cylinder he found the periodicity to be most marked for  $40 < R < 1000$ .

Using a dimensionless frequency (the Strouhal number,  $S = fd/U$ ) Kovasnay (27) and Roshko (28) determined for circular cylinders with viscous wakes:

$$S = 0.212 \left( 1 - \frac{21.2}{R} \right), \quad 40 < R < 150$$

and for the periodic component at higher Reynolds numbers:

$$S = 0.212 \left( 1 - \frac{12.7}{R} \right), \quad 300 < R < 5000$$

The latter's work shows that the higher  $R$  the shorter will be the

"body regime" which he defines as the region between the trailing edge and the point of full wake turbulence.

Den Hartog (1) attributes vibration of a smokestack for  $R = 7 \times 10^6$  to vortex shedding and reports actual failure of a large stack for  $R = 2 \times 10^7$  (29).

Both Pagon (30) and Dockstader (31) report values of  $R = 5 \times 10^6$  for similar cases.

Penzien (9) suggests, that such vibrations may be self-excited rather than forced in which case the natural frequency of the structure would be determinative. Indeed the work of Scruton (10) demonstrates that vibrations of cylinders occur over a range of  $S = 0.1$  to  $S = 0.2$  depending on the structural damping.

Even well below the periodic range, at  $R = 11$ , a vortex trail was obtained by Camiechel et al (32) for a cylinder mounted on springs such that natural frequencies below 40 were provided for.

Recent measurements by McGregor (33) and by Gerrard (34) reveal that up to  $R = 10^4 - 10^5$  (limit of the range of measurements) largely regular pressure variations are present on the surface of a circular cylinder.

Combining the above findings suggests that near the trailing edge of a circular cylinder the wake may remain essentially periodic up to an as yet undetermined high Reynolds number. It is apparently not the rapidity with which the energy contained in discrete vortices diffuses into random turbulence, but rather local effects at the trailing edge which are determinative in vibration questions. It follows that the shape of the trailing edge and the adjacent field are of prime importance. This leads to a consideration of shapes other than circular cylinders.

The wake behind elliptic cylinders was studied by Richards (35); that behind inclined flat plates by Fage et al (36); for a wide variety of rolled beam shapes by Nøkkentved (37), and for a large number of bluff cylinders by Delany (38) and Shaw (39). In many cases the value of  $S$ , based on the largest body dimension perpendicular to the direction of flow, is considerably below the 0.2 valid for circular cylinders with values ranging from 0.12 to 0.21. For higher Reynolds numbers Delany's work shows an increase in  $S$  to  $S = 0.4$ .

Of special importance, being another elementary form, is the flat plate. The significant work of Fage et al (36), (40), deserves particular attention. It constitutes one of the few studies of the wake immediately behind the object. Plates with sharp leading and trailing edges were tested at angles of incidence varying up to  $90^\circ$ . One of the conclusions was that from both sides of the plates almost equal amounts of vorticity are shed.

The Strouhal number, based on the projection of the plate perpendicular to the flow ( $B = 2b \sin \alpha$ ), increased from  $S = 0.14$  at  $\alpha = 90^\circ$  to  $S = 1.0$  to 1.6 at small  $\alpha$ 's. Replacing  $B$  by  $d'$ , i.e., the distance between the parallel

portions of the free shear layers (see Figure 1-d) it was shown that  $S \approx \text{Constant} \approx 0.16$ .

The velocity distribution close to a circular cylinder was described by Fage (41) in a subsequent report.

Another study of the free shear layers close to a circular cylinder was made by Schiller and Linke (42). The boundaries of the spreading vortex layers were determined at several Reynolds numbers. Again the shortening of the "body regime" with increasing  $R$  was shown. The lowest pressure is shown to be found at the end of the body regime where the free shear layers diffuse into each other. Towards the body there is a pressure increase.

Gongwer (20) suggested that the Strouhal numbers for vanes, based on the trailing edge thickness, have the customary values if the latter are corrected for local boundary layer thickness. Interesting visual evidence was given of 3-dimensional instability of the wake. Gongwer attributed this to scalloping of the trailing edge. An attempt was made to compute the alternating lift force associated with vortex shedding, from the occurrence of cavitating vortices. The force thus determined was of considerable magnitude.

Actual measurements of instantaneous lift forces seem to be limited to circular cylinders despite their obvious value in design. For a circular cylinder Schwabe (see (43), page 421) found at  $R = 735$  and  $C_D = 1.09$ , a periodic lift coefficient  $C_L = 0.45$ . Petrikat (44) found for cylinders in water  $C_L = 1.0$  to  $1.6$  at resonant conditions.

More recently Macovsky (45) determined by direct measurement on a rigidly held cylinder segment periodic lift coefficients as high as  $C_L = 1.5$ , with  $C_L = 1.0$  as an average value for  $R$  between  $2$  and  $6 \times 10^4$ . Toward  $R = 10^5$ ,  $C_L$  drops to  $C_L = 0.5$ .

Philips (46) attempted to infer  $C_L$  from velocity fluctuations near the shedding object. For a moving and vibrating string for which the emitted sound intensity was measured, final computations gave  $C_L = 0.5 C_D$  with a chance of 40% error.

McGregor (33) and Gerrard (34) attempted to determine  $C_L$  by integration of the measured pressure pulses at the surface of a cylinder thus in effect also considering only a segment of the cylinder. McGregor gives  $C_L = 0.60$  for  $R = 0.4 - 1.1 \times 10^6$ ; Gerrard found  $C_L$  to be a function of  $R$  :  $C_L = 0.3 - 1.0$  for  $R = 3 - 5 \times 10^5$ .

Theoretically isolated vortices are stable. If more vortices occupy a flow field, an interaction instability, already predicted by Kelvin (47), may occur. Gutsche (48) once attributed the singing of propellers to this periodic break up of vortices. Indeed, the long vortices depicted in Gongwer's photographs (20) are unstable, although Gongwer points to the mode of vane vibration as the primary cause. Three dimensional periodicity

and instability in the wake of a presumably rigid circular cylinder were demonstrated by Roshko (28). Even more clearly the 3-dimensionality of the wake is shown in Makovsky's pictures (45). This phenomenon most likely accounts for the variation in observed values of lift coefficient as well as its decline with increasing Reynolds Numbers.

## 2. Theoretical Work

Except for the viscous laminar wake theoretical considerations have not resulted in concise exact descriptions of wake flows.

In all practical cases a quasi-empirical approach is necessary. Almost all of these are extensions of either Kirchhoff's or Von Karman's theories. The latter's contribution is most widely known and possibly too quickly advanced as sufficient explanation in the event of hydroelastic vibrations such as the singing of propellers or the motions of smoke stacks.

At both sides of a bluff body the flow will separate when the velocity becomes large enough. Helmholtz (49) suggested that separation occurred because, at the edges, the velocity could not become infinite. Prandtl's boundary layer concept clarified this matter and pointed to the Reynolds number as determinative for the location of separation. Actual calculations of the separation point by boundary layer theory are elaborate for laminar layers; more difficult, if at all feasible, for turbulent boundary layers. Assuming for the moment that the separation points are known and fixed and following Kirchhoff's extension in 1869 of Helmholtz' original theory (50) the wake flow can be simplified by assuming that the wake is a body of stagnant fluid. This "dead water" region is then isolated from the main flow by the shear or vortex layers which originate at the separation points and which, within a few diameters behind the body, disintegrate into a turbulent mixing zone, (see Figure 1-b). Kirchhoff proceeds by replacing the shear layers by surfaces composed of "free streamlines". He assumes that the free streamline velocity,  $U_1$ , is everywhere equal to the free stream velocity, so that by Bernoulli's law the pressure in the wake would equal the ambient pressure outside of it. For a given shape of the free streamlines, a simple momentum analysis would yield the drag.

The assumption of constant velocity along any free streamline insures that the mapping of it onto the hodograph plane always becomes a circle facilitating greatly a transformation to the complex potential plane. This mathematical convenience led to the appearance in the literature of a large number of free streamline solutions. However, in all cases this theory overestimates the base pressure,  $P_b$ , so that in actuality the velocities near the free shear layer must exceed the free stream velocity. This was indeed borne out by measurements in the shear layers of inclined flat plates and circular cylinders made by Fage and Johansen (40) (41). They noted maximum velocities up to 1.45 x the free stream velocity. Also infinite free streamlines, assumed for the sake of mathematical formulation, are not in accord with reality. The shear layers develop into alternating vortices which, depending on Reynolds number, may persist far downstream or

diffuse quickly into random turbulence.

At the same time Fage's measurements (36) uphold part of the free-streamline theory. Even along the rear of inclined flat plates nearly constant pressures were measured. Furthermore, measurements (43), p. 553 indicate that close to the body the theoretical free streamline shapes are not unrealistic. Observations of the wake beyond the point where the shear layers roll up, i.e., outside the "body regime", definitely demand another model.

In 1911-12 Von Karman published a different approach to the determination of the drag of bluff bodies (51), (52). His now classic theoretical discussion of periodic wakes was built on a mathematical model of two parallel rows of equally spaced and staggered point vortices in an otherwise irrotational and infinite flow (see Figure 1-c). Three arbitrary parameters are involved: the longitudinal spacing  $a$ , the transverse spacing,  $h$ , and the strength,  $\mathfrak{z}$ , of each vortex. The complex potential  $W$  of the flow field could be determined in terms of these parameters. From  $W$  the velocity  $u_s$  with which the vortices moved relative to the fluid at infinity may be computed and hence the rate of vorticity discharge  $K$ . The drag of the body then may be calculated from the geometrical pattern of the eddies (53), p. 132. However, Von Karman's formulas cannot yield  $K(U,d)$ ,  $a(U,d)$  and  $h(U,d)$ . Determination of these relations would involve prediction of the Strouhal number, of  $K/U^2 = \lambda$ , of  $u_s/U$  and  $h/a$ . Von Karman showed that in a non-viscous fluid, expect for  $h/a = 0.281$ , the equilibrium of the vortex array was unstable to the first order. Schmieden (54) showed, however, that this "stable spacing ratio" has a higher order instability and Birkhoff (55) advances another prediction of  $h/a$  based on inertia considerations. He arrives at  $h/a = 0.35$  also in agreement with the scattered experimental values.

A prediction of  $\lambda$ , based on boundary layer theory was given by Heisenberg (56). Since  $D\mathfrak{z}/Dt = \nu \nabla^2 \mathfrak{z}$ , the boundary layer approximation of the vorticity,  $\mathfrak{z} = \partial u / \partial y$ , is carried into the wake by convection and diffusion. On each side the rate of vorticity shedding then may be approximated by

$$K_1 = \int_0^{U_1} \left( \frac{\partial u}{\partial y} \right) u \, dy = 0.5 u_1^2 \quad [2]$$

a relation confirmed by Fage's measurements (36). If  $\beta$  is the fraction of vorticity of each sign remaining after the initial diffusion into vorticity of opposite sign, then  $\beta = K/K_1$ ; Heisenberg sets  $\beta = 1$ , Prandtl stated on empirical grounds that for the periodic wake regime  $\beta = 0.5$ .

Heisenberg thus made an attempt to join the two theoretical solutions of Kirchhoff and Von Karman. For a flat plate normal to the flow there is reasonable agreement. As Von Karman pointed out (discussion of 55), however,



the drag coefficients for other shapes have the same value.

The insertion of an empirical factor, indicated by Prandtl, may still save the useful features of the free stream line approach. This idea has been pursued recently by Roshko (57) who corrected the separation velocity  $u_1$  by introducing  $u_1 = \bar{k}U$ , where  $\bar{k}$  is a constant larger than unity. The constant  $\bar{k}$  is replaced by 1, when the free streamlines become parallel to the direction of flow (since at infinity the flow must have returned to a uniform one), which results in a notch in the circular hodograph. As long as the factor  $\bar{k}$  cannot be deduced from the dynamics of the wake close to the body, it must still follow from actual measurements.

If, given a  $\bar{k}$ -value, it was possible to obtain a description, in terms of  $\bar{k}$ , of the wake beyond the transition from body regime to wake regime, a complete solution could be obtained.

Von Karman's analysis showed that the two parameters needed to relate the wake regime to the body producing it are the dimension  $h$  and the velocity  $U-u_s$ . Once these are fixed the wake can be considered independent from the body. Therefore, in a subsequent experimental study, Roshko (58) assumed that  $h = d'$ , where  $d'$  is the distance between the parallel free streamlines. By means of the notched hodograph method it then is possible to relate  $d'$ , for a given  $\bar{k}$ -value, to the body dimension  $d$  ( $d =$  largest dimension perpendicular to the flow). For the second relation between  $\bar{k}$  and the periodic wake Roshko (58) reverts to the above assumption of Prandtl:  $\beta = \text{constant} \approx 0.5$  ( $\beta$  is the  $\epsilon$  in Roshko's paper;  $K/K_1 = \epsilon = U^2/(\bar{k}U)^2 = \bar{k}^{-2}$ ). The value  $\beta = \epsilon = 0.5$  is substantiated by the often mentioned work of Fage and his colleagues, whereas Jeffreys (59) suggests the same value on the basis of symmetry of perturbation of a single boundary layer. This contention was criticized by Rosenhead (60) who noted that this symmetry is but temporary.

In any event the reduction of experimental variables needed for the description of the complete wake to a single quantity would be a significant development in the systematization of wake phenomena. It promises further the determination of the drag from a single measurement such as for example the shedding frequency.

It may be noted that in the above no mention is made of the actual mechanism of vortex shedding. Von Karman noted that his theory did not offer such an explanation. In fact a better understanding of the dynamics of the early wake is the key to the complex problem of periodic and turbulent wakes. It is probably erroneous to speak of vortex shedding. Vortices are gradually developed some distance behind the body. Richardson(61), fig. 2, shows that the zone of maximum velocity fluctuations,  $v'_{\max}$ , is at some distance behind a circular cylinder and shifts toward the body while decreasing in magnitude, with increasing  $R$ :  $v'_{\max} = 1.2$  at  $y/d = 0.3$  for  $R = 1.25 \times 10^4$  to  $v'_{\max} = 0.7$  at  $y/d = 0.1$  for  $R = 4.25 \times 10^4$ . In that region which Roshko termed the "coupling region" (coupling the free streamline wake to the Von Karman wake) the mean pressure falls well below the ambient pressure (42), (58) (see Figure 1-b). Associating these low

pressures with the cores of the vortices being formed and assuming that the base pressure coefficient  $\phi$ , which is directly associated with  $\bar{k}$  by  $\phi = 1 - \bar{k}^2$ , depends mainly on the vortex pressure, it follows that the vortex dynamics close to the trailing edge are of primary importance. Further it may be expected that the vortex formation will be related intimately to both the boundary layer development and the trailing edge geometry.

### C. Wake Dynamics and Trailing Edge Geometry

In the discussion of periodicity in wake flows and its effects, the fundamental importance as well as the inadequate understanding of the early wake were stressed. The foregoing review suggested that the significant variables of this problem are:

- a. the trailing edge geometry of the structural component,
- b. the location of the separation points,
- c. the maximum distance between the free shear layers,
- d. the history of the shear layers.

#### 1. Trailing edge geometry

Among these interrelated variables the shape of the trailing edge is probably the most prominent single factor. Relevant references from which this may be inferred indirectly deal with the reduction of the form drag coefficient due to apparently small interferences in wake flows near the trailing edge. (It is recalled that the drag coefficient and the vortex street can be related to each other by means of momentum considerations (53) and that therefore changes in  $C_D$  are indicative of alterations in wake structure).

Pankhurst (62) reports a reduction of  $C_D = 1.11$  to  $C_D = 0.94$  for a circular cylinder after it had been fitted with a small flap at the rear.

Nøkkentved (37) shows a decrease in drag coefficient of  $D_D = 1.9$  to  $C_D = 1.6$  for a structural T-shape of which the leg points upstream and downstream respectively.

Particularly noteworthy is the work by Roshko (58). He noticed a reduction in  $C_D$  of 40 % by placing a small plate along the center line of the wake close behind a circular cylinder. A similar arrangement for a flat plate normal to the flow resulted in a decrease of  $C_D$  by 20 %.

The experimental work presented in this report was designed to substantiate the inference that the trailing edge geometry was of decisive influence on the structure of the early wake and thereby on the periodic lift forces acting on the structure. This point of view was vindicated in a recent publication by Heskestad and Olberts (63) which appeared when the present experimental program drew to a close. The paper reports on measurements of vibrational amplitudes and frequencies for a large number

of trailing edge geometries fitted onto a thin flat plate. The frequency of vibration of the plate and in particular the amplitudes of motion were shown to be markedly effected by changes in the trailing edge shape (see Figure 1-e).

## 2. Location of the separation points.

Besides being a direct function of trailing edge geometry, the separation points may recede with increasing free stream velocity thus making the Strouhal number dependent on the Reynolds number as is clearly shown in Delany's work (38). As an attendant effect the separating boundary layers may become more directed toward each other resulting in an increased annihilation of vorticity before it can diffuse into the wake proper.

For vibrating objects with rounded trailing edges the separation points will be unstable resulting in a "flapping" motion of the low velocity portion of the wake. This effect is clearly involved in the sustained motion of cylinders reported by Meier-Windhurst (64).

This periodic motion of the early wake led Birkhoff (55) to an attempt to predict the Strouhal Number based on a consideration of the inertia of the swinging portion of the wake.

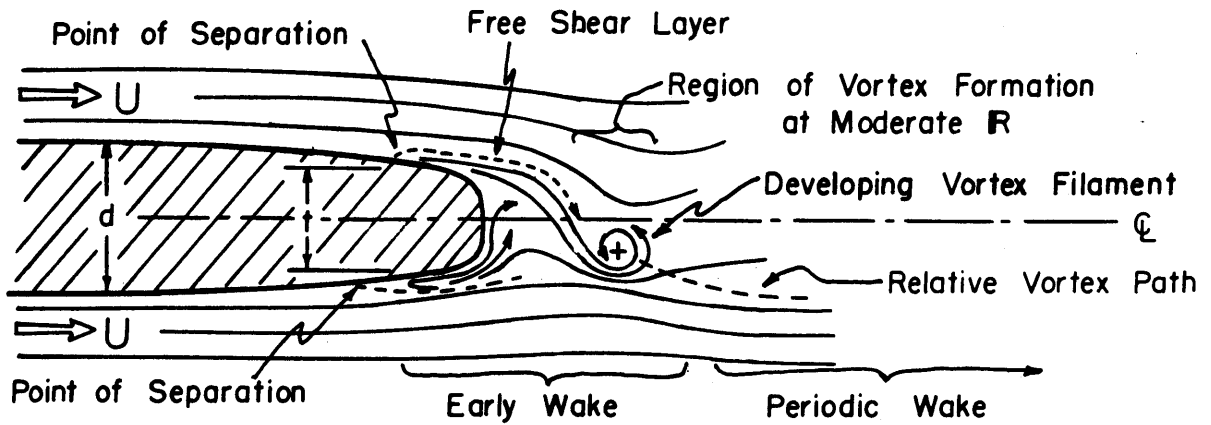
## 3. Distance between the shear layers.

For bluff bodies the maximum distance  $d'$  between the free shear layers is an important parameter in the dynamics of their wakes. Fage and his associates (36) found advantage in using  $d'$  instead of  $d$  in the computation of the Strouhal number. This dimension is fundamental in the theoretical treatment by Roshko (58), which was mentioned in section II-B. Roshko's formulation of the "Universal Strouhal Number",  $S^* = fd'/u_1$  in which  $d'$  for a number of cases can be obtained from the notched hodograph transformation, however, can not account for the effect of trailing edge shape downstream of the separation points.

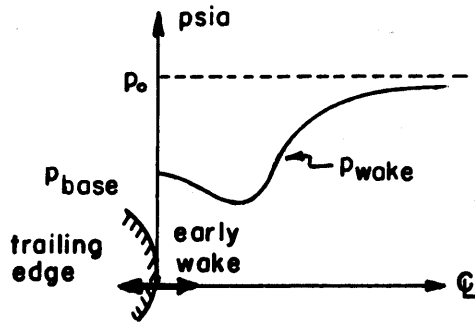
When  $d'$  approaches zero, the amount of discrete vorticity carried into the wake tends to zero. This is illustrated by the work of Chuan and Magnus (65) a.o., who found that vortex induced vibrations of an airfoil were only possible for angles of attack above  $6^\circ$ .

## 4. History of the shear layers.

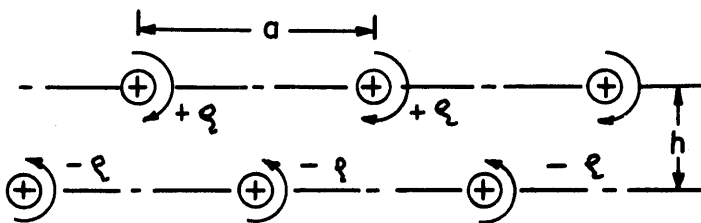
For streamlined shapes the temporal and spatial boundary layer growth must be taken into account because they will form the free shear layers. As mentioned before, Gongwer (20) went a step in that direction by increasing the physical trailing edge thickness with a portion of the turbulent boundary layer thickness. This approach will have to be supported by more experimental data. For bluff bodies such a correction will in general have little significance.



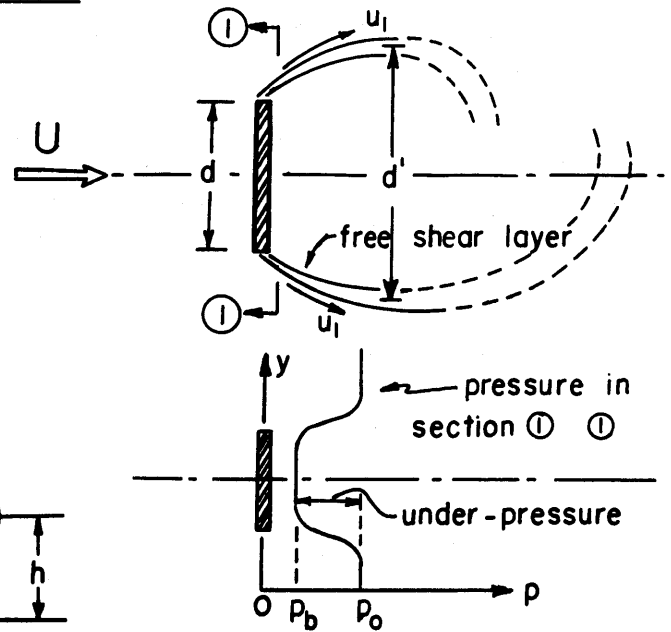
a. Scheme of Trailing Edge Flow



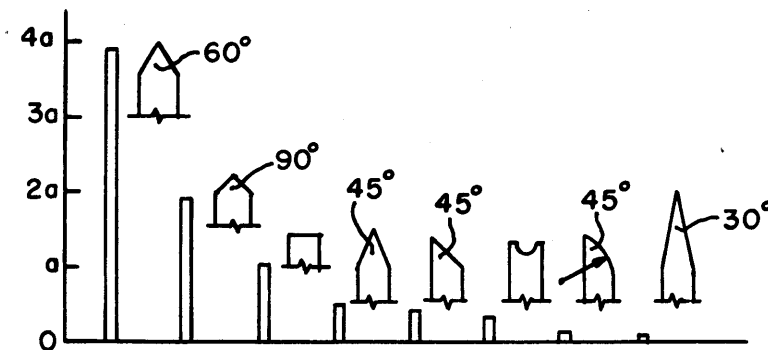
b. Pressure along Center Line



c. Von Kármán Vortex Trail



d. Wake behind Flat Plate



e. Amplitude of Vibration as Function of Trailing Edge Geometry - from Reference 63

Figure I. Wake Flows - Amplitude of Vibrations

In the case of slender vibrating bodies boundary layer considerations will be particularly important. At the same time, however, these are of considerable difficulty; no specific treatment of this aspect has been found in the literature.

#### D. Summary

1. From the large number of references in the engineering literature which associate structural vibrations with the formation of a periodic wake, two categories were discussed in section II-A:

- a. vortex-induced vibration of cylinders
- b. the singing of ship propellers

The circular cylinder, being an elementary shape, is of frequent occurrence both in structural applications and in research work. Some recent publications pertaining to that shape were therefore included in the review.

Secondly, references about the singing of ship propellers were selected for discussion since the shape of the propeller blade resembles most that of the flat plates employed in the experimental work presented in this report. This literature reflects the complexity of the vortex induced vibration phenomenon.

2. In section II-B-1 the wake with which vortex-induced vibrations are associated is considered. After a discussion of the wake structure and periodicity as a function of Reynolds Number, attention is drawn to the flow field around the trailing edge.

The few reported attempts to determine the lift forces associated with vortex shedding point to their difficulty as well as the need for further investigation. Demonstrated three-dimensionality of the wake was assumed to be responsible for variations of the lift coefficient.

Section II-B-2 deals with the theoretical treatment of wake flows. Following Kirchhoff many authors employed free stream line theory to obtain a description of the wake close to the body. Others bypassed the early wake by using the Von Karman model of an idealized periodic "asymptotic" wake.

It was shown that among the attempts to join both theoretical treatments the recent work of Roshko merits attention. Again the review suggested that the trailing edge geometry and the flow field, or "early wake", surrounding it are of basic importance.

3. In the section II-C further support is given to the point of view that the early wake and the trailing edge geometry constitute the basic variables of the vibration phenomenon.

Interference with the early wake flow may substantially reduce the drag. Evidence of the direct influence of trailing edge geometry on the

severity of the vibrations is presented.

The formulation of the Strouhal Number should be based on the (variable) distance between the free shear layers rather than on a body dimension.

The location of the separation points deserves attention since instability of these points has been suggested as determinative for sustained wake periodicity. Receding of the separation points with increasing  $R$  explains part of the scatter in quoted values of  $S$ . The boundary layer thickness at the trailing edge may have to be incorporated in the definition of  $S$ .

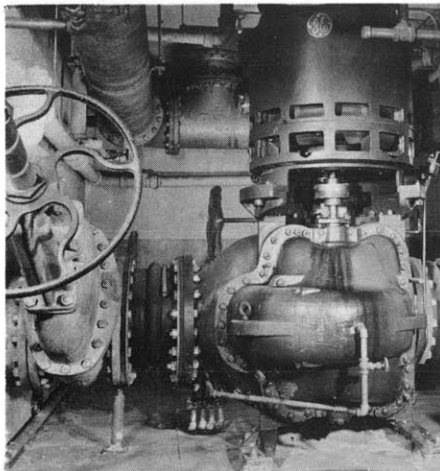
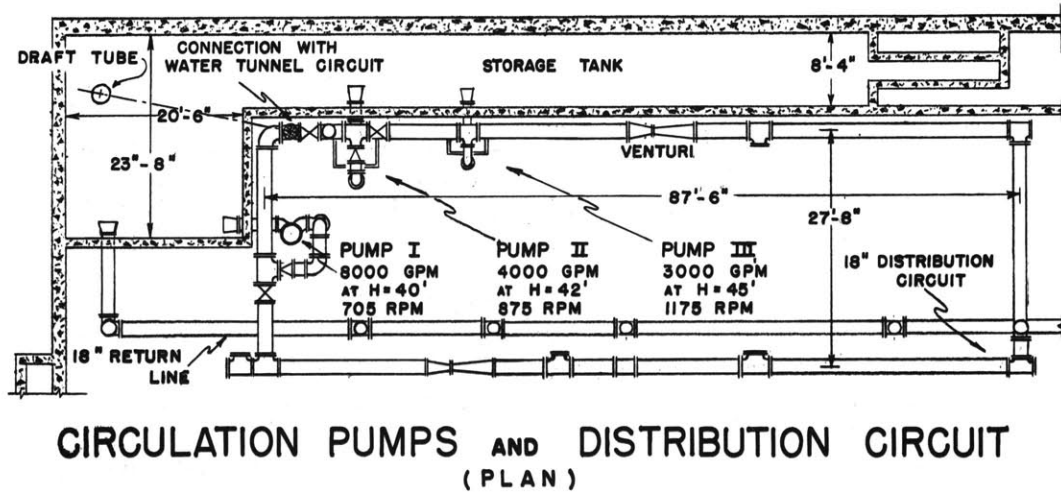
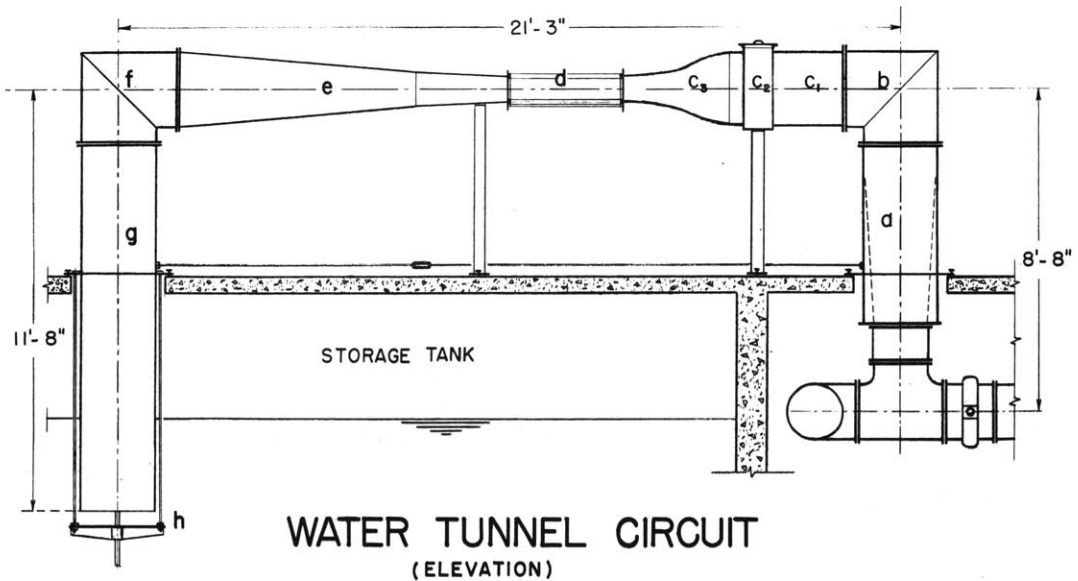
### III. EXPERIMENTAL EQUIPMENT AND PROCEDURES

#### A. General Description of Water Tunnel

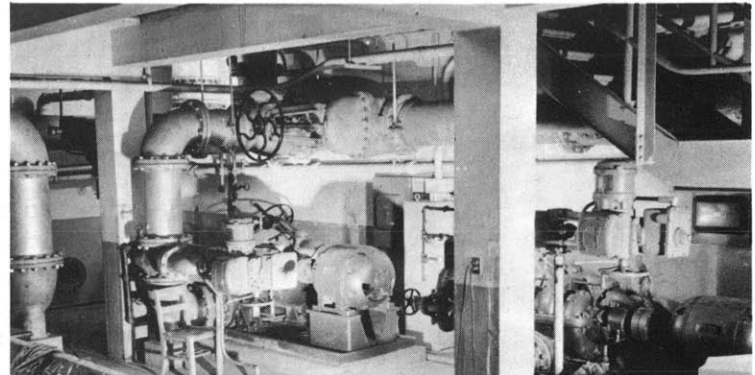
A detailed study of the wake behind flat plates held at zero angle of attack as well as an investigation into the hydroelastic response of these structural shapes required that the plates be suspended in a uniform flow with a low turbulence level. To this end a water tunnel has been constructed which is indicated schematically in Figure 2. The facility is connected to an 18-inch diameter header pipe suspended in the basement of the laboratory. It may receive water from any or all of three centrifugal pumps which have rated capacities of 8,000; 4,000; and 3,000 gallons per minute, respectively, at heads of approximately 40 feet. The flow rates may be regulated by motor operated valves located on the discharge side of the pumps. All pumps draw water from a common reservoir in the basement.

The water tunnel itself is connected to the header pipe and consists of a series of elements designed to produce a flow of desired character in the test section. Proceeding downstream from the junction with the header pipe and referring to the lettered items of Figure 2 there are:

1. An expanding riser which brings the water from the 18-inch header up to a 24-inch diameter at a suitable elevation above the main floor of the laboratory hall.
2. A 24-inch mitered elbow fabricated from 24-inch pipe and including 15 guide vanes situated in the mitered plane.
  - . A composite transition, screen housing and contraction with over-all length of 6'2". This item includes:
    - a. a 24-inch long transition from the 24-inch round elbow section to an octagonal one of slightly larger area,
    - b. a screen assembly housing,
    - c. a 33-inch long contraction composed of 8 pieces of thin steel plate dressed to carefully shaped ribs. This unit provides a transition from the octagonal screen section to the filleted rectangular test section,



Pump I



Pump II and III

Figure 2. Water Tunnel, Pressure Circuit and Circulation Pumps

4. A 36-inch long test section of essentially rectangular shape, 9 inches high and 7-1/2 inches wide. This unit is fabricated from 1 inch thick plexiglass reinforced by external aluminum members.

5. A 9-foot long diffuser fabricated from steel plate and divided into four equal flow channels by two continuous orthogonal splitter vanes. By means of this unit the 7-1/2 inch x 9 inch test section is brought back to a circular section of 24-inch diameter.

6. A second mitered elbow similar to the bend mentioned under b.

7. A 10-foot long draft tube of circular cross-section 24 inches in diameter. The downstream end of this unit is below the free surface in the water storage tank.

8. A plate valve for regulation of pressure level within the tunnel.

A more detailed description of the structural features of the facility may be found in Reference 66 while the measured hydraulic characteristics of the tunnel are presented in Appendix A of this report.

An overall view of the tunnel and its associated equipment is given in Figure 3 and a closeup of the test section in Figure 4.

## B. Test Plate Assembly

### 1. Selected Test Plates

A total of ten flat plates have been tested in the test section of the water tunnel for their vibrational behavior. The plates spanned the 9" dimension of the test section. Each of the plates had a length in the direction of flow of 2" and was given a leading edge of semi-cylindrical shape. Two plate thicknesses were tested: a set of six 1/8"-thick plates and a set of four 1/4"-thick test plates. The trailing edge configuration was varied from test to test; the motivation for the selection of the employed shapes, depicted in Figure 5, will become apparent later. All plates were fabricated of aluminum which combines a low weight with adequate strength and rigidity.

Tests on the 1/8" plates were conducted first. The results of these measurements dictated changes in the mounting of the plates as well as in the instrumentation. The second series of experiments utilizing 1/4" plates was carried out under different mechanical restraints using different instrumentation. These two tests are consequently discussed separately below.

### 2. Mounting of the Test Plates

The usual mounting of the test plates provided for a pivoting motion around the center of the semi-cylindrical leading edge. This method of mounting was motivated by the desire to prevent lateral motion of the



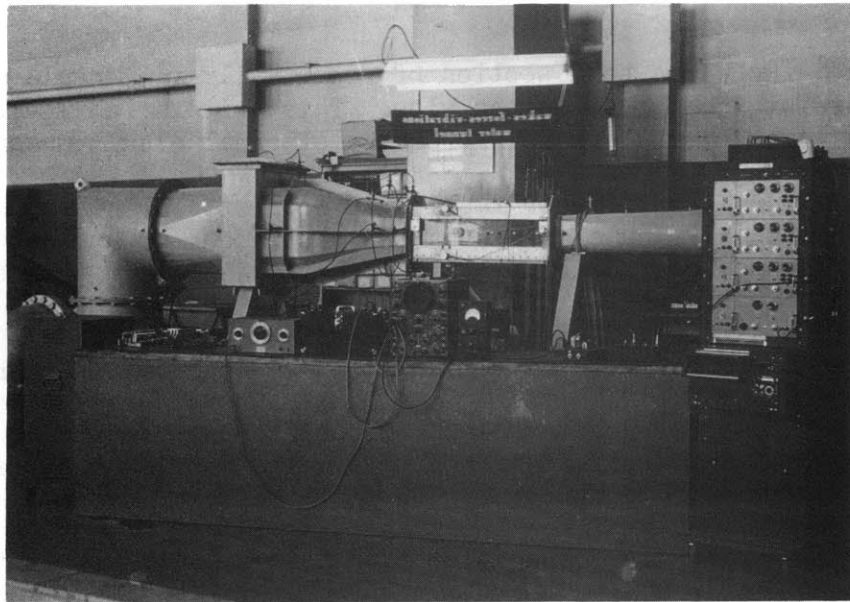


Figure 3. Overall View of Water Tunnel and Instrumentation

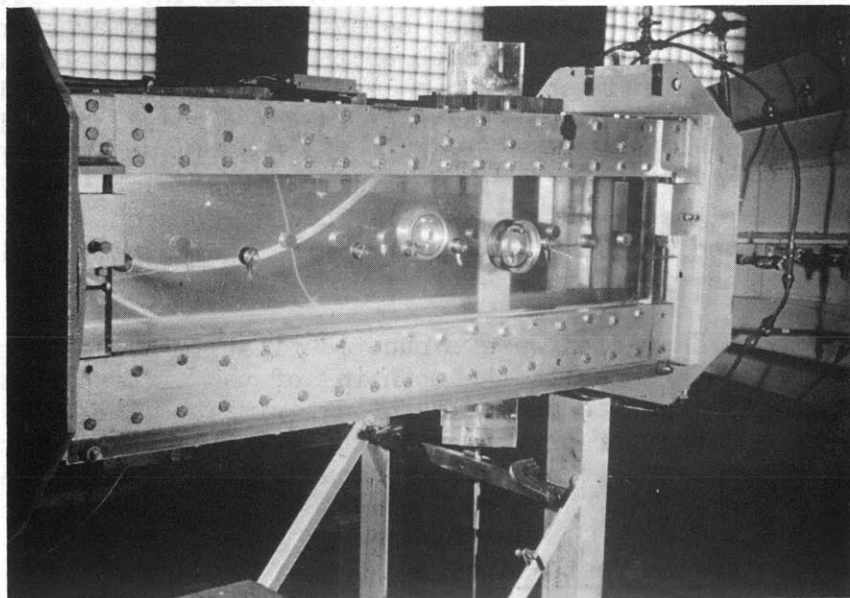


Figure 4. Test Section With Mounted 1/4"-Test Plate

leading edge, so that no vortices or even boundary layer disturbances would be created at that location. The rotational motion was restrained by springs as illustrated in Figures 5 and 6, thus making the test plate assembly a simple single degree of freedom system. Aside from simplifications in the analysis this mounting greatly reduced the danger of classical flutter of the plates.

All test plates were mounted vertically in the test section in order to eliminate the effect of gravitational forces on the plate motion.

The  $1/8$ " test plates were supported at each end by an  $0.27$ " diameter aluminum spindle passing through a pair of self-aligning ball bearings. Outside of the bearings the upper spindle was restrained by a leaf spring which carried strain gages for measurement of the frequency and amplitude of the vibrational plate motion.

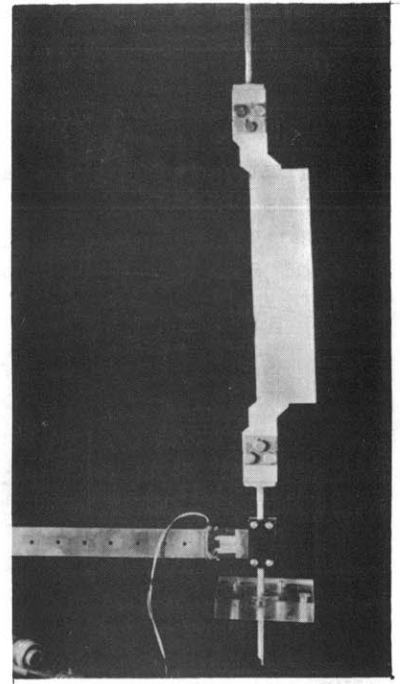
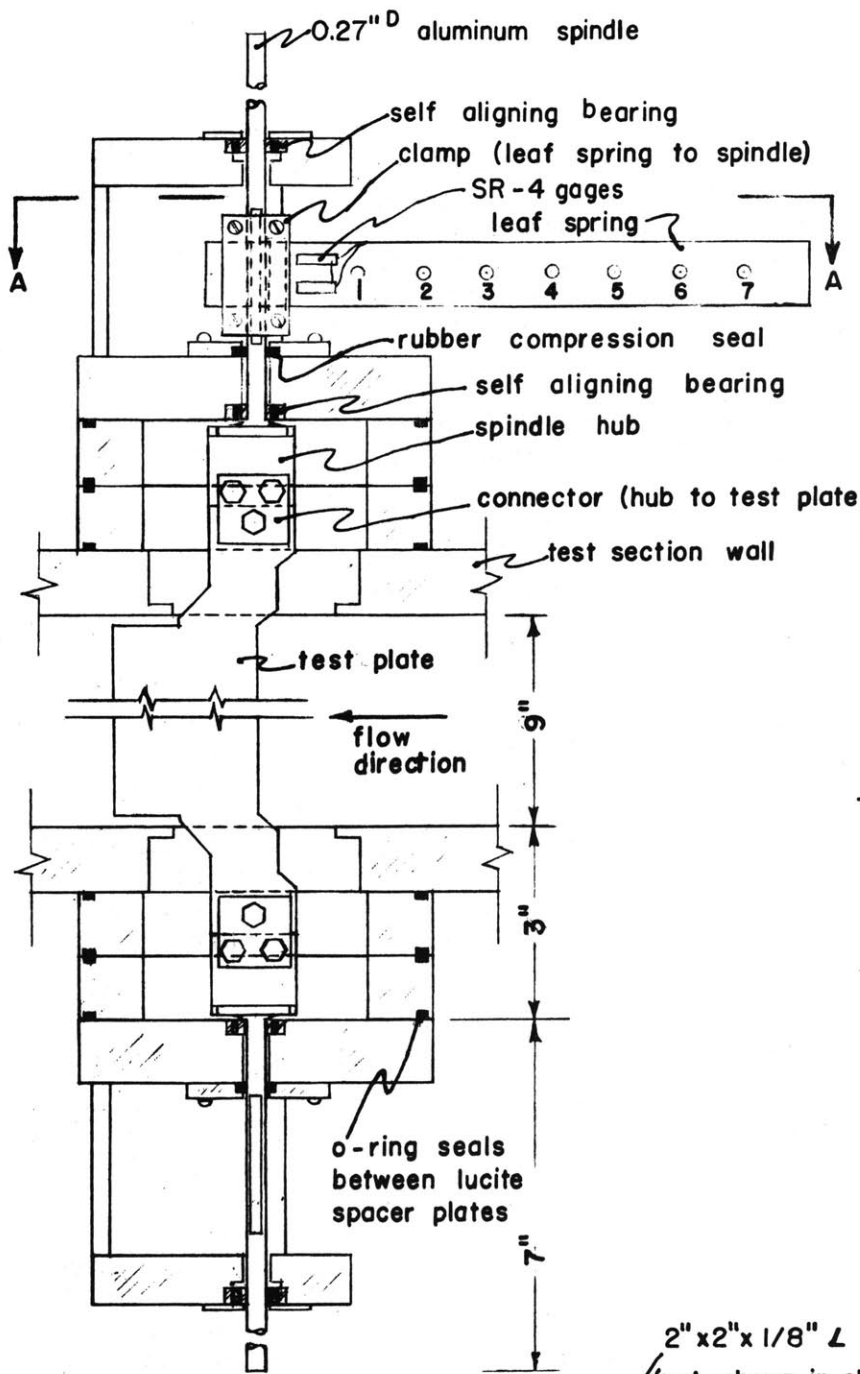
For the  $1/4$ " plates the upper spindle was replaced by a short aluminum stub and the lower spindle by a step-tapered stainless steel rod. Onto the rod a small arm was mounted which carried a crystal type accelerometer with which the motion was sensed. Small streamlined plates were also added which covered the ends of the trailing edge in order to prevent end effects. In addition the connection between plate and spindles allowed for selection of the axis of rotation at  $0.5$ " downstream of the leading edge. In the following this mounting will be referred to as "pivot at  $1/4$ -chord".

### 3. Spring Constants and Viscous Damping

One of the program objectives was to investigate the explicit role of support stiffness on the vibrational response of the plates. For the  $1/8$ " plates provision was made to vary the support stiffness by changing the free length of the restraining leaf spring. For the systematic series of measurements, discussed in section V, only one stiffness was employed. For all those measurements the clamp with which the leaf spring was fixed at the steady end was kept in position #5 (see Figure 5), resulting in a natural frequency for the entire test plate system of  $f_n = 40$  cps when suspended in air. For suspension of the test plate in water this was reduced to  $f_n = 25$  cps due to the apparent mass.

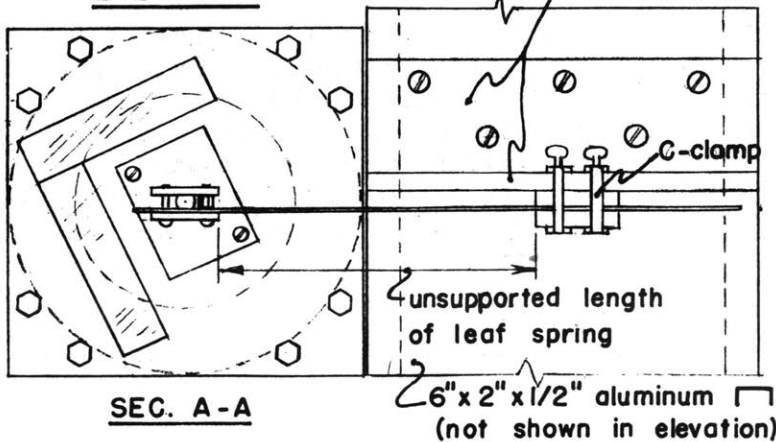
Based on the experimental results from the first test series the lower spindle which acted as a torsion spring for the  $1/4$ " plates was designed to permit variation of the system natural frequency from  $f_n = 40$  cps to  $f_n = 100$  cps. This variation could be effected by rigidly clamping the lower spindle at various positions along its length (see Figure 6). The modified support also intended to realize as far as was practically possible a one degree of freedom system. Test results show that this objective has largely been attained.

The calculated or measured values for  $f_n$ , the stiffness,  $k$ , and the damping coefficient,  $c$ , are given as a function of clamp position in Figure 17.



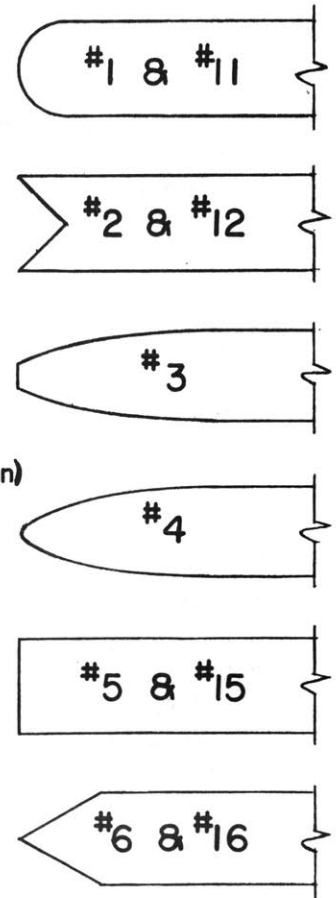
TEST PLATE & LEAF SPRING

ELEVATION



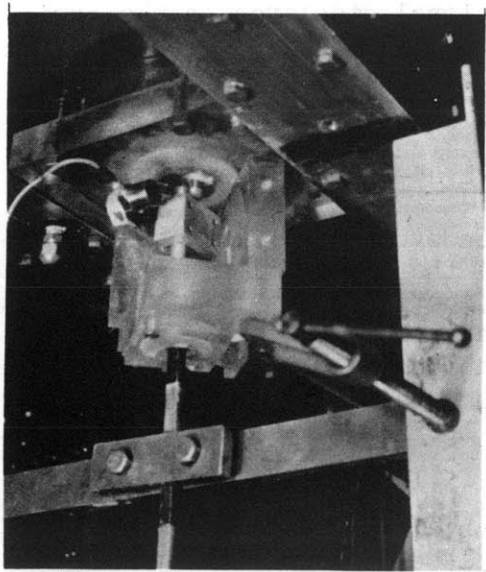
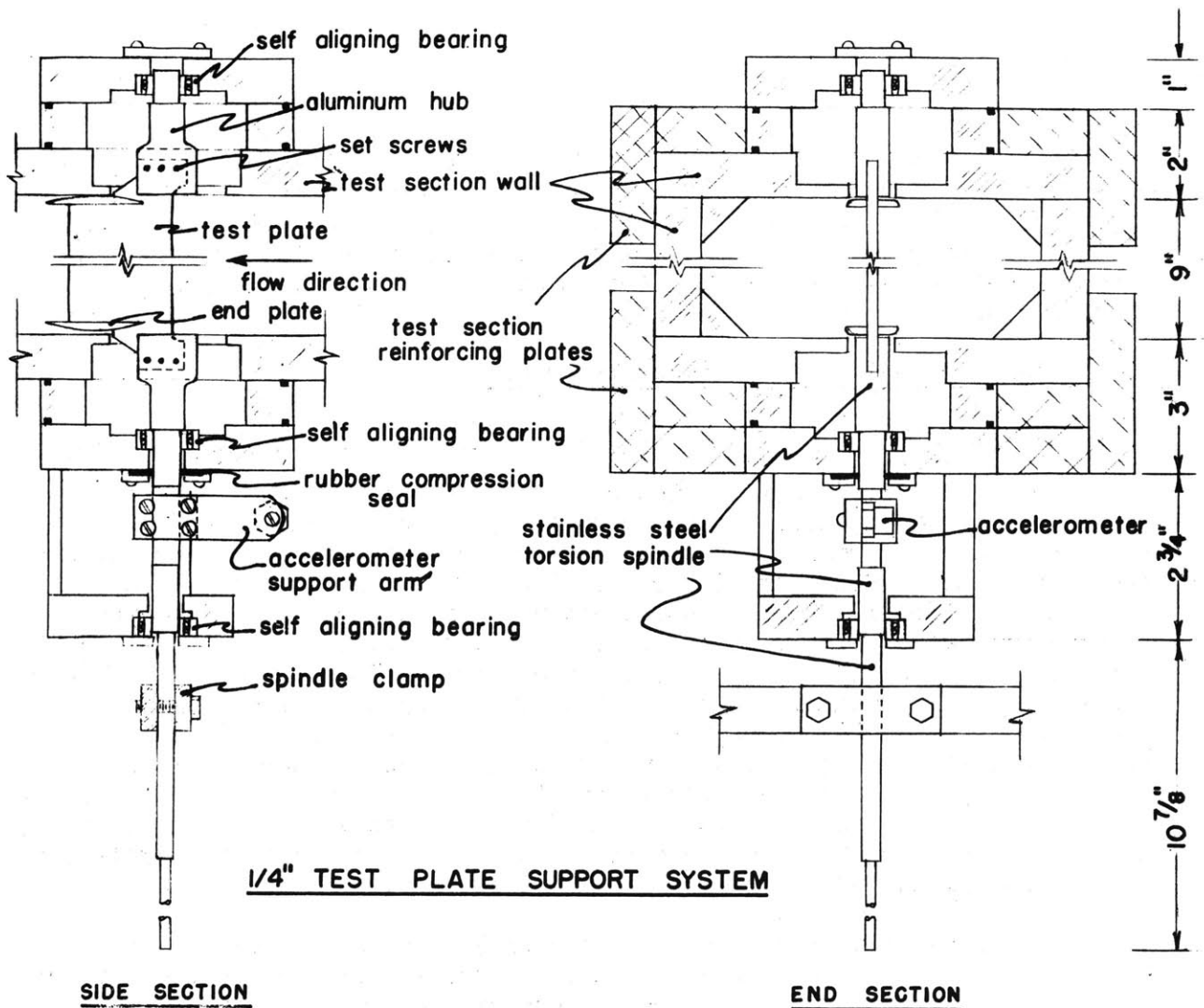
SEC. A-A

1/8" TEST PLATE SUPPORT SYSTEM

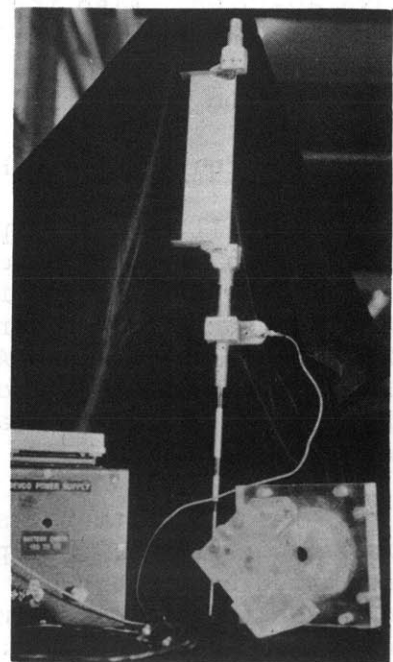


TRAILING EDGE GEOMETRIES

Figure 5. Test Plate Assembly for 1/8"-Plates



**View of Mounted Accelerometer**



**Test Plate and Torsion Spindle**

**Figure 6. Test Plate Assembly for 1/4"-Plates**

For the lower values of  $k$ , the damping for the plate-spring system with plate #11 suspended in water was found by determining the logarithmic decrement,  $\delta$ , of recorded damped free vibrations. The ratio of damping to critical damping was found to average  $c/c_c = 0.05$  which is low. It was assumed that the values for the other test plates would be of the same order of magnitude.

### C. Electronic Equipment and Data Procurement

#### 1. Equipment and Procedures for the 1/8"-thick Plates

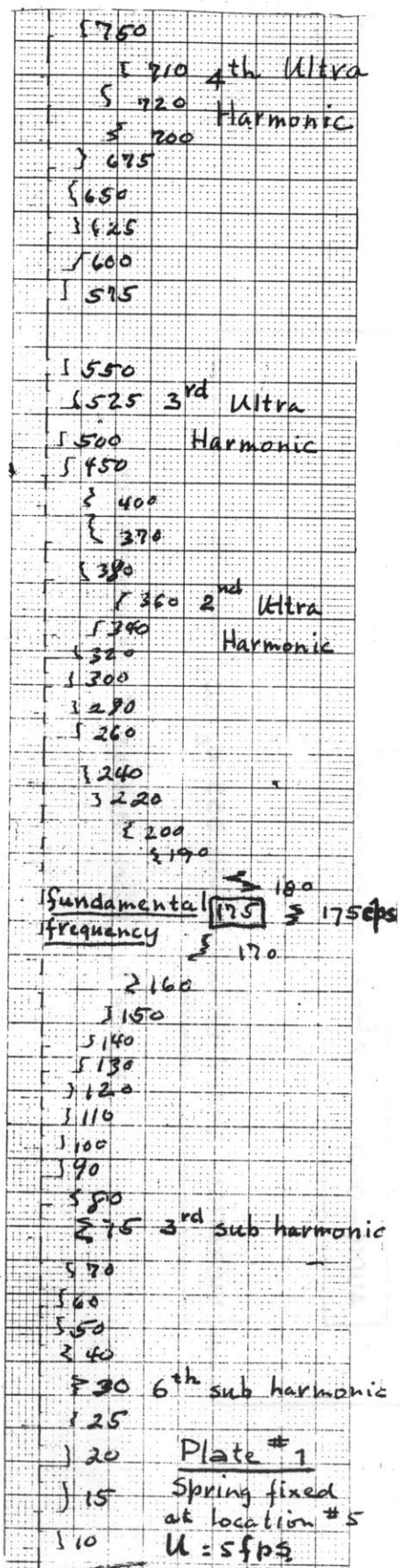
The bronze leaf spring which restrained the 1/8" plates carried 4 straingages located close to the spindle. The excitation voltage was 22.5 Volts and the wiring such that the temperature effects were eliminated. Via a Ballantine Decade Amplifier the straingage signal was led to a General Radio Model 762-B Vibration Analyzer or, alternately, onto the horizontal plates of an oscilloscope. The wave analyzer output (i.e., the RMS vibrational amplitude at a given frequency) was displayed on a Sanborn 150 oscillograph. At each value of the free stream test section velocity the entire spectrum of the transducer signal was scanned. After location of the amplitude peaks a Sanborn record was taken at those and surrounding frequencies. A sample of a representative spectrum is reproduced in Figure 7. The records are to be interpreted by means of the curves given in Appendix B which are based on a systematic calibration of the Wave Analyzer employing an incoming signal of known strength and frequency.

The transducer signal led to the oscilloscope was modulated by impressing the output of a Hewlett-Packard audio-oscillator on the vertical oscilloscope plates. Often a more or less stable Lissajous figure could be formed which facilitated and checked the frequency determinations from the wave analyzer. Also the amplitude of the signal displayed on the oscilloscope screen was measured. From these readings the total strength of the incoming signal could be converted to a representative angle of rotation by means of the calibration graph of Figure 2, Appendix B.

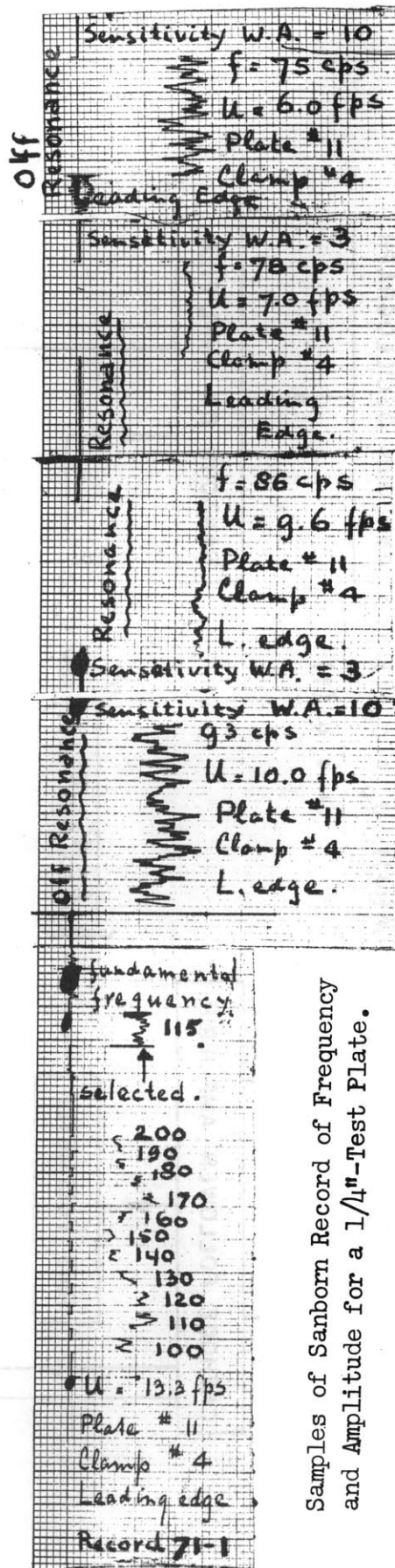
#### 2. Equipment and Procedures for the 1/4"-thick Plates

A small crystal-type accelerometer (Endevco Model 2200) weighing 1.1 oz. was mounted between the bearings of the lower spindle on an arm at 1-11/16" from the axis of rotation. Amplification for this high impedance piezo-electric transducer was provided by a cathode follower, the Endevco Model 2607 Subminiature Amplifier. The transducer output was subsequently led into a Ballantine Model 643 root-mean-square voltmeter, a General Radio Model 762-B Vibration Analyzer or onto the horizontal plates of an oscilloscope.

The RMS voltmeter scale was read to obtain the average strength of the transducer signal. Except for vibrations close to resonance the signal exhibited continuous and sometimes large fluctuations. To facilitate readings and also to obtain a permanent record, this averaged but yet fluctuating signal was recorded by the Sanborn recorder. With the wave analyzer the



Sample of Sanborn Record of Amplitude Spectrum for an 1/8"-Test Plate



Samples of Sanborn Record of Frequency and Amplitude for a 1/4"-Test Plate.

Figure 7. Sample of Wave Analyzer Records

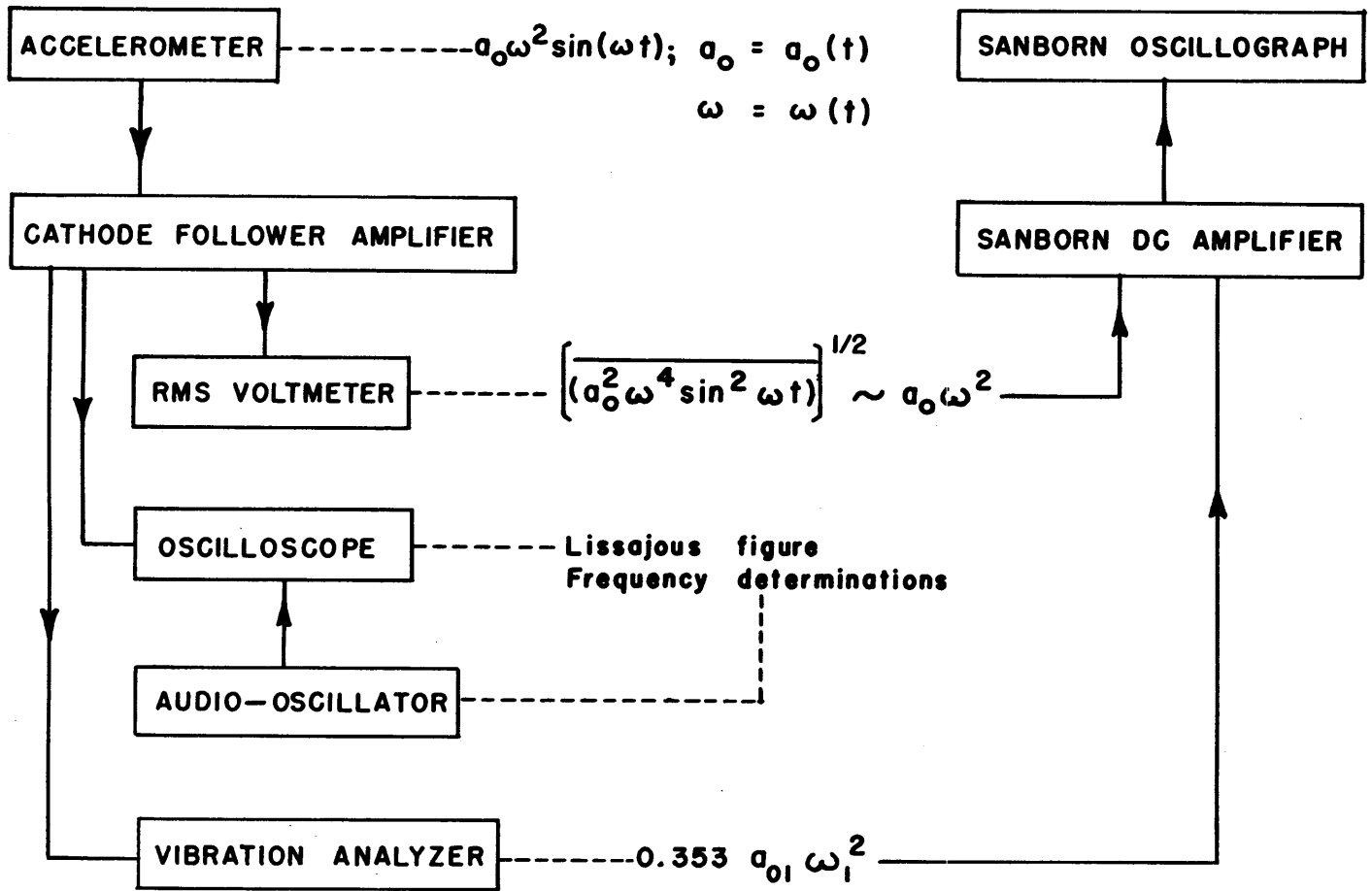


Figure 8. Block Diagram of Instrumentation



transducer signal was scanned for particular predominant frequencies. The frequency components and if need be the whole spectrum of the transducer signal, were amplified by a Sanborn D.C. amplifier and recorded by the Sanborn oscillograph. A block diagram of the equipment employed is shown in Figure 8.

The audio-oscillator was again employed to assist in the frequency determination of the accelerometer signal. This signal was modulated until a more or less stable Lissajous figure was formed on the oscilloscope screen. The figure would tell at a glance whether the motion was harmonic, whether one or more harmonic components were present or whether the frequency was unstable and wandered over a certain range. The latter case usually occurred for excitation of the test plates at frequencies well removed from the natural frequency provided for in the system.

The accelerometer has been calibrated on a precision shaker. The result is presented in Appendix B, Figure 2 and shows that the RMS value of the output of accelerometer plus cathode follower equals 111 mV/g. ( $g = 32.17 \text{ ft/sec}^2$ ).

#### IV. THEORETICAL CONSIDERATIONS

##### A. The Common Model of Vortex Induced Vibrations.

In this section will be presented the model for vortex induced vibrations as it is usually found or implied in discussions of this vibration phenomenon.

##### 1. Theoretical Determination of Periodic Lift Forces.

##### a. The Analysis of von Karman

The usual model of vortex induced vibrations is illustrated in Figure 9a, b, and c. For  $R > 50$  the separating boundary layers behind a test plate roll up periodically to form vortices. This happens alternately on either side resulting in a trail of staggered patches of vorticity which move with a velocity  $u_v$  with respect to  $U$ .

Von Karman (51), (52) has determined a complex potential,  $W$ , descriptive of such a trail or "vortex street":

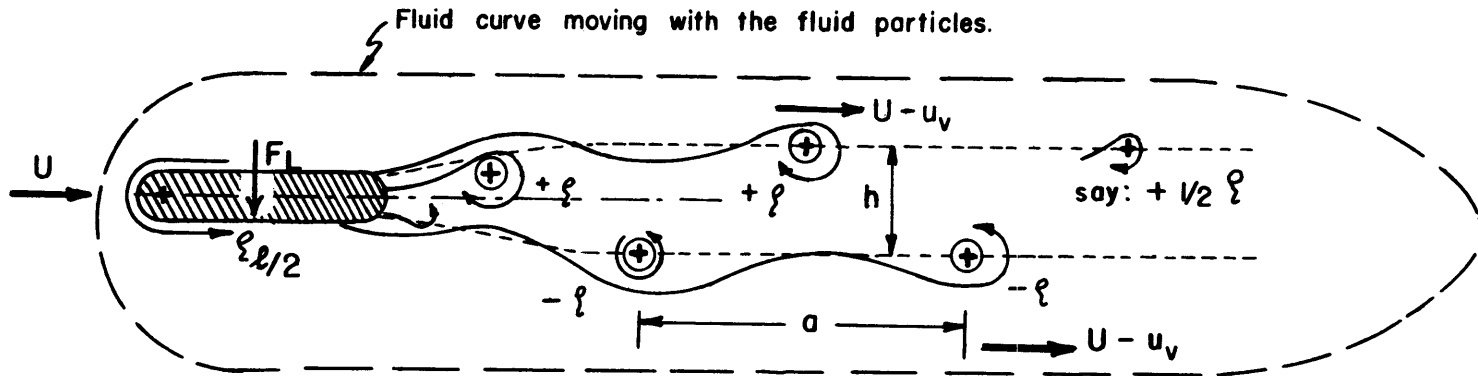
$$W = \frac{i\mathcal{S}}{2\pi} \left[ \log \sin \frac{\pi}{a} \left( z - \frac{ih}{2} \right) - \log \sin \frac{\pi}{a} \left( z - \frac{a}{2} + \frac{ih}{2} \right) \right] \quad [1]$$

in which

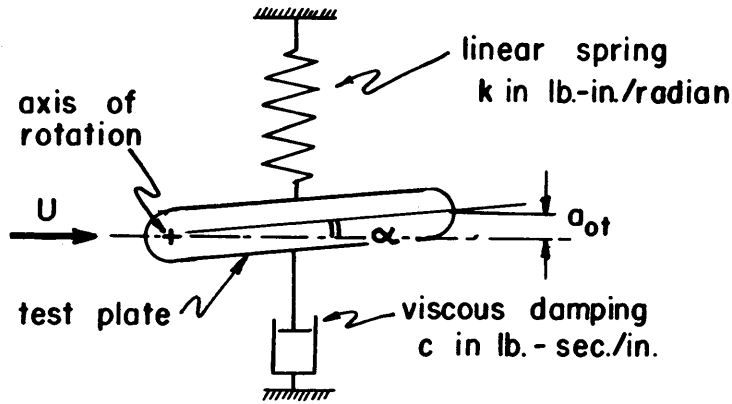
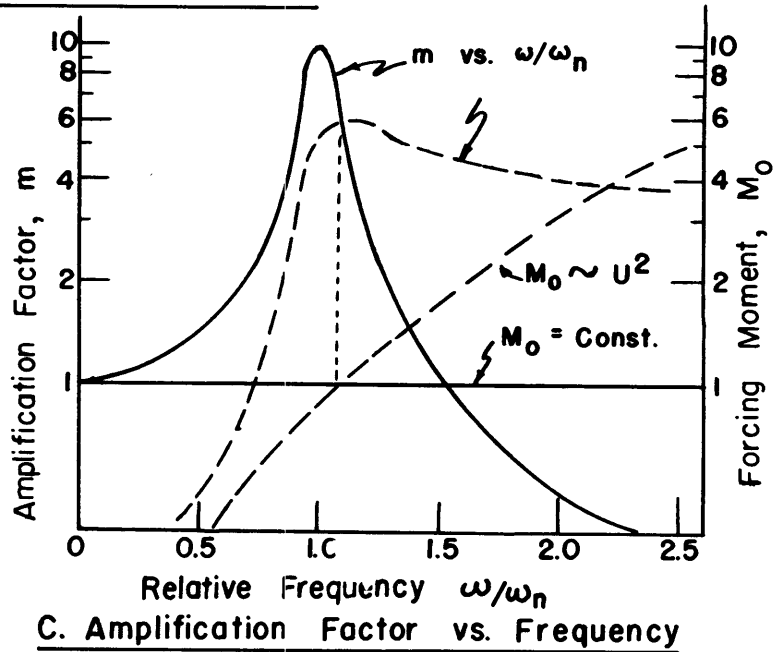
$a$	=	longitudinal vortex spacing
$h$	=	transverse vortex spacing
$\mathcal{S}$	=	strength of each vortex.

Differentiation of Eq. [1] with regard to  $z$  and separation of the obtained complex velocity into real and imaginary parts leads to:





**A. Characteristics of the Vortex Street**



**b. Scheme of Test Plate - Spindle System**

**C. Amplification Factor vs. Frequency**

Figure 9. The Common Model of Vortex Induced Vibrations

$$u_v = \frac{\mathcal{G}}{2a} \tanh \frac{\pi h}{a} \quad [2]$$

Von Karman also showed that, except for:

$$h/a = \pi^{-1} \cosh^{-1} \frac{\mathcal{G}}{\sqrt{2}} = 0.281 \quad [3]$$

the equilibrium of the vortex array was unstable to the first order. In the application of von Karman's analysis this "stable spacing ratio" is usually accepted as being required by the dynamics of the wake.

b. The Prediction of Vortex Strength and Frequency of Shedding.

The problem of relating von Karman's vortex street to structural vibrations is concerned with the determination of the strength of the individual vortices,  $\mathcal{G}$ , as well as the (dimensionless) frequency of vortex shedding,  $S = ft'/U$ , for a particular structure; this involves the prediction of:

$$\mathcal{G}(U, t'); \quad h(U, t'); \quad a(U, t') \quad \text{and} \quad S(U, t'),$$

in which  $f$  = frequency of vortex shedding  
 $t'$  = a characteristic dimension of the body creating the wake  
 (in the present study  $t' =$  test plate thickness)  
 $U$  = free stream velocity.

Along the lines indicated in section II an estimate for the vorticity may be obtained from boundary layer considerations. Accepting the value of  $K/U^2 = \lambda = 0.4$ , mentioned in II-B-2, one finds:

$$\mathcal{G} = \frac{aK}{U - u_v} = \frac{0.4 aU}{(1 - u_v/U)} \quad [4]$$

Eliminating  $\mathcal{G}$  by means of Eq. [2] and acceptance of the stable spacing ratio  $h/a = 0.281$  leads to:

$$\frac{u_v}{U} \left(1 - \frac{u_v}{U}\right) = 0.2 \tanh \pi \left(\frac{h}{a}\right) = 0.14$$

from which:

$$\frac{u_v}{U} = 0.17 \quad [5]$$

so that:

$$\mathcal{G} = 0.48 aU \quad [6]$$

Von Karman (52) also gave the relation between the wake vorticity and the form drag, D:

$$D = \rho \frac{h}{a} (U - 2u_v) + \rho \frac{\mathcal{S}^2}{\pi 2a} \quad [7]$$

Using Eqs.[3],[5] and[6]this reduces to:

$$D = 0.128 \rho a U^2$$

so that the drag coefficient,  $C_D$ , is equal to:

$$C_D = 0.26 a/t'$$

from which  $a = 3.8 t' \cdot C_D$  [8]

Employing once more the ratio  $h/a = 0.281$ , there follows:

$$h = 1.1 t' \cdot C_D \quad [9]$$

The dimensionless frequency of vortex shedding may be estimated by means of Eqs. [5] and [8]:

$$S = \frac{f \cdot t'}{U} = \left(1 - \frac{u_v}{U}\right) t'/a = \frac{0.22}{C_D} \quad [10]$$

Finally for a number of shapes the drag coefficient can be estimated by free stream line theory along the lines discussed in II-B-2. Thus an entirely theoretical estimate of relevant quantities is obtained.

In general, however, it will be easier to estimate  $C_D$  with the aid of the large number of such data available in the literature. Conversely a direct measurement of  $S$  is indicative of the drag coefficient.

### c. Magnitude and Frequency of Periodic Lift Forces.

The usual manner of relating the vortex strength,  $\mathcal{S}$ , to a lift force utilizes Kelvin's circulation theorem which states the circulation around a fluid curve is constant. Referring to Figure 9a it is seen that the circulation around a test plate,  $\mathcal{S}_1$ , would vary between:  $-\mathcal{S}/2$  and  $+\mathcal{S}/2$ .

Employing the Kutta-Joukowski relation, the lift force per unit length is then estimated to vary between:

$$F_{L_o} = -\rho U \mathcal{S} / 2 \quad \text{and} \quad F_{L_o} = +\rho U \mathcal{S} / 2$$

Commonly the lift force is assumed to vary harmonically so that:

$$F_L = 1/2 \rho U \mathcal{L} e^{i\omega t} \quad [11a]$$

in which  $\omega$  = circular frequency =  $2\pi f$ , or also using Eqs. [4] and [10]:

$$F_L = \frac{0.4t'}{S} \rho \frac{U^2}{2} \cdot e^{i\omega t} = F_{L_0} e^{i\omega t} \quad [11b]$$

in which  $\omega$  is the circular frequency of vortex shedding related to the (supposedly constant) Strouhal number by:

$$\omega = 2\pi SU/t' \quad [12]$$

## 2. Structural Response to a Periodic Lift Force.

### a. Usual Equation of Motion for the Test Plates.

The test plate-torsion spindle combination, indicated schematically in Figure 9b, can be regarded as a simple, single degree of freedom system. The usual equation of motion is:

$$I\ddot{\alpha} + c\dot{\alpha} + k\alpha = l_r \cdot 1/2 \rho U \mathcal{L} e^{i\omega t} = M_{V_0} e^{i\omega t} \quad [13]$$

in which:

- $I$  =  $I_{total} + I'$ ;
- $I_{total}$  = polar mass moment of inertia around the axis of rotation of test plate, spindles and attached masses,
- $I'$  = apparent mass moment of inertia,
- $c$  = coefficient of viscous damping,
- $k$  = spring constant,
- $M_{V_0}$  =  $l_r \cdot F_L$ ,
- $l_r$  = distance of the line of action of  $F_L$  to the axis of rotation of the test plate,
- $\alpha$  = instantaneous angle of attack.

The numerical values for  $I$ ,  $c$  and  $k$  are discussed in II-B and Appendix C. It was found that  $c \approx 0.05 c_c$  [ $c_c$  = critical damping =  $2(kI)^{1/2} = 2I\omega_n$ ]. The linear differential equation [13] expresses the fact that at any instant the resultant of the mass moment, the damping moment, the spring moment and the forcing moment is equal to zero.

The steady state solution of [13] is of the form:

$$\alpha = \alpha_0(\omega) e^{i\omega t} \quad [14]$$

i.e., an harmonic motion of frequency  $\omega$  and maximum amplitude  $\alpha = \alpha_0$ .

At low frequencies the lift moment  $M_{V_0} e^{i\omega t}$  will counteract the spring moment, which then may be much larger than the inertial moment. For large  $\omega$ ,  $M_{V_0} e^{i\omega t}$  overcomes the inertial moment which then is larger than the spring moment. At some intermediate frequency the spring- and inertial moments will balance each other and the forcing moment merely counteracts the damping moment. The frequency,  $\omega_r$ , at which this occurs, is the "resonant frequency". Since  $c$  was found to be small  $\omega_r \approx \omega_n$ , where  $\omega_n$  is the undamped frequency of the test plate system. It is readily shown that:

$$\omega_n = (k/I)^{1/2} \quad [15]$$

and

$$c_c = 2I\omega_n \quad [16]$$

b. Resonant Amplitudes.

At resonance the work per cycle by the external moment,  $\pi M_{V_0} \alpha_0$ , equals the work per cycle dissipated in damping:  $\pi(\dot{\alpha})_{\max} c \alpha_0$ . Hence:

$$\pi M_{V_0} \alpha_0 = \pi c \omega \alpha_0^2 \quad [17]$$

so that at resonant conditions:

$$\alpha_0 = M_{V_0} / c \omega_n \quad [18]$$

It is seen at once that for small damping, which obtains in the present case, resonant amplitudes of appreciable magnitude may occur.

c. Vibrational Amplitude as Function of Frequency.

In connection with the following discussions it is useful to further investigate the amplitude of the vibration [14] as a function of  $\omega$ . After disappearance of the transient part, the solution of [13] may be written as:

$$\alpha = \alpha_0 e^{i\omega t} = \frac{M_{V_0} e^{i\omega t}}{[(c\omega)^2 + (k - I\omega^2)^2]^{1/2}} \quad [19]$$

Making use of Eqs. [15] and [16] there follows:

$$\frac{\alpha_o}{M_{V_o}/k} = \frac{1}{\left[ \left(1 - \frac{\omega^2}{\omega_n^2}\right)^2 + \left(2 \frac{c}{c_c} \cdot \frac{\omega}{\omega_n}\right)^2 \right]^{1/2}} = m \quad [20]$$

Since  $M_{V_o}/k$  equals the static rotation of the test plate under the action of the (constant) moment  $M_{V_o}$ , the amplification factor,  $m$ , indicates how much, at a given frequency  $\omega$ , the static deflection is being amplified. In Figure 9c the factor  $m$  for the case  $c/c_c = 0.05$ , has been indicated by a solid line. It is seen that for  $\omega = \omega_n$ , the static rotation is magnified by a factor 10.

### 3. The Common Model of Vortex Induced Vibrations.

The accepted model of vortex induced vibrations states that such vibrations are brought about when the frequency of the forcing moment, given by Eq. [12], coincides with the natural frequency of the structure; i.e.:

$$\omega = 2\pi S U/t' = \omega_n \quad [21]$$

It is to be noted that the foregoing considerations are based on the concept that vortex induced vibrations are forced vibrations for which the frequency is a linear function of the free stream velocity. Also von Karman's mathematical model of the vortex street is made the basis of all quantitative evaluations. For this reason the vibrations are often referred to as "von Karman vortex vibrations".

### B. Shortcomings of the Notion of "von Karman Vortex Vibrations".

The foregoing exposition makes plausible the occurrence of "von Karman vortex vibrations". However, a number of the more important shortcomings and objections of the treatment will be pointed out below. The discussion is limited to the case of the employed test plates.

#### 1. Inadequate formulation of the Forcing Moment.

Many publications concerning vortex induced vibrations are accompanied by a sketch of an amplitude response curve as given by the solid line in Figure 9c. Such a presentation implies that the maximum forcing moment,  $M_{V_o}$ , would be constant. From the equations [11b], [12] and [13], however, follows:

$$M_v = (0.2 \rho l_r) \frac{U^3}{f} e^{i\omega t} \quad [22]$$

which shows that, even if the Strouhal number,  $S = ft'/U$ , remains constant, at least  $M_v \propto U^2$ . This fact, and its consequence for the amplitude of vibration, is illustrated in Figure 9c by dashed lines.

There is experimental evidence Refs. (20), (10) and (64) that the frequency of vibration and presumably the frequency of vortex shedding, may remain fairly constant over a range of velocities. This tends to broaden further the region of velocities (see Figure 9c) over which nearly resonant amplitudes of vibration may occur.

## 2. Neglect of the Trailing Edge Geometry.

As far as the theory of the von Karman vortex vibrations is concerned the geometry of the structure downstream of the separation points is of no consequence. In the discussion of section II-C, however, it was found that the trailing edge geometry constituted a most important variable. This shortcoming in the theoretical considerations is a direct consequence of relating von Karman's mathematical model for the periodic wake to an element of the theory of mechanical vibrations, without regard for the dynamics of the early wake.

An immediately related question is how the delicate dynamic equilibrium of the flow near the trailing edge may be influenced by vibrations of the structure. Particularly for flat plates a definite hydroelastic effect (i.e. modifications of the hydrodynamic loading due to the plate motion) is expected as a result of an increase in two-dimensionality of the wake. A direct dependence of this effect on trailing edge geometry is anticipated.

## 3. Disregard of the Relation between Wake Structure and Reynolds Number.

The theoretical discussion of the "von Karman vortex vibrations" based on the assumptions of an ideal fluid cannot reveal a dependence on the Reynolds number. Yet experiments show the existence of such a relation.

In the first place the Strouhal number which was tacitly assumed to be a constant, is a function of the Reynolds number. For a circular cylinder e.g. the Strouhal number varies as shown in Refs. (43), (27) and (38), from:

$$S = 0.11 \text{ at } R = 60 \quad \text{to} \quad S = 0.20 \text{ at } R = 10^3$$

and from:

$$S = 0.19 \text{ at } R = 10^5 \quad \text{to} \quad S = 0.35 \text{ at } R = 10^6$$

The last variation, which is more likely to fall in a Reynolds number of practical interest than the first one, can be explained by a rearward

shift of the separation points. If the Strouhal number were based on the new distance between the free shear layers,  $S$  would probably remain constant.

Secondly, there are the profound changes in wake structure that occur when  $R$  increases from low to high values; these changes were already indicated in Section II-B-1. In fact, for Reynolds numbers larger than  $R = 10^5$  to  $10^6$  all visual evidence of wake periodicity such as a vortex street is absent and only by statistical means is it possible to distinguish a predominant frequency component of the velocity fluctuations in the wake flow. It follows that in those cases a treatment of the vibration phenomena which employs relations following from the consideration of a vortex street (e.g. the use of the ratio  $h/a = 0.281$  as being necessitated by von Karman's stability argument) places an improper emphasis on the physical occurrence by directing attention to the asymptotic wake behavior rather than to the early wake. Larger  $R$ 's will bring three-dimensional conditions and an attendant phase shift of the lift force between locations along the trailing edge. This may result in a decrease in the magnitude of the net lift force.

The experimental findings of Roshko (28), McGregor (33), Macovski (45) a.o. indicate that even close behind a steady object an increase in  $R$  leads to three-dimensional conditions in the sense that the vortex formation at various points along the trailing edge may not be in phase. Rather than the increase in lift force with increasing  $U$  (and hence  $R$ ) according to Eq. [22], the net lift force may remain constant or even decrease. In any case instability of the net lift force may be anticipated with increasing  $R$ .

#### 4. The Occurrence of Instabilities in Vibrational Amplitude.

Results obtained by Price (7) and by Penzien (9) clearly indicate that the amplitude of vibration of a circular cylinder suspended in a fluid flow, exhibits marked instabilities. The sudden changes of the vibrational amplitude, shown in Price's sample record, are an indication that non-linear effects may be involved in the vibration phenomenon.

However, the equation of motion, Eq. [13], is a linear differential equation with constant coefficients. The resultant solution of Eq. [13] should therefore show the continuity characteristic of linear systems.

It follows that the noticed instabilities point to an unsatisfactory formulation of the basic equation of motion.

#### C. Test Plate Vibrations of Hydroelastic Origin.

A number of shortcomings in the usual formulation of von Karman vortex vibrations have been noted above. In this section a reformulation of the problem is sought by taking into consideration some hydroelastic characteristics of the vibration. After a formulation of these characteristics in section IV-C-1, a possible form of the equation of motion is derived (section IV-C-2) which, in order to simplify its discussion, is reduced



in section IV-C-3. In section IV-C-4, finally, the properties of the reduced equation of motion are discussed and the anticipated amplitude response curve indicated.

## 1. Hydroelastic Characteristics of the Test Plate Vibrations.

A priori the following hydroelastic effects (i.e. substantial changes in the hydrodynamic loading due to elastic deformations) may be anticipated:

### a. Apparent Mass Forces.

The fluid particles along a vibrating plate must be accelerated transversely causing a reaction force of considerable magnitude. This periodic force is the familiar apparent mass force. The theoretical determination of this force, discussed in Appendix C, shows that its magnitude is about twice as large as the inertia force for a 1/4" test plate.

### b. Periodic Lift Force due to Plate Vibration.

A periodic motion of the plates will result in a continuously varying angle of attack,  $\beta = \beta(\alpha, \omega, U)$ , which gives rise to a periodically changing circulatory flow around the plates and hence to a periodic lift force acting on the plates.

### c. Wake Structure along Trailing Edge.

With increasing Reynolds number the two-dimensional wake structure near the trailing edge will be replaced by a three-dimensional one. That at non-resonant conditions, there still obtains a periodic net lift force seems to point to a unifying action of the proximity of the trailing edge on the developing vortex filaments.

Conversely it is likely that fast transverse motions of the trailing edge influence the wake structure and even restore its two-dimensionality.

A vibration of the test plates may thus bring into play a greatly increased lift force (compared to the force acting in the steady object). This hydroelastic element could lead to self-excited plate vibrations.

## 2. Formulation of a Hydrodynamic Forcing Function.

The objective of the following attempt at a qualitative formulation of a reasonable forcing function is to make plausible the shape of the amplitude response curves determined for the test plates as well as the character of the investigated vibrations.

In formulating a hydrodynamic forcing function the assumption will be made that the circulatory flows associated with "vortex shedding" are practically confined to the boundary layer region. Above discussions then suggest regarding the flow and forces as a superposition of the elements

indicated in Table 1. A more detailed description of the lift forces associated with each of the flows of Table 1 is given below:

Flow	gives rise to:	due to:	estimate on the basis of:
a. Viscous Flow.	Circulatory boundary flow; lift force assumed to act near the trailing edge.	Pulsating discharge of boundary layer = "vortex shedding".	Assumptions.
b. Potential Flow.	Circulatory potential flow; lift force acting at 1/4-chord.	Necessity of satisfying the Kutta-condition.	Thin Airfoil Theory.
c. Potential Flow.	Transverse flow; apparent mass moment and lift force acting at 1/2-chord.	Transverse plate motions as result of pitching and translation of plate elements.	Thin Airfoil Theory.

Table 1. Assumptions regarding the Forcing Function.

a. Lift Forces due to Vortex Shedding.

In keeping with the above assumption the formation of vortex filaments will be accompanied by periodic increases in boundary layer discharge from either side of the plate. Since vortices mature the greater part of a half cycle and are swept away fairly suddenly at the end of that period, the second leading term in a Fourier series development of the periodic, symmetrical lift force per unit length of plate is anticipated to have a negative coefficient:

$$L' = \frac{U^2}{S} \sum_n B_n e^{in\omega t} = \frac{U^2}{S} \left[ B_1 e^{i\omega t} - B_2 e^{i3\omega t} + \dots \right] \quad [23]$$

in which:  $B_i$  = dimensional coefficients.

Since the mechanical spring-test plate system is a linear one the amplitude of motion is then expected to be given by:

$$\alpha = \sum_n A_n e^{i(n\omega t + \phi_n)} = A_1 e^{i(\omega t + \phi_1)} - A_3 e^{i(3\omega t + \phi_3)} + \dots [24]$$

A most important hydroelastic effect is that the two-dimensionality of the wake increases with amplitude. To take this into account Eq. [23] may be multiplied by a magnification factor M:

$$M = M(A_n^i, G, R_t, R_\delta)$$

in which G is a factor depending on trailing edge geometry,  $R_t = Ut'/v$  is related to the stability of the downstream wake and  $R_\delta$  is indicative of the boundary layer thickness at the trailing edge. It is considered that the role of R is secondary in the case of large amplitude vibrations. It is also assumed that a large G is associated with a trailing edge geometry which is suitable to enhance two-dimensionality of the wake. As a consequence of these assumptions the above relation may be written:

$$M/G = M(A_n^i).$$

It is sufficiently general to assume M to be a linear combination of  $(A_n^i)^n$ :

$$M/G = a_s/G + a_1 A_1^i + a_2 A_1^{i2} + a_3 A_1^{i3} + \dots [25]$$

so that the net lift force,  $L_v$ , becomes:

$$L_v^i = (U^2/S) \left[ G \sum_m a_m (A_1^i)^m \right] \left( \sum_n B_n e^{in\omega t} \right) [26]$$

The choice of the coefficient  $a_m$  in Eq. [25] depends on physical considerations. Even if the object is steady a net lift force will be present, so that  $a_s$  is a positive constant. When the motion develops a rapid increase in M may be expected. Ultimately, however, M must tend to a constant as the wake approaches nearly two-dimensional conditions. Such a trend is e.g. given by:

$$M/G = a_s/G + \tanh a_1 A_1^i = a_s/G + \tanh A_1$$

in which case Eq. [25] reduces to:

$$M/G = a_s/G + A_1 - \frac{1}{3} A_1^3 + \dots [27]$$

Employing Eqs. [23] and [27] to expand Eq. [26]:

$$L_V^i = (U^2/S) (a_s + GA_1 - \frac{1}{3} GA_1^3) B_1 e^{i\omega t} - (a_s + GA_1 - \frac{1}{3} GA_1^3) B_3 e^{i3\omega t} \quad [28]$$

Near resonance  $GA_1 \gg a_s$ . Further, for nearly harmonic motions the influence of  $a_s B_3 e^{i3\omega t}$  will be small relative to that of  $a_s B_1 e^{i\omega t}$ . Therefore the term  $a_s B_3 e^{i3\omega t}$  will be neglected.

To the same order of approximation as implied in Eq. [25],  $A_1$  is given by  $A_1 = \alpha e^{-i\omega t}$ , the phase angle  $\phi_1$  being irrelevant in this connection. Substitution in the foregoing equation then gives (per unit length of plate):

$$L_V^i = \left[ -GB_3 (e^{i2\omega t} - \frac{1}{3}\alpha^2) \alpha + (M) B_1 e^{i\omega t} \right] U^2/S \quad [29]$$

The point of application of this force is unknown, so that the moment around the leading edge can only be given by  $M_V = XbL_V^i$ .

#### b. Non-Circulatory Potential Flow

Forces and moments due to unsteady pitching of a two-dimensional thin flat plate about its leading edge have been calculated in the classical work of Theodorsen (67). These techniques still serve for flutter calculations and have been interpreted and summarized by Bisplinghoff et al. (70) among others.

It is first assumed that the flow along the plate is composed of a uniform portion  $(U, 0)$  and a perturbation  $(u', v')$  so that  $u' \ll U$  and  $v' \ll U$ .

Laplace's equation

$$\nabla^2 \phi' = 0$$

is then solved for the disturbance potential,  $\phi'$ , under the boundary condition

$$v^i = \frac{Dy_P}{Dt} = \frac{\partial y_P}{\partial t} + (U+u') \frac{\partial y_P}{\partial x} + v' \frac{\partial y_P}{\partial y} \approx \frac{\partial y_P}{\partial t} + U \frac{\partial y_P}{\partial x} \quad [30]$$

where  $y_p = 0$  and  $-b \leq x \leq b$ .

Referring to Fig. 10-a;

$$\frac{Dy_p}{Dt} = -U\alpha - (b+x)\dot{\alpha} \quad [31]$$

Theodorsen distributes sources and sinks along both sides of the line  $y = 0$ ,  $|x| \leq b$  to obtain  $\phi'$  in terms of  $v'$ . Since  $-p' = \rho\phi'$  in incompressible flow the pressure distribution and thus the lift force and moment may be obtained.

The oscillations of the plate about its leading edge can be resolved into an oscillating translation of its mass center and an oscillating rotation about that point. The apparent mass effect will then be in two terms:

A lift force applied at mid-chord:

$$L'_I = -\pi\rho b^3\ddot{\alpha}$$

and an apparent moment of inertia about the centroidal axis:

$$M'_I = 1.125 \pi\rho b^4\ddot{\alpha}$$

The total moment acting due to the non-circulatory potential flow is thus (per unit of length):

$$M'_{n.c.} = \pi\rho b^4 \left( 1.5 \frac{U}{b} \dot{\alpha} - 1.125 \ddot{\alpha} \right) \quad [32]$$

### c. Circulatory Potential Flow

In order to satisfy the Kutta-condition of finite velocities at the trailing edge Theodorsen superimposed a flow pattern consisting of vortices along the line of the plate coupled with counter vortices moving with the flow along the x-axis in the wake.

The Kutta-condition applied to a thin flat plate of chord  $2b$  in steady flow yields the familiar equation for lift per unit of length:

$$L_c = 2\pi\rho b U^2 \sin \alpha \quad [33]$$

in which  $U \sin \alpha$  may be called the "downwash",  $w$ .

For unsteady pitching about the leading edge Theodorsen obtains:

$$L'_c = 2\pi\rho b U w_{3/4} C(k)$$

and

$$M'_c = -\pi\rho b^2 U w_{3/4} C(k) \quad [34]$$

in which  $w_{3/4}$  is the "downwash" at the 3/4 chord point for the pitching plate and is given, for small  $\alpha$ , by:

$$w_{3/4} = U \alpha + 1.5 b \dot{\alpha} \quad [35]$$

For simple harmonic motions:

$$\alpha = A_1 e^{i\omega t}$$

$$C(k) = C\left(\frac{wb}{U}\right) = \text{Theodorsen Function}$$

$$= \frac{K_1(ik)}{K_0(ik) + K_1(ik)} \quad [36]$$

In the Theodorsen function  $K_0$  and  $K_1$  are modified Bessel functions and the reduced frequency,  $k$ , is related to the Strouhal number,  $S$ , by:

$$k = 2\pi S \quad [37]$$

for the 1/4" thick and 2 inch long plates used.

For the present range of interest;

$S$	$k$	$C(k)$
0.27	6.7	0.501 + 0.021 i
0.20	5.0	0.503 + 0.025 i
0.14	3.5	0.505 + 0.035 i

[38]

The moment due to the circulatory flow is thus:

$$M_c = -\pi \rho b^2 U^2 C(k) \left[ \alpha + \frac{3b}{2U} \dot{\alpha} \right] \quad [39]$$

Combining Eqs. [29], [32] and [39] the equation of motion per unit length of test plate becomes;

$$I_t \ddot{\alpha} + c \dot{\alpha} + k \alpha = M_v + M_c + M_{n.c.} = M \quad [40]$$

### 3. Formulation of the Reduced Equation of Motion

The shape of the amplitude response curves following from Eq. [40] is complicated by the fact that  $M' = M'(U, f)$ . In this section a reduced form of Eq. [40] is introduced which facilitates the discussion of the differential equation.

The equation of motion for the ( $H = 9''$ ) test plate-torsion spring system is given by:

$$I_t \ddot{\alpha} + c \dot{\alpha} + k\alpha = H M'_v + H M'_c + H M'_{n.c.} = H M' \quad [41]$$

The only term on the r.h.s. not dependent on  $U$  is due to the apparent mass force associated with the translation and pitching of plate elements:

$$I' = (H) 1.125 \pi \rho b^4 \ddot{\alpha};$$

$I'$  may be combined with the mass moment of inertia.

As long as the non-linearities introduced by the influence of the plate motion on the wake structure are not too pronounced, the amplitude of vibration should be approximately proportional to  $U^3/f \propto U^2/S$  (see Eq. [22]). Upon dividing the measured amplitudes of plate vibration by  $U^2/S$ , the expected amplitude response curves should resemble, in form, those of the system:

$$\begin{aligned} (I_t + I') \ddot{\alpha} + c \dot{\alpha} + k\alpha = & - H X b G B_3 (e^{i2\omega t} - \frac{1}{3} \alpha^2) \alpha \\ & + H X b B_1 (M) e^{i\omega t} - \pi \rho H b^2 S C(k) (\alpha + \frac{3}{2} \frac{b \dot{\alpha}}{U}) + \frac{3}{2} \pi \rho H \frac{b^3 S}{U} \dot{\alpha} \quad [42] \end{aligned}$$

which was obtained by dividing the moment,  $M'$ , of Eq. [41] by  $U^2/S$ .

By making use of the relation  $\frac{bS}{U} \dot{\alpha} = 25iS^2\alpha$  and selecting:

$S = 0.27$  so that according to Eq. [38]:

$$C(k) = F'(k) + G'(k) = 0.501 + 0.021 i$$

Eq. [42] reduces to:

$$\begin{aligned} & (I_t + I')\ddot{a} + (c - \frac{3}{2} \pi \rho H b^3 \frac{S}{U})\dot{a} + \left[ k + \frac{1}{2} \pi \rho H b^2 (S - 1.5 S^2) \right. \\ & \left. - \frac{1}{3} H X b G B_3 \alpha^2 + H X b G B_3 e^{i2\omega t} \right] \alpha = H X b B_1(M) e^{i\omega t} \quad [43] \end{aligned}$$

Equation [43] now is an equation of motion for a one-degree-of-freedom system with non-linear restoring spring and slowly varying damping. This equation will be called a "reduced equation of motion" since the explicit role of the free stream velocity has been eliminated.

However, the terms in the coefficients of  $\ddot{a}$ ,  $\dot{a}$  and  $\alpha$  can no longer be contracted numerically. Therefore the conclusions from Eq. [43] will be qualitative only and the equation is best written:

$$\begin{aligned} & I\ddot{a} + (c - m_1 \frac{S}{U})\dot{a} + (k + m_2 S - 1.5 m_2 S^2 - m_3 \alpha^2 \\ & + m_4 \cos 2\omega t)\alpha = m_5 (M) \cos \omega t \quad [44] \end{aligned}$$

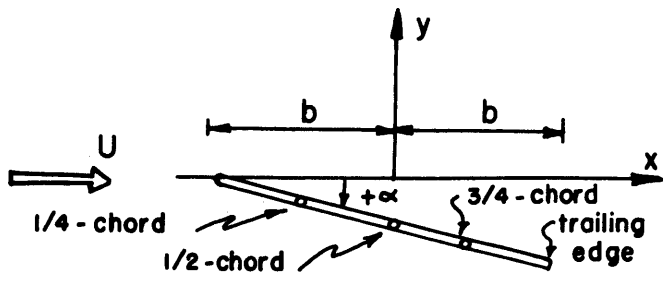
It is seen that for the reduced equation the hydrodynamic damping increases with the velocity  $U$ . A decrease in  $S$ , mentioned in Section IV-B-1, which may occur when  $\omega_p \simeq \omega_n$  will have a similar effect. In addition the decrease of  $S$  is equivalent to a decrease in the effective spring stiffness which shows algebraically how the deviation of the frequency of vortex formation from its "steady object" value leads to a non-linear effect. Even if  $S$  were constant (as has been assumed in most previous discussions) non-linear effects, discussed in the next section, will be present.

#### 4. The Reduced Amplitude Response Curves.

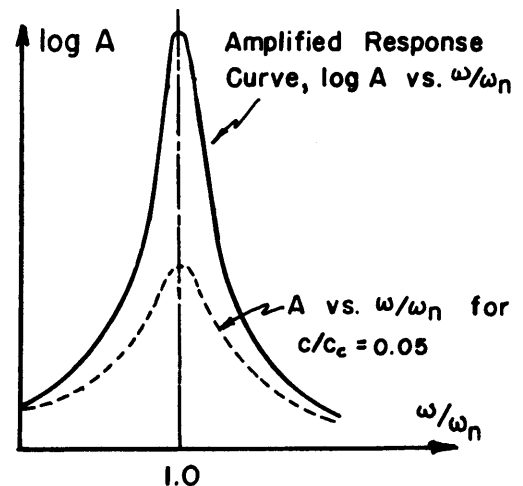
There does not seem to be an established theory by which an equation of the type of Eq. [44] may be solved. Without the presence of the term  $m_3 \alpha^2$  the equation would still be linear and could be identified as a "Mathieu's equation". The theory of this function has been treated in detail. The form of the solution depends on the values of  $(k - m_2 S)/I$  and  $m_4/I$  as has been indicated in Figure 10c. In the case of a "stable" solution the vibration may be nearly harmonic except for the continuously varying amplitude of vibration (case A - Figure 10c). In the unstable case the amplitude grows until non-linear effects in the system limit or even diminish it. Probably the process then starts anew (case B).

If the term  $m_4 \cos 2\omega t$  were absent, but  $m_3 \alpha^2$  present the now non-linear Equation [44] can be identified as "Duffing's equation". Methods to obtain approximate solutions are treated elsewhere, (68). The resulting amplitude response curve can be thought of as formed by bending over to

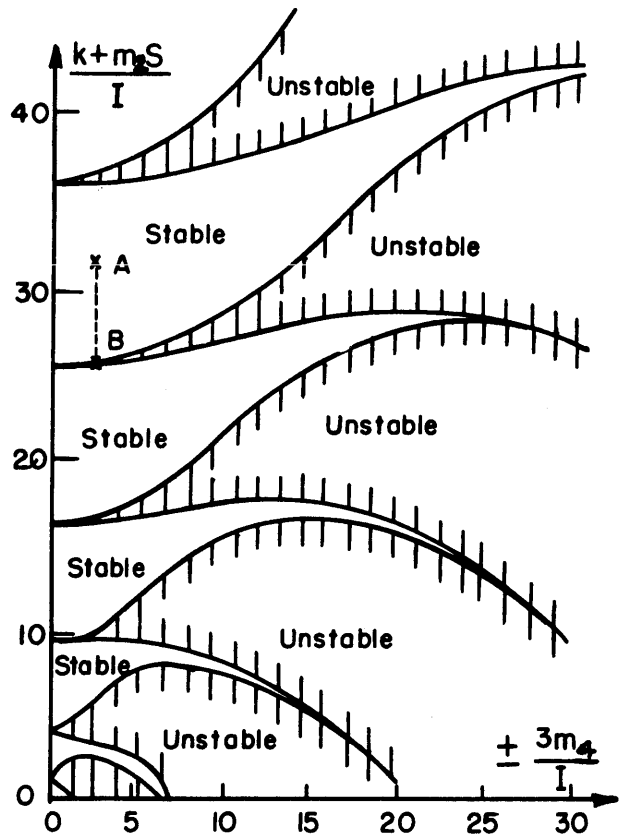




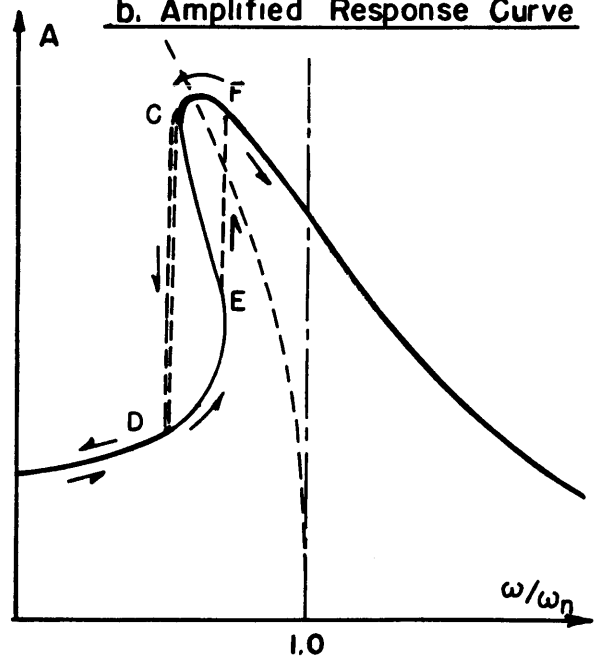
**a. Notations**



**b. Amplified Response Curve**



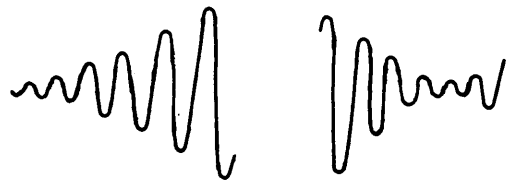
**c. Part of Stability Chart for Mathieu's Function**



**d. Amplitude Response for System with Soft Spring**



**Case A**



**Case B**

**Figure 10. Expected Amplitude Responses**

the left the usual response curve for the linear case. It is seen that then 3-valued solutions arise for the vibrational amplitude. In actuality jumps in the amplitude will occur as has been indicated in Figure 10d.

On the basis of these considerations the amplitude response curves, plotted as a function of the frequency of plate vibration are expected to exhibit the following features:

- a. The reduced amplitude response curve will resemble the curve for a linear system after it has been bent to the left (see Figure 10d); it is bound to the left by a vertical portion D-C of unstable amplitude.
- b. For certain trailing edges the factor G in Eq. [28] may be large, making for a larger forcing moment. The response curve will in that case give the impression of being stretched vertically compared to the usual curve resulting from a constant forcing moment of varying frequency (see Figure 10b).

And on the basis of Figure 10c it is concluded that:

- c. The vibration may be slightly unstable in its amplitude or that the vibration may be unstable and appear spasmodic.
- d. It has been mentioned before (10), (20), (64) that near resonant conditions the frequency of vibration may remain fairly constant over a range of free stream velocities so that the Strouhal number, S, may fall below its customary (or "steady object") value. Referring to Figure 10c it is seen that (going from A to B) an unstable condition may then be reached, which could limit such a decrease in S. Instabilities in the vibrational amplitude will namely terminate the two-dimensional structure of the early wake which is instrumental in causing the deviation of S from its customary value.

The reduced equation [44] may obscure the fact that the actual damping coefficient,  $c'$ , in the complete equation of motion is:

$$c' = c + m_1 U \quad [44a]$$

which would indicate that a sufficient increase in free stream velocity leads to negative damping. Physical reality would then dictate a non-linear damping coefficient so that at relatively high velocities instabilities are expected in the form of relaxation oscillations (cf. van der Pol's equation). This latter effect can not be revealed, however, by the linear thin airfoil theory employed in this development.

The decrease in hydrodynamic damping together with the proportionality between forcing function and  $U^2$  may render a higher mode of vibration more dangerous than the fundamental one.

## V. PRESENTATION AND DISCUSSION OF RESULTS

### A. Some Exploratory Tests with 1/8"-Thick Test Plates

#### 1. Amplitude and Frequency of Plate Vibration

The first plate tested had a semi-circular trailing edge (see Table 2). It was reasoned that the instability of the separation points at the trailing edge might be the principal cause of a variation in lift which the plate motion itself could then sustain. For this reason, the trailing edge of plate #2 was given a 90° groove resulting in two fixed separation points. The amplitudes of vibration were indeed substantially smaller.

Pursuing this approach, plates #3 and #4 were tested. It was thought that easier curvatures near the trailing edge would promote instability of the separation points. However, these plates exhibited hardly any vibration at all, whereas plate #6 with two definite separation points appeared the most susceptible to "singing".

The magnitudes of plate motion given in line 3 of Table 3 were obtained by considering the amplitude of the modulated strain gage signal in the cases for which a clear and stable Lissajous figure was observed on the oscilloscope. By means of a static calibration curve for rotation vs. transducer output, it was found that the maximum plate rotation from the neutral position was of the order of 0.015 radians for plate #6 to 0.003 radians for plates #3 and #4. This corresponds to a transverse motion at the trailing edge of  $0.25 t'$  and  $0.05 t'$  respectively where  $t'$  is the plate thickness. For non-resonant conditions this decreased to at least  $0.02 t'$ , i.e., 0.0025" or less. In determining these maximum amplitudes from the Sanborn record traces, values associated with frequencies between 150 and 225 cps were not taken into consideration. For this frequency range an unwanted amplification of the strain gage output due to resonance of the restraining leaf spring could be expected.

The predominant frequencies,  $f$ , obtained from the wave analyzer records are correlated with free stream velocity,  $U$ , for the various trailing edges in Figure 11. All data were obtained for the same support stiffness. For plates #1 and #6, in particular, discontinuities in the frequency response curve are noticeable which give the curve a stepped appearance. In line 2 of Table 3 the test plates have been grouped in order of increasing "step behavior".

In order to arrive at a representative Strouhal number,  $S = ft'/U$ , straight lines were drawn through the origin and the points of maximum amplitude which, as a rule, were located near the middle of a step. The Strouhal numbers thus determined are given in line 4 of Table 3. If the straight lines are drawn such that all data points lie just to the right of it, somewhat higher Strouhal numbers result as indicated in line 5 of Table 3.

In an attempt to explain the appearance of the steps in the "f vs. U curves" the predominant frequencies have been tabulated in Table 3 for each of the test plates. A predominant frequency is defined as the frequency for which the amplitude of plate motion reached a maximum. This was often evidenced by audible singing of the plate. Since the maxima in general occurred in the middle of a step the predominant frequencies could be defined alternately as those frequencies of vibration which tended to persist during small changes of the free stream velocity.

## 2. Discussion of Results and Conclusions

### a. Frequency vs. Velocity

The results obtained with the series of six test plates show appreciable variation of response as a function of trailing edge geometry as may be seen from Table 3. Not only are there large differences in maximum amplitude of vibration but also the susceptibility to vibration as evidenced by the number of discrete frequencies (line 6, Table 3) varies considerably amongst the test plates.

Table 3 shows a noticeable correlation between step behavior, amplitude of vibration, Strouhal number and excitability of the plates.

No direct explanation can be advanced for the order in which the plates appear in Table 3. If the argument about the stability of the separation points is eliminated as unsatisfactory, the behavior of plates #3 and #4 can still be made plausible by assuming that the Strouhal number is proportional to the distance between the free shear layers at the trailing edge,  $t'_{s,1}$ , rather than to the trailing edge thickness itself. For both these plates the displacement of the separation points to the rear could increase the frequency of vortex formation such that the relatively large mass forces cannot be overcome any more and the plate is steady.

Another explanation could be that a decrease in  $t'_{s,1}$  leads to an increase in annihilation of vorticity at the trailing edge due to diffusion of one shear layer into the other.

The behavior of plate #6, which presumably has well defined separation points, remains unexplained, however.

### b. "Step" Behavior

It is seen in Table 3 and Figure 11 that frequencies around 165, 180 and 510 cps are present irrespective of the particular trailing edge geometry. This is a strong indication of structural resonances in the plate-spring system. In order to substantiate this computations were made of the possible natural frequencies of the plate-spring system lying below 700 cps. Most of these calculations involve assumptions so that the answer can only be approximate. The leaf spring was chosen very weak so that the natural frequency,  $f_n$ , of the system would be below 40 cps (in air). The computed apparent mass effect reduces this to 25 cps in water. This frequency

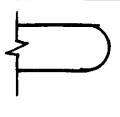
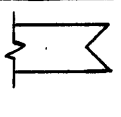
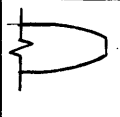
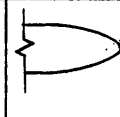
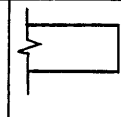
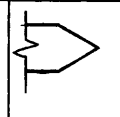
1. Trailing Edge Geometry						
2. Plate number and order of testing:	#1	#2	#3	#4	#5	#6

Table 2. Trailing edge shapes of 1/8"-test plates.

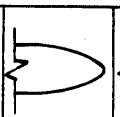
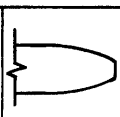
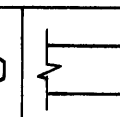
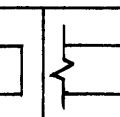
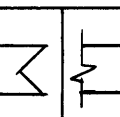
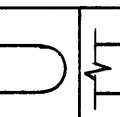
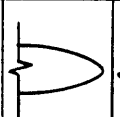
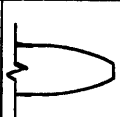
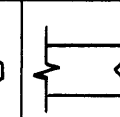
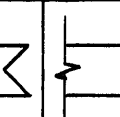
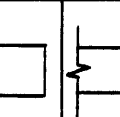
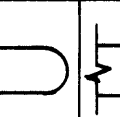
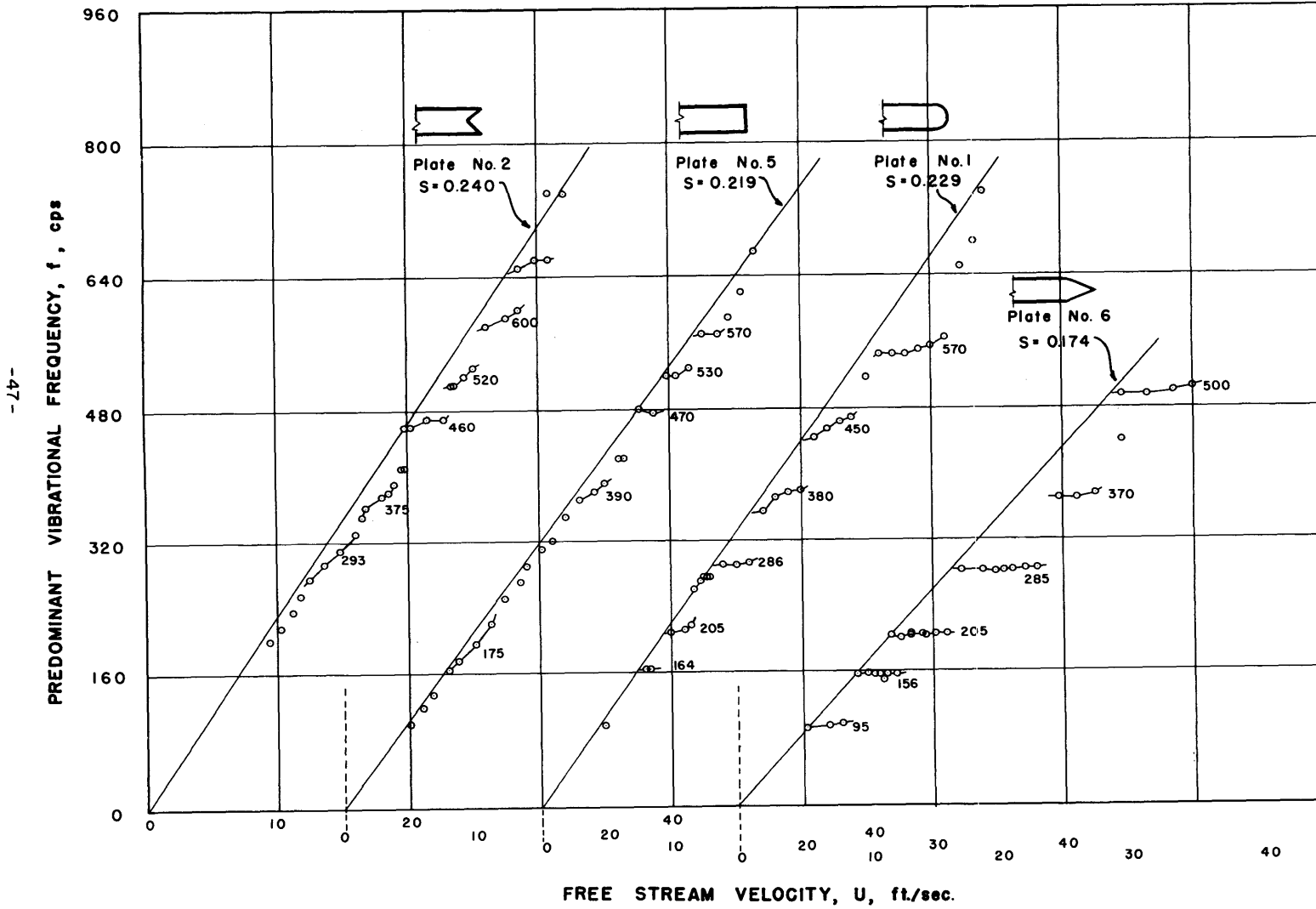
1. Plates in order of increasing step behavior:						
2. Plates in order of increasing amplitude of motion:						
3. Observed maximum amplitudes in radians for the plates in the order of line 2:	.003	.0035	.004	.005	.014	.016
4. Strouhal numbers for the plates in the order of line 2 and based on maximum amplitude data:	-	.237	.224	.212	.206	.146
5. Strouhal numbers for the plates in the order of line 2 and based on maximum frequencies:	-	.251	.240	.219	.229	.174
6. Frequencies associated with larger amplitudes for the plates in the order of line 2:	165 380	165 380 620	293 375 520 600 740	85 175 390 470 530 570 670	80 164 205 286 380 450 510 615 740	95 156 205 285 370 500 680

Table 3. Experimental results for 1/8"-test plates.



**Figure II. Strouhal Graph for 1/8" Test Plates**

is apparently not involved in the results shown in Table 3.

Depending on the assumptions concerning the fixity at the test plate ends the natural frequency for bending vibrations in air is 90 and 200 cps. The apparent mass effect reduces this to between 45 and 100 cps. Possibly the 80 to 90 cps component which often stood out somewhat in the noise of the lower part of the frequency scale is thus accounted for.

Elimination of the effect of the natural frequency of the leaf spring itself was provided for by making the stiffness of the spring support easily variable. The reported series of test, however, were limited to a support stiffness yielding a natural frequency in flexure of from 145 to 221 cps for the first mode and from 460 to 590 cps for the second mode. Comparison of these values with the observed frequencies recorded in Table 3 shows that the 205 cps and 570 cps vibrational components can possibly be explained.

The aluminum spindles around which the plate rotated also possess natural frequencies in bending and torsion. The fundamental bending frequency was computed to lie between 450 and 600 cps. The comparable value is not unrealistic in many cases and is seen to be markedly present in the data. Finally the 380 cps component of the data can possibly be explained as a combination of a second torsional mode of the spindle and a second bending mode of the leaf spring.

In short, these computations indicate that the steps in the  $f$  vs.  $U$  curves and the singing (i.e., audible vibration) which was often associated with it were due to resonance at natural frequencies present in the system. Thus the conclusion was drawn that the lift forces due to the periodic discharge of vorticity of alternating sign were so small that singing could only occur at a natural frequency of the vibrating object.

In addition to a possible reformulation of the Strouhal number technical interest is, in the light of the above, centered on the resonant and near-resonant plate behavior.

### 3. Apparent Mass Forces

In the formulation of a mechanism for the test plate vibrations an accurate knowledge of the apparent mass forces will be useful. Mainly due to end-effects these forces can only be computed approximately. They were therefore compared with experimental determinations of the apparent mass. Both the computed and experimental data are presented in Appendix C and show that the apparent mass moment of inertia is about four times as large as the moment of inertia of the plate itself.

### 4. Modification of Equipment

It therefore was decided to study in detail the response near or at a natural frequency of the system as a function of trailing edge shape and

restraint. To this end the test plate - leaf spring system should essentially behave as a single degree of freedom system. The 1/8" plates and the leaf spring were judged inadequate for this purpose.

To prevent bending vibrations of the plate its own flexural frequency should be much higher than the natural frequency of the plate-support "system". Added stiffness means added mass, however, which is detrimental from the standpoint of accuracy when measuring small forces. The alternative, provision for very low system frequencies, is unsatisfactory since the forcing forces become quite weak in the low frequency range. Plates 1/4" thick were finally selected, a new torsional restraint was installed and an accelerometer was substituted for the strain gages.

## B. Vibrational Frequency vs. Free Stream Velocity (1/4"-plates).

### 1. "Strouhal Graphs"

In Figures 12 through 16 are presented a series of "Strouhal Graphs", i.e., a correlation of predominant vibrational frequency and free stream velocity, similar to those presented in Figure 18 for the 1/8" plate. The data for each trailing edge and rotational axis are shown on separated plots. On each plot the data are identified according to the particular plate restraint used. These positions are indicated in the records and on the Figures 12 through 16 as #1, #4, #5, #7 and free, meaning that the spindle was clamped 1, 4, 5, .... inches below the transition between the 0.6" diameter and 0.375" diameter portions of the spindle.

As expected the data for the "free" case usually plot along a straight line in the Strouhal graphs. The slope of this line then gives the Strouhal number. When a particular natural frequency is provided in the system the points in the Strouhal graph deviate from the line found in the free case as soon as the frequency of vortex shedding is sufficiently increased to nearly coincide with  $f_n$ . The deviation may be so large that a nearly horizontal step is formed in the Strouhal line. After a sufficient increase in velocity the rate of vortex shedding is no longer controlled by the proximity of the  $f_n$  of the system and points plot again according to the Strouhal relation provided a region of secondary resonance has not been reached. For a qualitative explanation of the discontinuity at the end of each step in the Strouhal graph see the discussion in Section IV, C-2-iiii.

The Figures 12 through 16 are actually combinations of 3 or 4 "Strouhal graphs" prepared individually for each plate and each stiffness condition. Strouhal numbers determined from the individual plots have been presented in Table 4, showing that for non-resonant conditions the stiffness has little influence on the value of the Strouhal number.

The average of the Strouhal numbers for each of the plates as found in column 6, Table 9, have been compared, in Table 4, with values found previously for the 1/8" test plates:



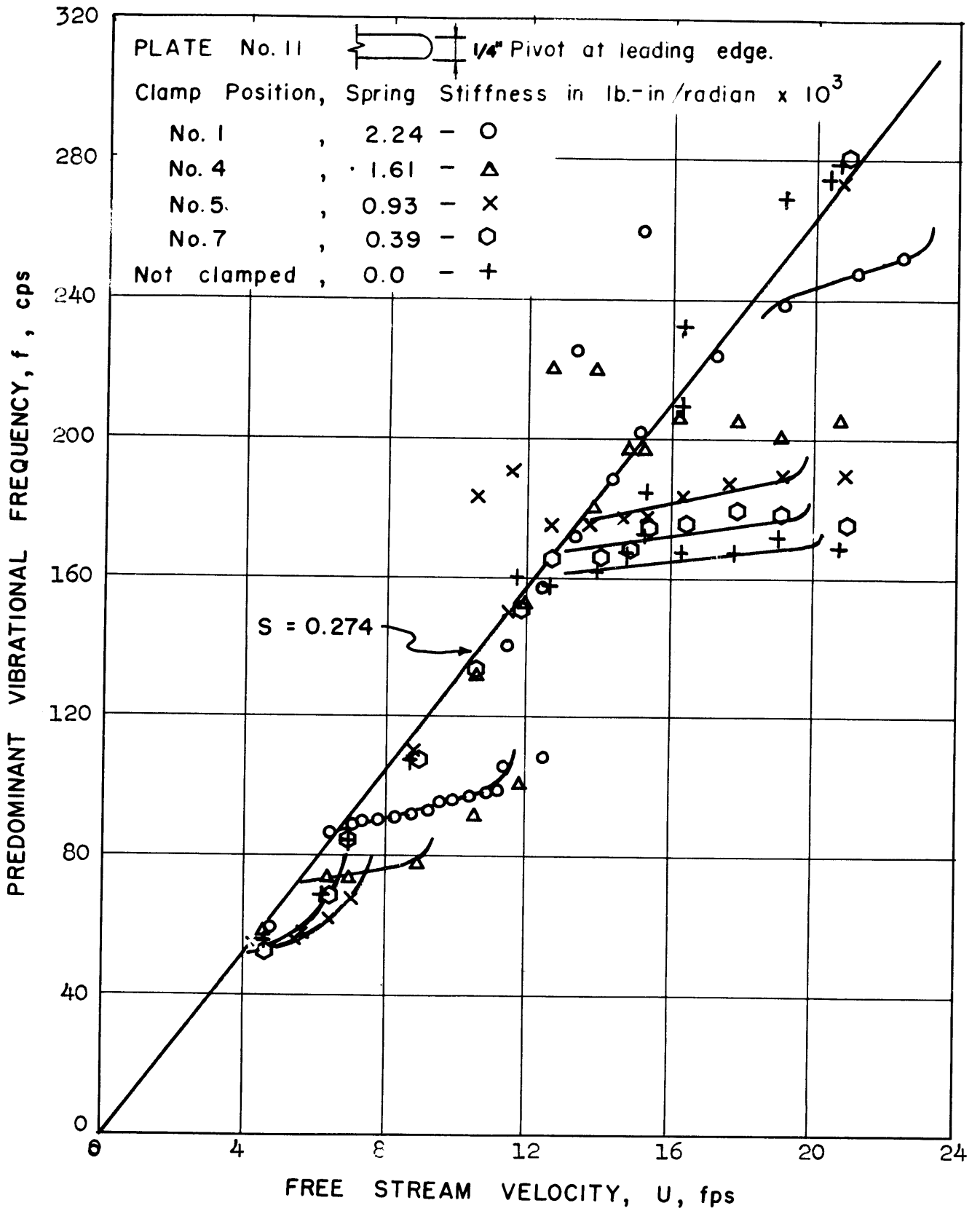


Figure 12. Strouhal Graph for Plate #11 - Pivot Leading Edge

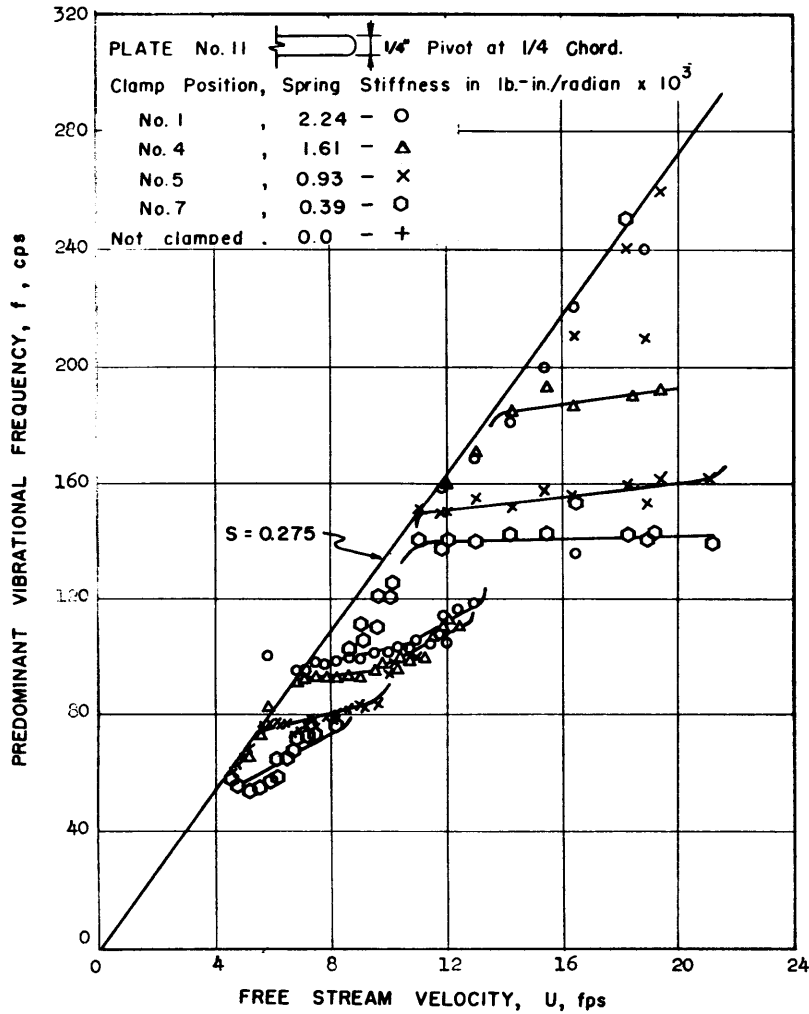


Figure 13. Strouhal Graph for Plate #11, Pivot at 1/4-chord

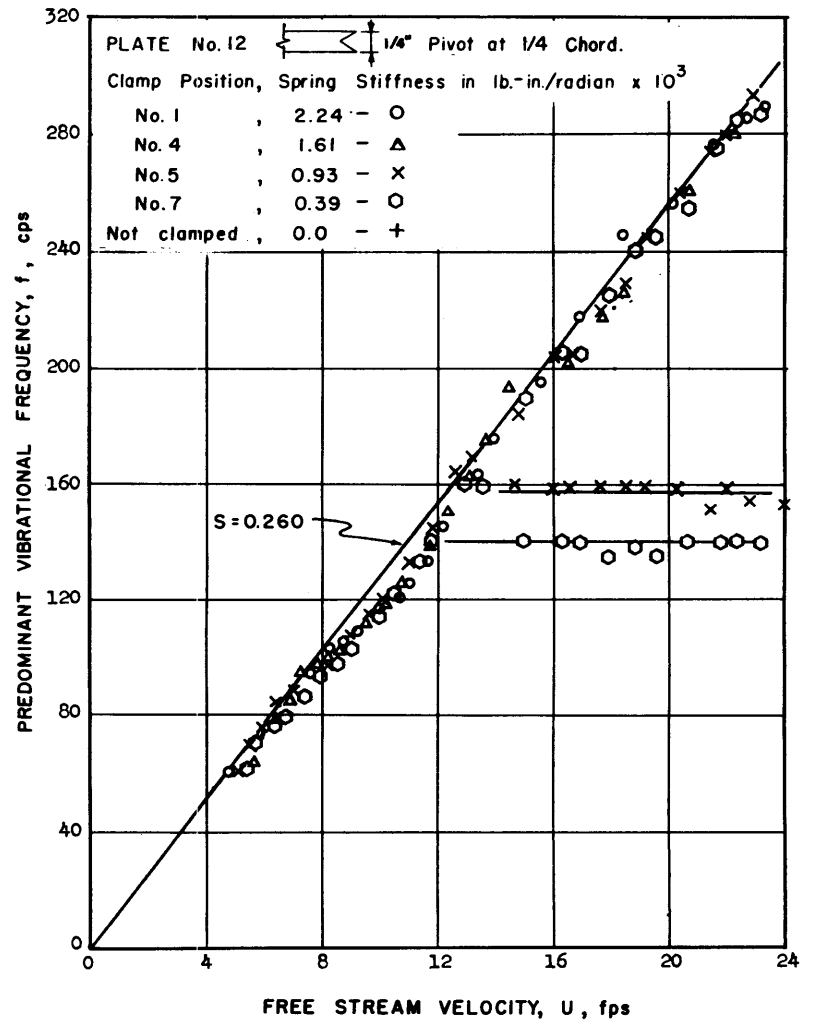


Figure 14. Strouhal Graph for Plate #12, Pivot at 1/4-chord

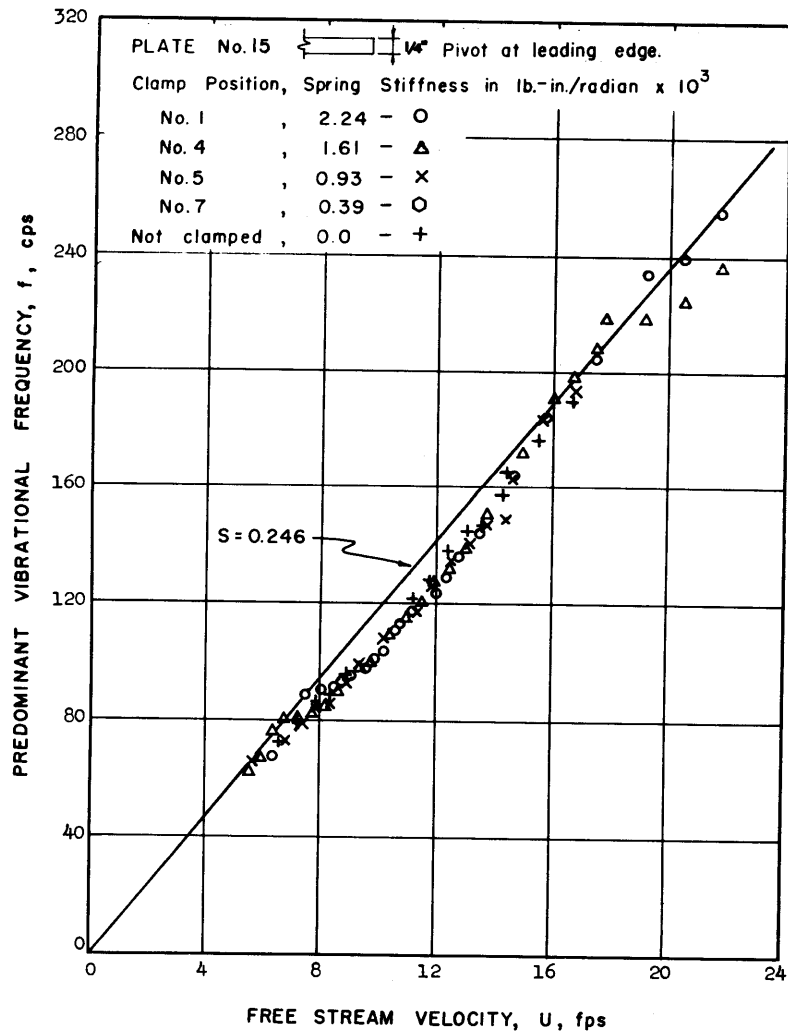


Figure 15. Strouhal Graph for Plate #15, Pivot at Leading Edge

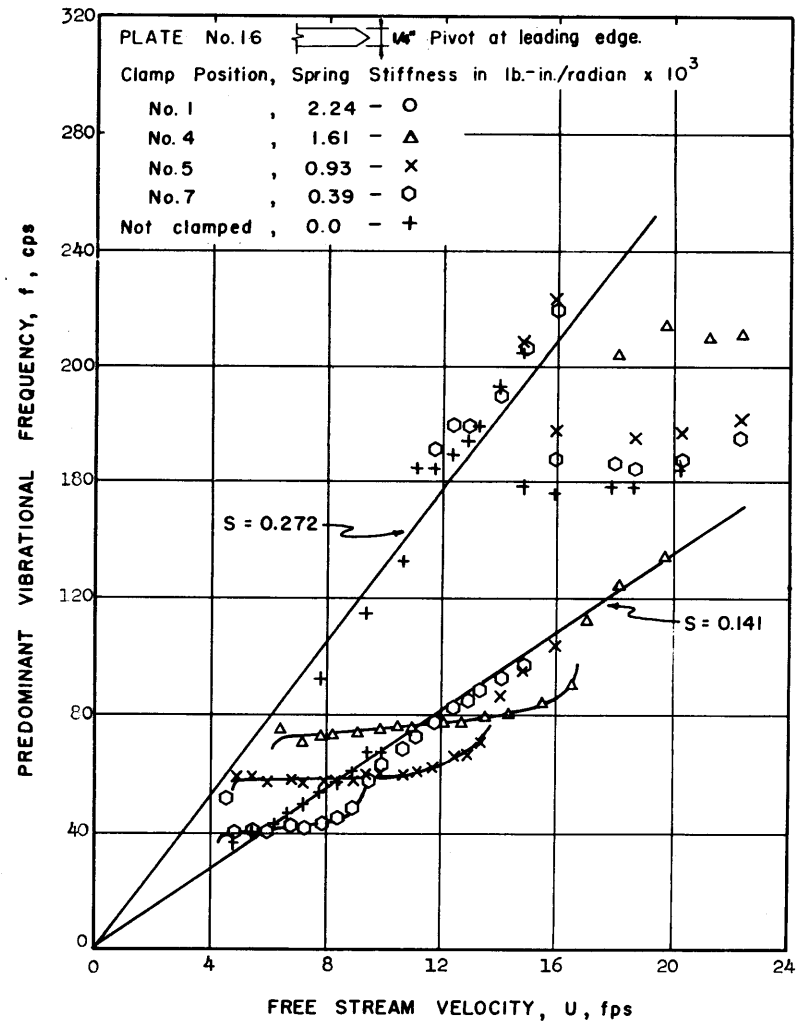


Figure 16. Strouhal Graph for Plate #16, Pivot at Leading Edge

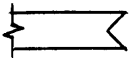
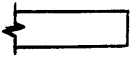
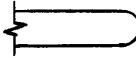
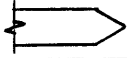
Strouhal Numbers for Plate No.		2 or 12	5 or 15	1 or 11	6 or 16
Test Plates	pivoted at				
1/8" plates	leading edge	0.219	0.240	0.229	0.174
1/4" plates	leading edge	0.249	0.246	0.275	0.139
1/4" plates	1/4-chord	0.258	-	0.274	-

Table 4. Comparison of Strouhal Numbers

It is seen that in three out of four cases the Strouhal numbers for the 1/4" plates are higher than those for the corresponding 1/8" plates. For plate #16, however,  $S_{16}$  is below  $S_6$ . The reason for these differences is not immediately clear.

The exceptionally low value of  $S_6$  and  $S_{16}$  are attributed to a boundary layer separation effect. The transverse plate motion may temporarily prevent separation at the beginning of the tapered trailing edge so that the separation point is shifted to the end of the trailing edge. This results in a sizable decrease in  $S$ , since experimental findings (36), (58) indicate that  $S$  is proportional to the distance between the separating shear layers. With an increase in  $U$ , however, separation is expected to always occur at the beginning of the trailing edge. This trend is indeed present and has been indicated in Figure 16 by the line  $S = 0.272$ , which is more in line with the experimental results obtained for the other plates.

For the cases allowing for plate rotation around the leading edge and 1/4-chord respectively the difference in  $S$  is small. Reasonable agreement between these values could be expected, since  $S$  is found from the slope of a line determined by non-resonant frequency values. For non-resonant conditions the amplitudes of vibrations are so small that steady state conditions are approached.

From the Strouhal graphs it is possible to discern between the data which were strongly affected by the system  $f_n$  (points plotting on the nearly horizontal portions of the curve) and those which are essentially independent of this elastic characteristic (points plotting along the sloping lines).

## 2. Sub- and Ultra-harmonics

The Strouhal graphs are based on the predominant frequency present in the accelerometer signal. In many cases other frequencies were present simultaneously. Examples of test runs for which these frequencies were recorded, are given in Table 5.

During resonance the 3rd harmonic is present distinctly for the plates #11 and #16. Also the 7th harmonic often appears. Occasionally the 5th harmonic is encountered. For plate #15 on the contrary, the 2nd, 3rd, 4th and 6th harmonics proved present during resonance (for plate #12 no such record was kept).

Plate Pivot and Position of Clamp	U in fps	Frequency of Components, f, in cps	$\frac{f}{f_{pr}}$ predominant component,	
1	2	3	4	
#11 leading edge Clamp #1  $f_n = 96$ cps  $f_r = 95.5$ cps	7.0	89, 275, 630	1.0, 3.1, 7.1	
	8.2	91, 276, 645	1.0, 3.0, 7.1	
	9.1	93, 262, 660	1.0, 2.8, 7.1	
	9.9	96, 270, 670	1.0, 2.8, 7.0	
	10.8	98, 295, 690	1.0, 3.0, 7.0	
	-----			end of "step"
	12.3	108, 158	1.0, 1.46	
	13.3	172, 255	1.0, 1.48	
	14.3	188, 225	1.0, 1.20	
	#15 1/4-chord Clamp #1  $f_n = 121$ cps  $f_r = 103$ cps	7.3	random around 101	
9.5		105, 210, 315, 420, 630	1.0, 2.0, 3.0 4.0, 6.0	
9.8		104, 208, 312, 624,	1.0, 2.0, 3.0 6.0	
10.3		110, 220, 330 660	1.0, 2.0, 3.0 6.0	
11.5		125, 250, 375	1.0, 2.0, 3.0	
12.7		135, 270, 305	1.0, 2.0, 2.3	
#16 leading edge Clamp #1  $f_n = 96$ cps  $f_r = 96.5$ cps		8.2	82, 246	1.0, 3.0
	8.9	85.5, 256, 605	1.0, 3.0, 7.1	
	9.4	87, 262, 620	1.0, 3.0, 7.1	
	10.3	88, 265, 620	1.0, 3.0, 7.0	
	10.7	88.5, 265, 620	1.0, 3.0, 7.0	
	11.7	89, 268, 630	1.0, 3.0, 7.1	
	12.7	91, 272, 635	1.0, 3.0, 7.0	
	13.2	91.5, 274, 640	1.0, 3.0, 7.0	
	15.0	93, 280, 665	1.0, 3.0, 7.2	
	16.8	96.5, 288, 675	1.0, 3.0, 7.0	
	18.0	99, 297	1.0, 3.0	
	-----			end of "step"
	19.4	136, 300	1.0, 2.2	

Table 5. Ultra-harmonics at resonance.

The Strouhal graphs further show a second step at a frequency,  $f_{sr}$ , which is considered to be associated with the 2nd torsional mode of the torsion-spring rod. (For #15 no such record was taken). Table 6 shows, however, that  $f_{sr} \neq 3f_n$  in all cases which indicates that the spring stiffness is influenced by the amplitude of motion.

It is not clear why this effect should be so much more pronounced for plates pivoted about the leading edge than for plates pivoted around the  $1/4$ -chord line (see Table 6, column 4).

A further peculiarity is the fact that beyond the speed at which the secondary resonance sets in, the vibration possesses a frequency component which is given by the Strouhal number. This gives, if the vibration is regarded as forced by vortex shedding, the secondary frequency the character of a subharmonic frequency.

The presence of sub- and ultra-harmonic components is readily made plausible from the consideration of non-linear equations like the Duffing's- and Mathieu's equations (see Reference 68). It is difficult to assess, however, to which extent purely mechanical factors are present, e.g., due to the "step-tapered" shape of the torsion rod. In this connection the inexplicable appearance for the plates #11 and #16 of the step in the Strouhal graph for the "free" case is to be noted.

### 3. Natural Frequency and Apparent Mass Determinations.

The analytic determination of the torsional natural frequency,  $f_n$ , of the test plate - accelerometer - spindle system as well as the torsional stiffness,  $k$ , of the spindle can only be approximate. Both characteristics were therefore determined experimentally. They are presented in Figure 17 and discussed in the Appendix C.

From the established values of  $f_n$  and  $k$ , the apparent mass moment is readily computed. This determination, which also is found in Appendix C, shows that end-effects were eliminated by the addition of small end plates (see Figure 7) to the  $1/4$ " test plates.

A determination of  $f_n$  for plate mountings which allow for rotation around the  $1/4$ -chord is given in Appendix C.

## C. Vibrational Amplitude vs. Free Stream Velocity.

### 1. Presentation and Discussion of the Amplitude Records.

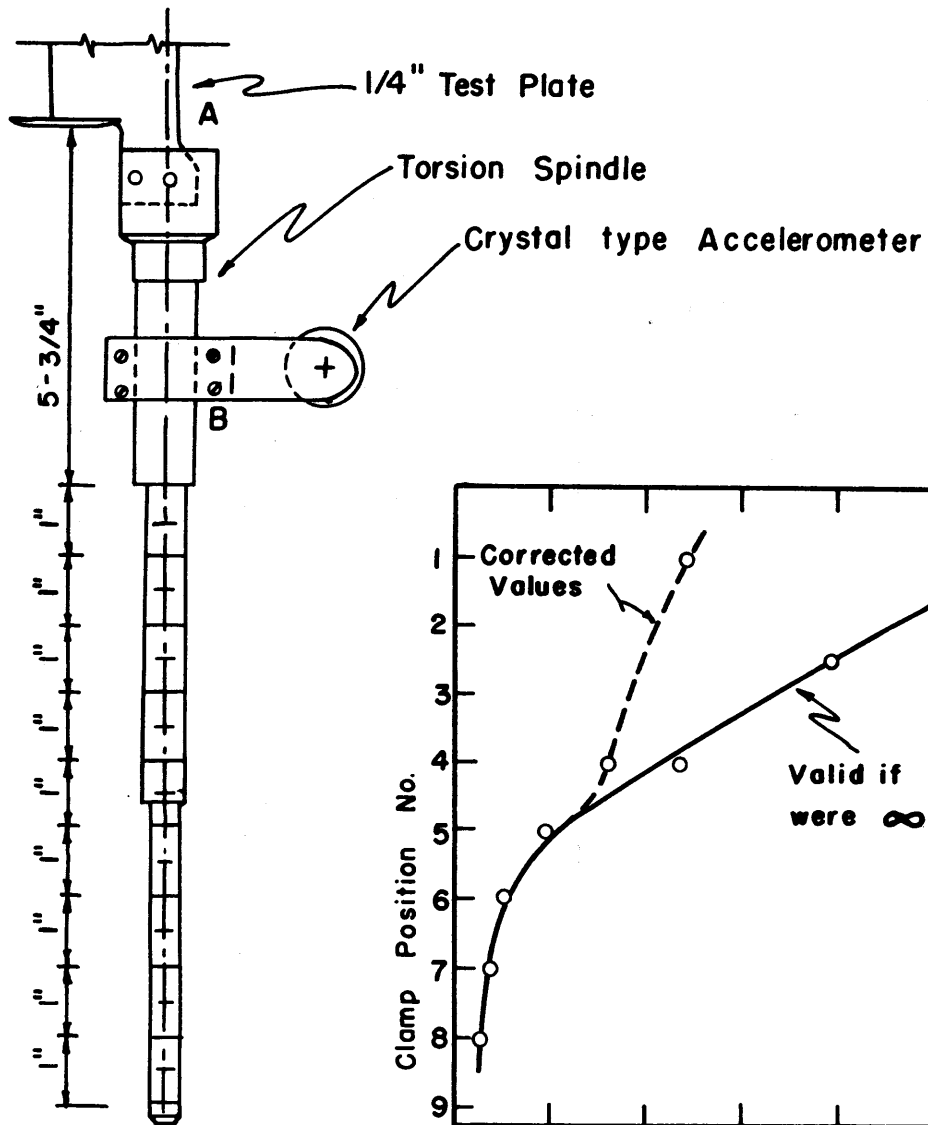
Simultaneously with the determination of the frequency components of the accelerometer signal, the total strength of the transducer output (measured with an RMS-Volt meter) as well as the strength associated with the predominant frequency components (measured with a Wave Analyzer) were recorded.

These data are presented and discussed as follows:

Plate and Pivot	Position of Clamp	Natural Frequency $f_n$	Frequency, $f_{sr}$ , of secondary resonance	$\frac{f_{sr}}{f_n}$
		cps	cps	
1	2	3	4	5
#11 leading edge	1	96	250	2.6
	4	81	205	2.5
	5	60	183	3.0
	7	41	177	4.2
	free	--	165	---
#16 leading edge	1	96	---	---
	4	81	210	2.6
	5	60	178	3.0
	7	41	168	4.1
	free	--	160	---
#11 1/4-chord	1	121	235	2.5
	4	103	185	2.3
	5	78	155	2.5
	7	51	140	2.7
#12 1/4-chord	1	121	---	---
	4	103	---	---
	5	78	158	2.0
	7	51	140	2.7

Table 6. Secondary Resonant Frequencies.

- a. the amplitude response curves (i.e., total transducer output vs. the free stream velocity ratio,  $U/U_r$ ) - section V-C.
- b. the maximum vibrational amplitudes taken from the amplitude response curves - section V-F.
- c. the extremes of the amplitude of the predominant component vs.  $U/U_r$  - section V-E.
- d. the reduced amplitude response curves (i.e., the amplitude response data divided over  $U^3/f$  vs.  $U/U_r$  - section V-G.



### Characteristics of TORSION SPINDLE

$$\delta = \frac{x_n - x_{n+1}}{x_n} = 2\pi C/C_c$$

$$\therefore C_{avg.} = \delta C_c / 2\pi = 0.05 C_c$$

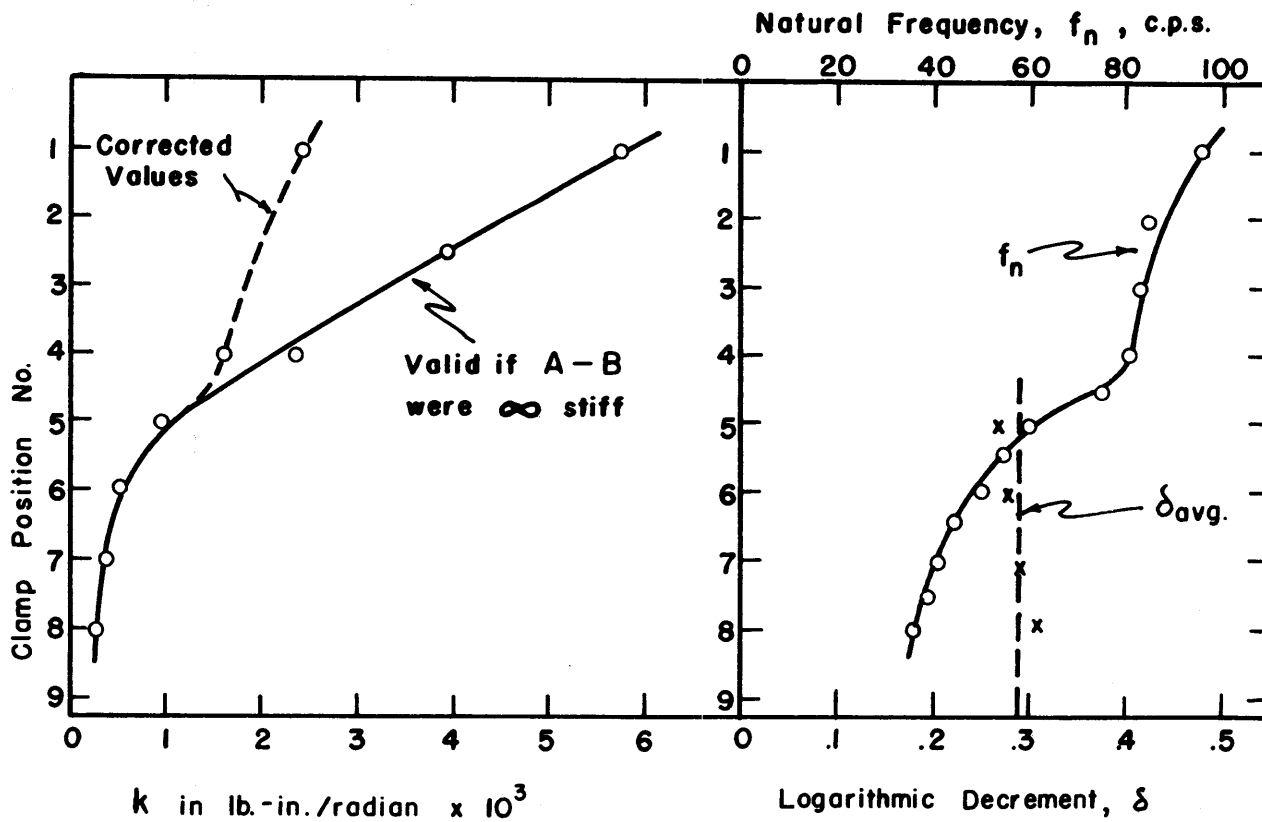


Figure 17. Characteristics of Torsion Spindle



## 2. Amplitude Response Curves

For a harmonic vibration of the test plate the Volt-meter reading of the total accelerometer signal is:

$$\text{RMS} = \left[ a_0^2 \omega^4 \sin^2 \omega t \right]^{1/2} \approx a_0 \omega^2 \approx a_{ot} \omega^2 \quad [45]$$

in which:  $\omega = 2\pi f$

$f$  = plate vibration in cps

$a_0$  = maximum amplitude of accelerometer motion

$a_{ot}$  = maximum amplitude of plate motion at trailing edge.

Therefore an indication of the amplitude of plate motion is obtained by dividing the Voltmeter reading by the square of the predominant frequency,  $f_p^2$ , determined by the Wave Analyzer.

During resonance the vibration could be reasonably harmonic, but for non-resonant conditions the frequency was unsteady in which case the  $\text{RMS}/f_p^2$  value leads to a fictitious amplitude.

The amplitude data are presented in Figures 18 through 21 and 23 in terms of a relative amplitude,  $2a_0/t'$ , in which  $t' =$  plate thickness = 0.25".

As shown in Appendix D, the ordinates of the amplitude response curves are to be multiplied by a factor 1.2 in order to obtain the vibrational amplitude at the trailing edge.

The determination of the conversion factor to convert the transducer output to the relative amplitude, is also given in Appendix D. For checking purposes some direct measurements were made of the amplitude of motion during resonance. The measurements, made by means of a micrometer and reported in Appendix E, agree reasonably with the amplitude values measured electronically.

From inspection of the Strouhal graphs the velocity at which structural resonance occurred was estimated. For speeds close to that velocity the record of amplitude values was inspected and a "resonant velocity",  $U_r$ , selected, which is defined as that velocity for which the amplitude data showed a maximum. The prevailing vibrational frequency was designated as the resonant frequency,  $f_r$ . The  $U_r$ 's and  $f_r$ 's thus found have been collected in Table 9.

All test section velocities below the influence of the secondary resonance were rendered dimensionless through division by  $U_r$  and the resulting ratio was plotted against the corresponding dimensionless amplitude,  $2a_0/t$ . The amplitude response curves are presented in Figures 18 through 21 and 23 for the four different 1/4" plates selected. For

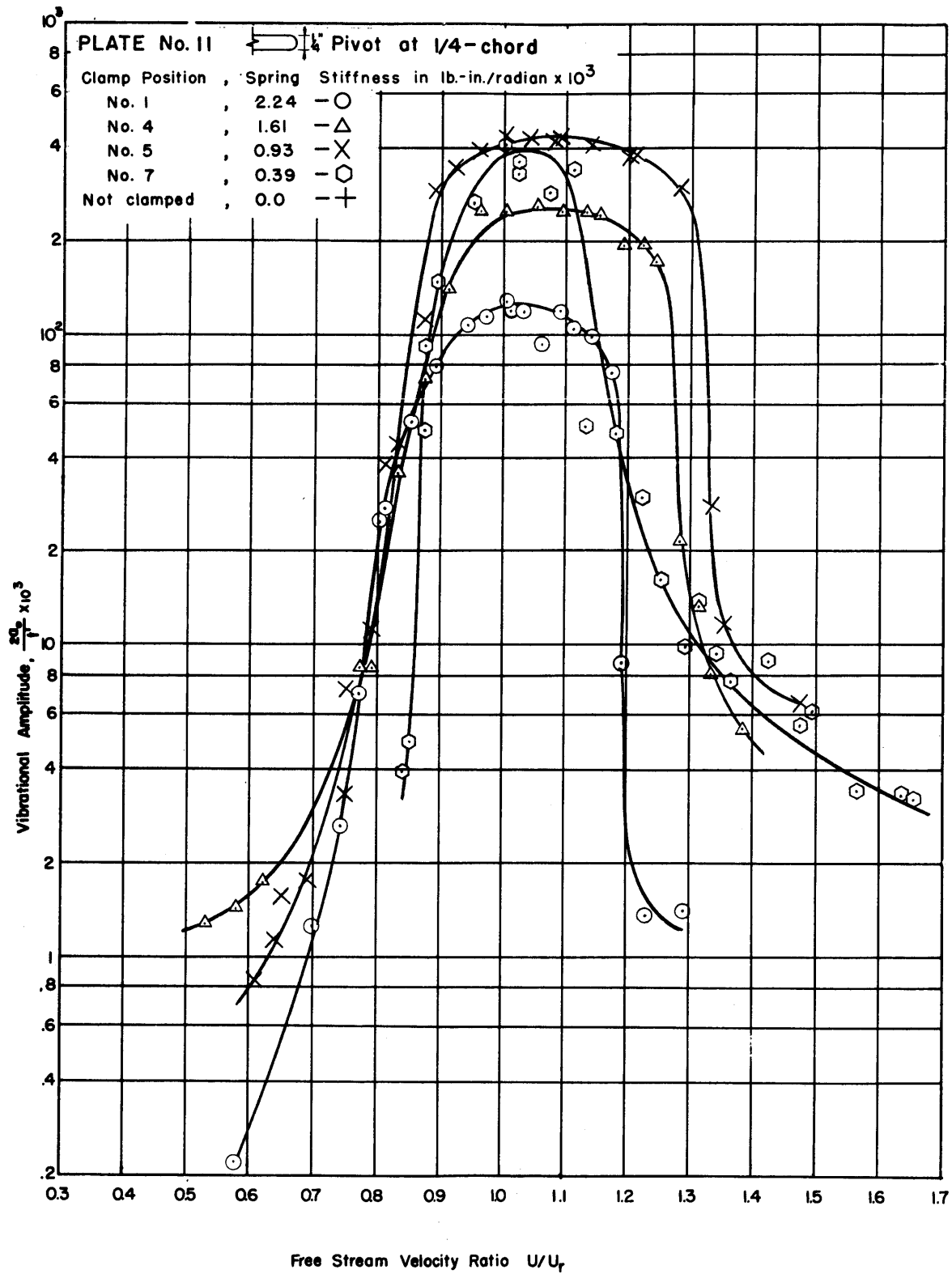


Figure 18. Amplitude Response Curve for Plate \*11, Pivot 1/4-chord

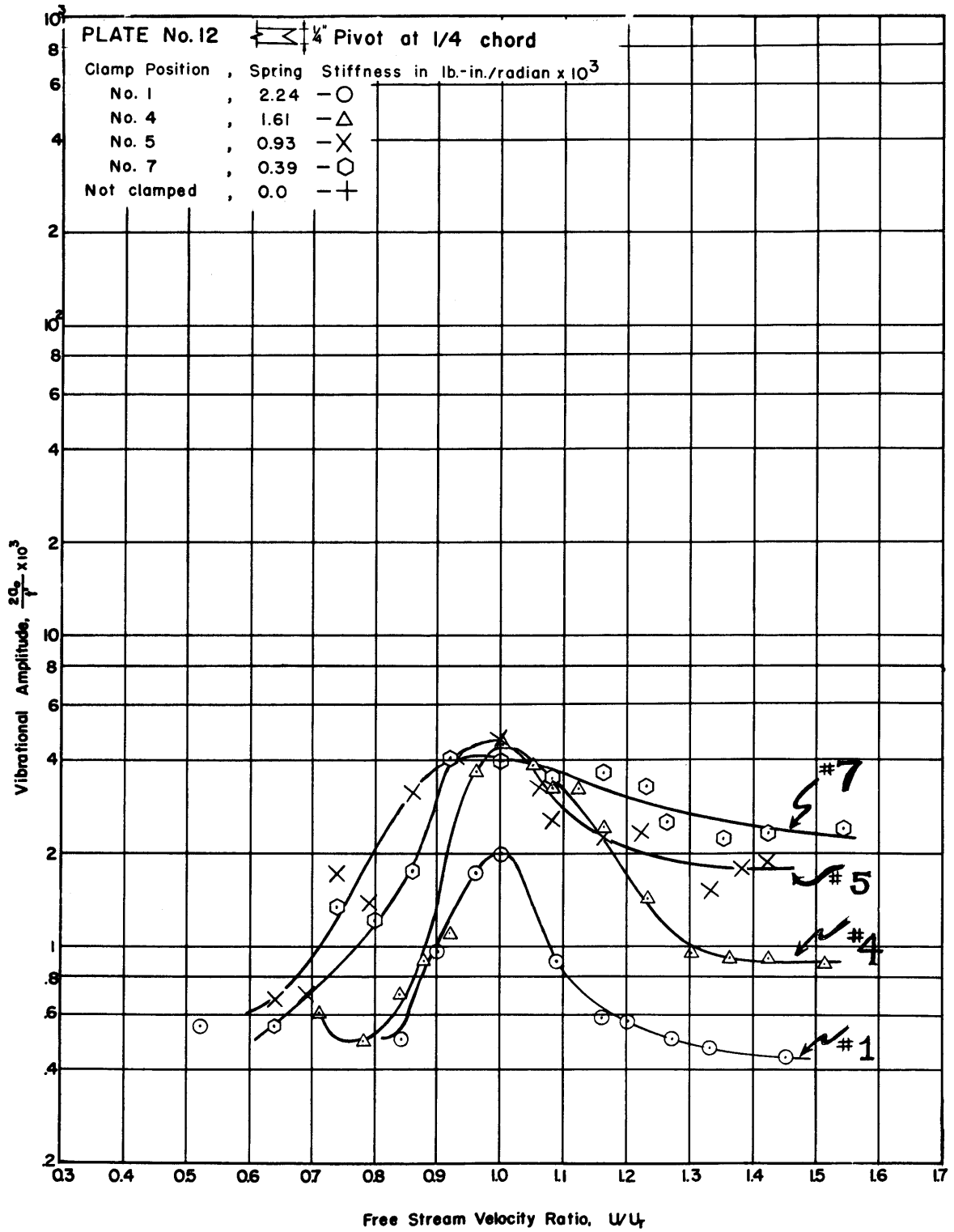


Figure 19. Amplitude Response Curve for Plate #12, Pivot 1/4-chord

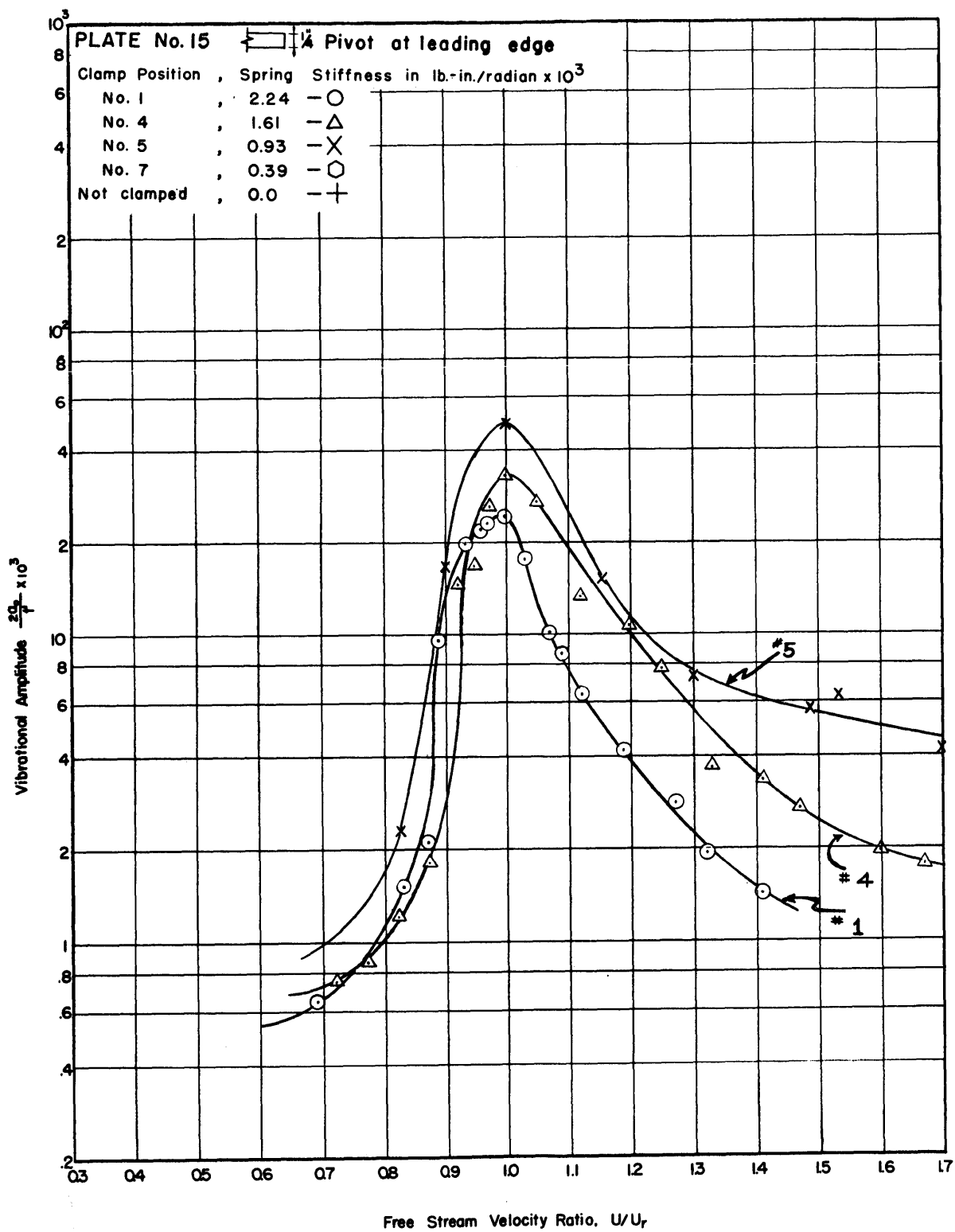


Figure 20. Amplitude Response Curve for Plate #15, Pivot Leading Edge

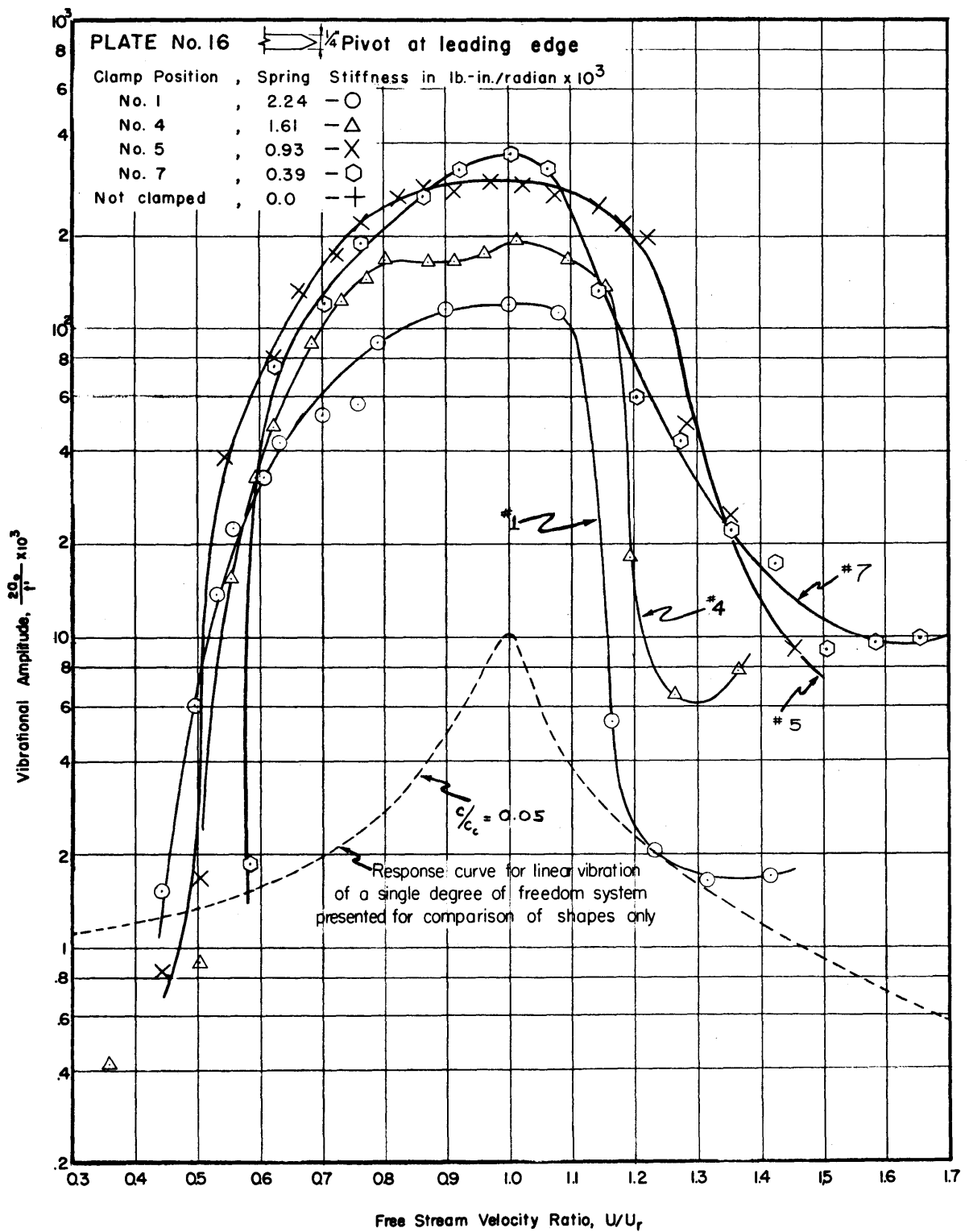


Figure 21. Amplitude Response Curve for Plate #16, Pivot Leading Edge

each plate several restraints or "clamp positions" have been used.

D. Reproducibility of Experimental Observations.

The phenomenon under investigation exhibits unstable features. Also the number of conceivably relevant variables is large. Therefore the question of how reproducible the experimental results are, is of particular importance.

1. Reproducibility of Vibrational Frequency and Amplitude

Figure 22 shows the results for three different test runs with plate #1, for which the mounting conditions were selected to be similar. No effort was made to also duplicate variables such as the ambient pressure in the test section, the amount of tunnel vibration and the sequence of measurements (i.e., increasing or decreasing test section velocity). It is seen that the steps in the Strouhal curve were well duplicated, but that agreement in the indicated vibrational amplitude was less favorable.

Similar features are shown in Figure 23 which presents data for two test series made for plate #11. In absolute value the maximum amplitudes differ by more than 100%. However, a subsequent redetermination of the maximum amplitudes for plate #15 showed very good agreement with earlier obtained values.

The resonant frequencies,  $f_r$ , and velocities,  $U_r$ , show good agreement as can be seen from the following data, in Table 7, taken from Figure 23:

Plate #11 Clamp Position	$U_{r1}$	$U_{r2}$	$f_{r1}$	$f_{r2}$	$\frac{(2a_0)}{t} 1$	$\frac{(2a_0)}{t} 2$
#1	9.9	10.1	96	95.5	1900	950
#4	7.9	7.9	76	81	2460	1545
#5	6.3	6.2	62	61	2700	2300

Table 7. Comparison of results for plate #11 of test series #1 and #2.

As may be inferred from the steep slopes of the amplitude response curves and their logarithmic ordinate scales, the increase in vibrational amplitude upon approaching resonant conditions, may be extremely rapid. Particularly for plate #11 this increase often occurs as a sudden jump in the amplitude. Keeping all mechanical conditions alike, the reproducibility of this transition velocity, (the velocity at which this amplitude change occurs) was investigated for plate #11, clamp position No. 5 and is reported in Table 8. The results show that the velocity of transition, for equal mechanical conditions is confined to a narrow range. The amplitudes of motion, however, were quite unstable at the transition velocities.

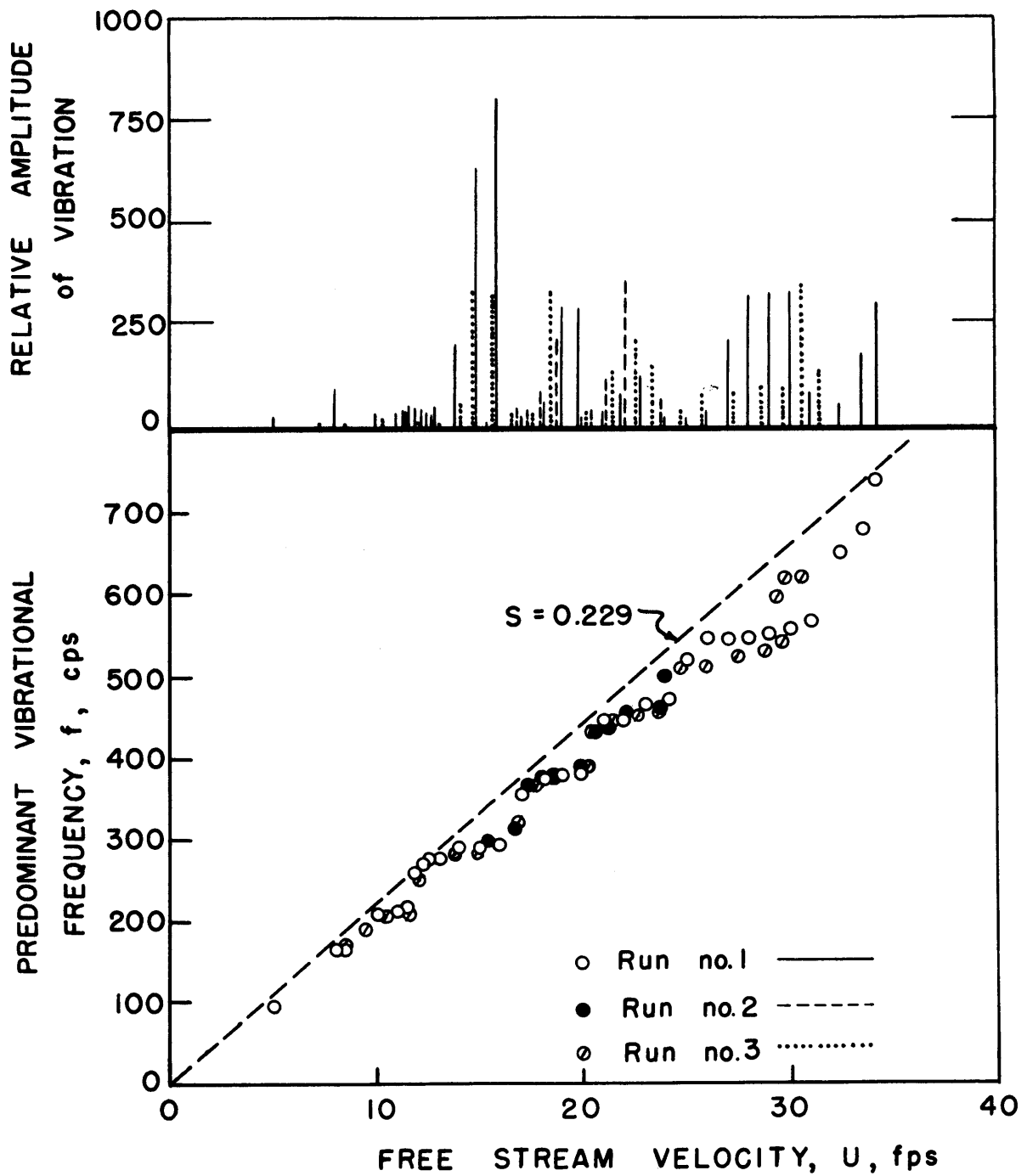


Figure 22. Reproducibility of Test Results for Plate #1

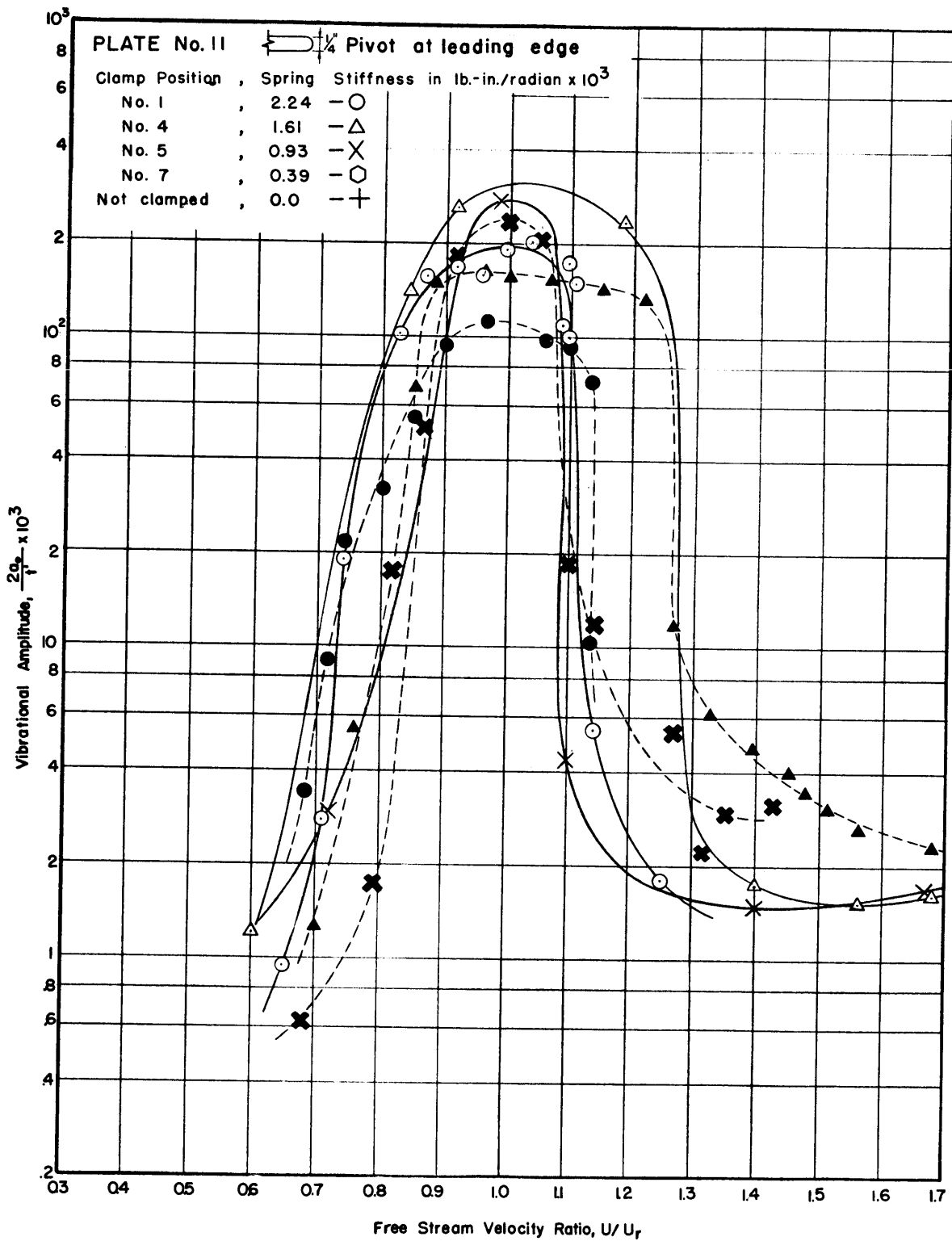


Figure 23. Reproducibility of Test Results for Plate #11



## 2. Effect of Ambient Pressure

Some measurements were also taken to determine the influence of the ambient pressure in the test section on the vibration phenomenon. The results (for plate #11 and clamp in position No. 4) are presented in Figure 24 and do not show such influence. Admittedly the conditions shown are those close to resonance. If that is not the case, however, the unsteadiness of the vibration would necessitate statistical comparison of the transducer signals.

Cavitation in the wake would conceivably alter the picture substantially. Since, however, the operating pressures were kept sufficiently high to avoid visible cavitation on the vibrating plates this effect was not further investigated.

## 3. Influence of Tunnel Vibrations

All the frequency spectra of the straining signal, indicative of the motion of the 1/8"-test plates, contained a band of noise between the frequencies of 10 cps and 100 cps. The noise level appeared to be influenced primarily by the fluid speed in the test section, rather than by test plate geometry or amount of restraint. The tunnel vibrations, mentioned before, were therefore held responsible for the noise.

The frequency spectra for the 1/4"-test plate series did not show the band of random frequencies which had been characteristic for the 1/8" plates. The vibration characteristics of the tunnel had not changed, however.

Apparently this improvement is related to the change in the displacement transducer. For the 1/8" plates straingages were mounted on the thin leaf spring which restrained the test plates. The spring was at either end in contact with the test section. These supports were 6-1/2" apart. Most likely the random test section motion caused bending vibrations of the leaf spring, resulting in the noticed noise.

The accelerometer used with the 1/4" plates on the other hand, is mounted on an arm which considerably amplifies the rotary vibration of the spindle compared to its transverse motion imparted by test section vibration. For the second test series the reproducibility of results therefore is not impaired by the water tunnel vibrations.

## 4. Summary

It thus appears that a satisfactory qualitative reproduction of the experimental conditions can be obtained, but that the quantitative duplication of vibrational amplitude may be poor. This implies that it will be possible only to indicate the order of magnitude of the forces exerted on the plates and that furthermore such correlations as the maximum vibrational amplitude as a function of elastic restraint, to be described later, may not be conclusive.

Velocity of Transition for increasing Velocity	Velocity of Transition for decreasing Velocity	Frequency $f_{pr}$	Amplitude $\frac{2a_0}{t^2}$
fps	fps	cps	---
6.60	----	62	2080
6.65	----	66	460
----	6.50	66	640
----	6.55	60	2090
5.60	----	60	446
5.65	----	60	1600
----	5.50	60	611
----	5.45	60	1390

Table 8. Reproducibility of Transitional Velocity and Vibrational Amplitude for Plate #11 clamp position No. 5.

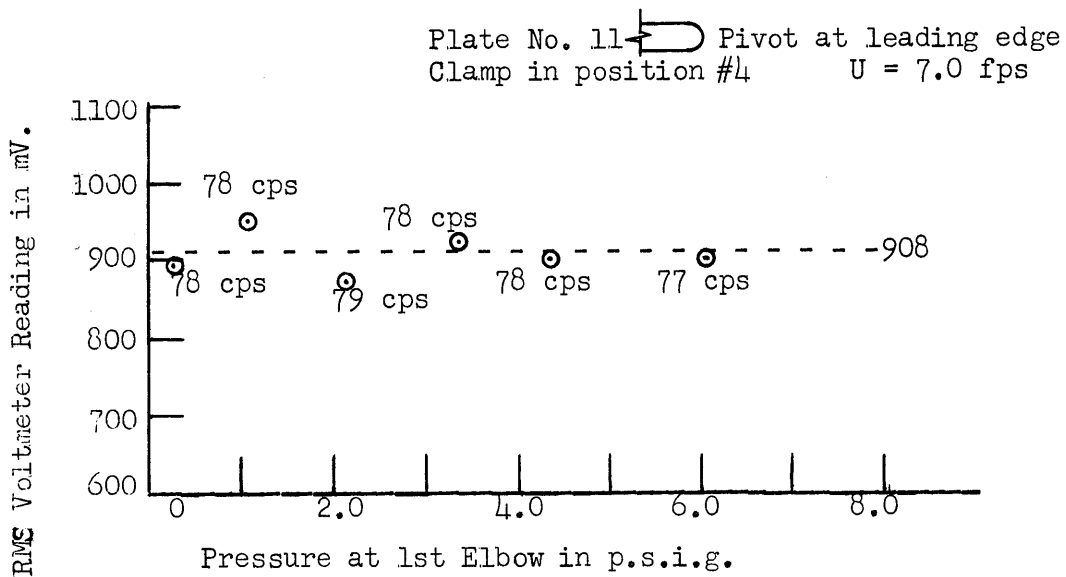


Figure 24. Influence of Ambient Pressure

One reason for variation in the mean vibrational amplitude from one test series to another may be found in the variation of viscous damping. For the motion which establishes itself at resonant conditions the work done per cycle by the periodic lift forces nearly equals the energy dissipated in viscous damping. Small changes in the damping due to a thick water repellent grease in the ball bearings around the spindles, might therefore lead to substantial differences in the observed amplitudes of vibration.

A second reason is found in the technique of test plate mounting which does not eliminate the possibility of small initial angles of attack. In view of the relatively small motions involved this circumstance might well be reflected in the variation of resonant amplitudes.

A third source of deviations among experimental values is the unsteadiness exhibited by the vibrations. Since the occurrence of unsteadiness is of importance for the understanding of the vibration phenomenon, the next section is devoted to its consideration.

#### E. Stability of Vibrational Amplitude and Frequency.

##### 1. Comparison of Wave Analyzer and Volt meter Signals

The total strength of the transducer signal was measured with an RMS-Volt meter. The reading included the effect of any harmonics present other than the fundamental one. Also it did not indicate whether the signal frequency was steady or unsteady. A comparison of the Volt meter reading with the analysis simultaneously made by the wave analyzer, however, provided a means for a qualitative evaluation of the transducer output.

Such a comparison for plates #11 through #16 with  $k = 1.61 \times 10^3$  lbs-in/radian and pivoted at the leading edge is shown in Figures 25 through 28. The dashed curves in these figures represent the ratio of the wave analyzer reading to the Volt meter reading.

##### 2. Stability of Vibrational Amplitude

For all plates the strength of the predominant component at non-resonant conditions was but a fraction of the total strength of the transducer signal. When the resonant condition was approached the strength of the predominant harmonic became a larger and larger portion of the total transducer output. This feature is shown by the dashed curves in Figures 25 through 28 which represent the average of the wave analyzer readings in mV divided by the average of the Volt meter readings in mV as a function of the free stream velocity ratio.

In many cases the strength of the predominant component was quite unsteady. This is reflected by the distance between the two solid curves in Figures 25 through 28, which represent the ratios,  $\Sigma$ , of the maximum

and minimum amplitude of the predominant vibrational component measured from the wave analyzer record, and the average Volt meter reading. This distance is indicative of the fluctuations in vibrational amplitude and thereby of the instability of the net circulation,  $\Gamma_{net}$ , at a given free stream velocity.

### 3. Stability of Vibrational Frequency

For all plates the frequency of the predominant component,  $f_p$ , at non-resonant conditions was quite unsteady. The frequency spectrum was broad and no Lissajous figure could be obtained on the oscilloscope screen. Approaching the resonant condition,  $f_p$  became more and more steady even though the amplitude of the signal could remain fluctuating appreciably. A more steady  $f_p$  was evidenced by a more peaked frequency spectrum as well as a stable (as far as frequency is concerned) Lissajous figure.

A decrease of the ratio of wave analyzer to Volt-meter signal always appeared to be associated with a decrease in the stability of  $f_p$ . The distance between the dashed curve in each of the Figures 25 through 28 and their horizontal tangents near  $U/U_r = 1.0$  is therefore considered a measure of the instability of the frequency  $f_p$ .

In the following discussions the Figures 25 through 28 will be referred to as "stability (of vibration) graphs" since the plots are indicative of the stability of  $f_p$  as well as of  $\Gamma_{net}$ .

### 4. Discussion of the Stability of Vibration Graphs

The only features which the stability graphs have in common is the occurrence of  $\Sigma_{max}$  near resonant conditions and the instability in the frequency when removed from resonant conditions. Near resonance the vibration is apparently forced to resemble most a harmonic vibration on account of the large inertia forces involved.

Test Plates	#16	#11	#15	#12
Maximum Amplitude $(\frac{2a_0}{t})_{max}$	0.159	0.155	0.033	0.002
Relative Max. Ampl. in %	100 %	97 %	21 %	1.3 %
$\Sigma_{max} \times 100 \%$	87 %	59 %	85 %	44 %
Instability in net circulation in terms of $\Delta \Sigma_{max} \times 100 \%$	6 %	8 %	35 %	71 %

Table 9. Comparison of Stability Graphs

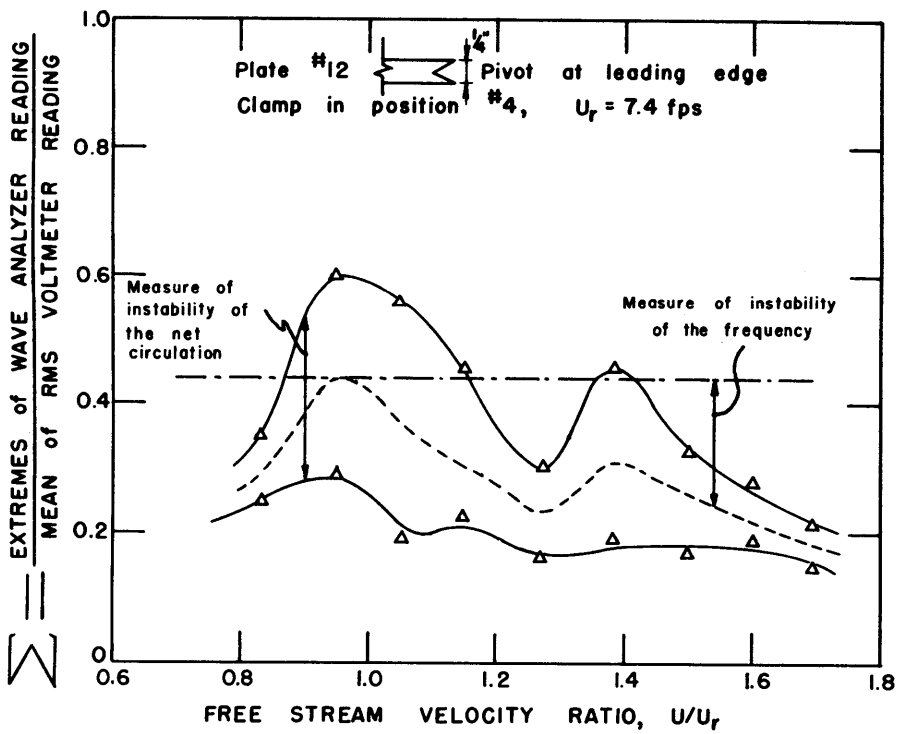


Figure 26. Stability Graph for Plate #12

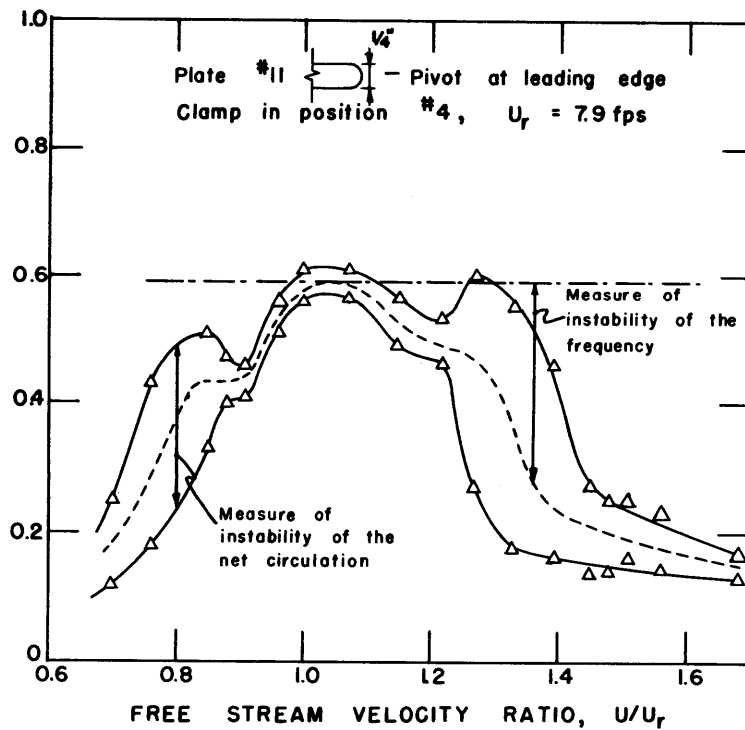


Figure 25. Stability Graph for Plate #11

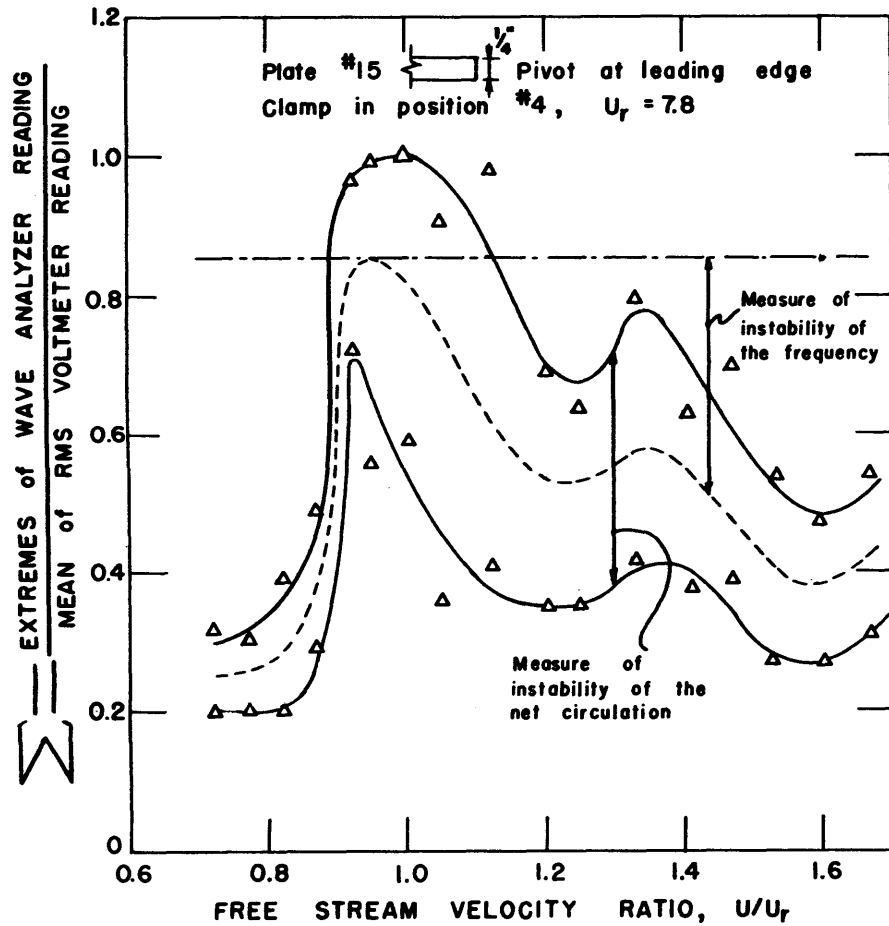


Figure 27. Stability Graph for Plate #15

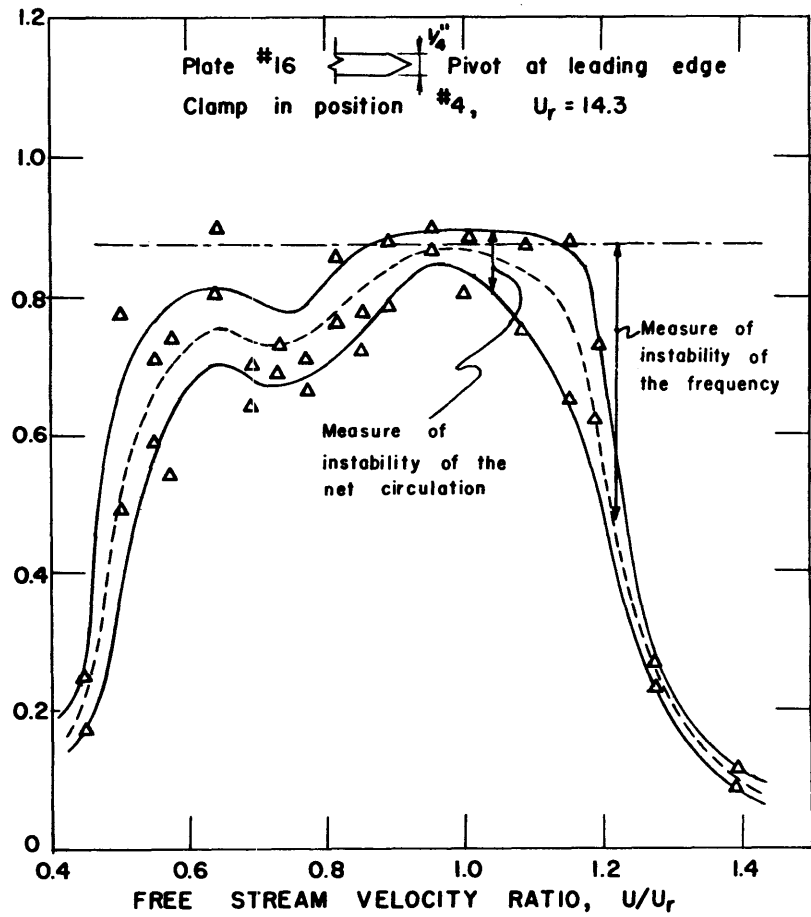


Figure 28. Stability Graph for Plate #16

Off resonance the motion seems to lose control over the wake structure, which most likely assumes an increasingly three dimensional and turbulent character. The randomness of the latter is considered to be reflected in the instability or random variation of the vibrational frequency.

In other respects the curves in Figures 25 through 28 are as different from each other as their associated amplitude response curves are dissimilar. The values  $\Sigma_{\max}$  vary appreciably. A value of  $\Sigma_{\max}$  approaching unity would indicate a purely harmonic vibration. Values less than unity point to the presence of higher harmonics near resonance. It would be expected that high values of  $\Sigma_{\max}$  are associated with larger amplitudes of motion in view of the larger elastic and inertia forces involved. Table 9 shows, however, that this correlation does not exist. An explanation is not immediately obvious.

Perhaps the most conclusive feature of the stability graphs is the correlation, found in Table 9, between stability of net circulation and large amplitudes of motion. During the tests it had already been noticed that at resonance the amplitude of plate #15 varied rapidly and regularly, whereas the frequency of vibration remained practically constant. It looked as if the plate motion excited itself at one moment and lost control over its wake at the next instant. In contrast to the easily excited plates #11 and #16 for which the trailing edge between the separation points extends somewhat into the wake, no such extension is present for plate #15. Growing transverse motion will increase the local velocities near the separation points resulting in increased instability of the separating shear layers. Apparently the plate extension into the early wake counteracts the growing instability of the free shear layers by furnishing them with transverse support. This support tends to keep the wake two dimensional whereas for plate #15 the building up of the motion ends in a breakdown of the two dimensional wake structure. Such an inherent instability of the vibrational amplitude is clearly shown by the stability graph for plate #15.

For the plate #12 the stability graph points to a maximum of instability at resonant conditions. The reasoning given for plate #15 need not necessarily apply for plate #12. There exists a difference of an order of magnitude between the exhibited amplitudes of vibration for these two plates. The relation to the argument of Heskestad and Olberts (63) about a counter circulation of the fluid in the groove of the trailing edge, is not obvious.

#### F. Maximum Vibrational Amplitudes.

##### 1. Comparison of the Maximum Vibrational Amplitudes

All maximum (double) amplitudes, which obtained during resonant conditions, are presented in Table 10, column 7, in terms of the plate thickness  $t = 0.250''$ .

Immediately apparent are the great differences (up to a hundredfold) between the listed amplitudes. The table clearly indicates that these differences are mainly a function of the trailing edge geometry.

When the plates are grouped in order of increasing vibrational amplitudes the same sequence obtains as was found for the 1/8" test plates (compare Tables 3 and 9).

The resonant frequencies,  $f_r$ , associated with the maximum amplitudes closely matched the natural frequency,  $f_n$ , of the test plate assembly in all cases where the mounting permitted rotation around the leading edge (see column 5 of Table 10).

## 2. Maximum Vibrational Amplitudes as a Function of Restraint

When the restraint of the test plates becomes very large, the amplitude of vibration may be expected to approach zero. If no restraint were present there would be no mechanism for the storage of kinetic energy which would again produce a negligible maximum amplitude response. Conceivably there exists an intermediate stiffness for which the amplitudes become a maximum. To answer this question Figure 29 was prepared which presents the resonant amplitudes (Table 10, column 7) as a function of support stiffness (Table 10, column 4) for each of the test plates.

Attention is drawn to the values in Table 10 denoted by asterisks, associated with the "free" case for which no "resonant" velocity nor frequency exists. In order to show the expected trend for stiffnesses which approach zero a small restraint,  $k = 0.10 \times 10^{-3}$  lb.in/rad, was arbitrarily selected for the free case and a characteristic vibrational amplitude for this case was chosen at a free stream velocity between the resonant velocities for clamping positions 4 and 5. These characteristic amplitudes were obtained from a test series on the unclamped plate.

Figure 29 indeed shows that for each of the plates there will be a critical stiffness for which the amplitudes will be a maximum for a given velocity.

It appears that there is little difference in amplitude between plates #11, #15 and #16 when the stiffness approaches zero. For increasing  $k$ , however, plates #11 and #16 are excited to amplitudes which are more than fifteen times as large as those for plate #15.

The amplitudes for plate #12 for  $k$  approaching zero are about 1/10th of those of plate #15. In particular considering the plate amplitudes for  $k \rightarrow 0$  it appears as if the particular trailing edge shape involved reduces the amplitude of motion below a more usual value. In this regard a suggestion by Heskestad and Olberts (63) is recalled concerning the relative slight vibration of a plate with a trailing edge geometry similar to plate #12. The idea was expressed that the fluid in the groove between the separation points always possessed a circulation which would be out of phase with the net circulation. This suggestion cannot be checked presently but it is not contradicted by the test results.



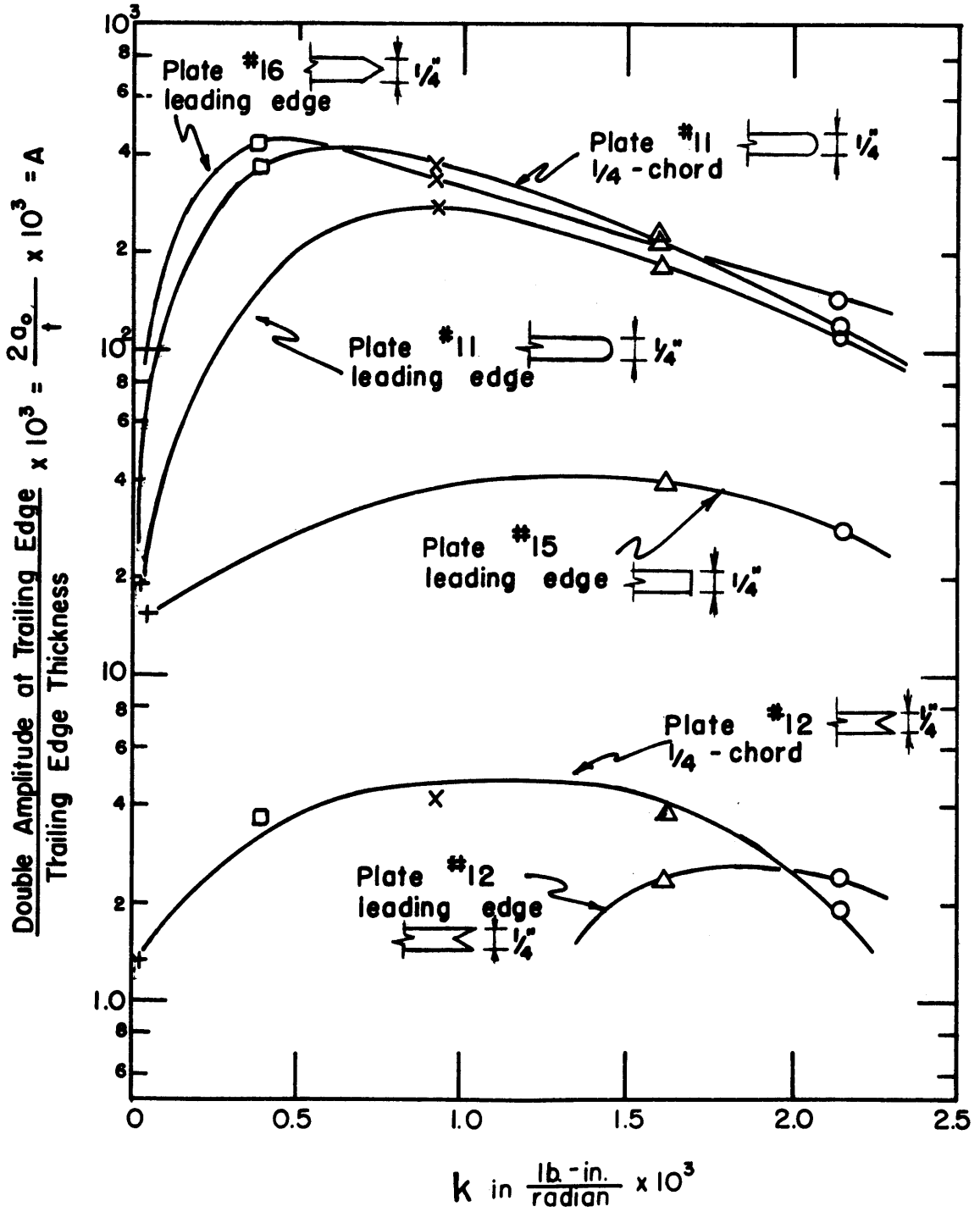


Figure 29. Maximum Amplitude as Function of Restraint

### 3. Influence of the Location of the Axis of Plate Rotation

A shift in the location of the axis of rotation will have two effects:

- a. modification of the boundary layer,
- b. modification of the magnitude of the forcing moment.

In particular the second effect may be expected to influence the maximum amplitude of vibration. This has been investigated for the case where the test plates were allowed to rotate around the 1/4-chord line.

When the axis of rotation does not coincide with the center of the semi-cylindrical leading edge, the stagnation point shifts continuously when the test plate vibrates. This likely results in boundary layer waves originating at the leading edge at a frequency equal to that of the plate vibration. It is conceivable that this influences both the Strouhal number and the magnitude of the forcing moment,  $M_V$ , associated with the vortex formation at the trailing edge.

Table 10 shows that Strouhal numbers for the 1/4-chord cases are somewhat larger than those for which rotation around the leading edge was permitted.

The effect of boundary layer disturbances on  $M_V$  cannot be separated from the consideration of the changes in the relative contributions to the net moment of the lift forces,  $L_V$ ,  $L_C$ , and  $L_{n.c.}$  (see Chapter IV) due to the shift in the axis of rotation. In order to consider these changes it is necessary to rewrite the Eq. [43] as follows:

$$\begin{aligned}
 I_{1.e.} \ddot{\alpha} + (c - \frac{3}{2}\pi\rho Hb^3U) \dot{\alpha} + [k + \frac{1}{2}\pi\rho H.b^2(1-1.5S)U^2 \\
 - \frac{1}{3} XbG^1 H.B_3 \alpha^2 U^2/S + X bGH.B_3 e^{i2\omega t} U^2/S] \alpha \\
 = \frac{U^2}{S} Xb B_1 H.(M) e^{i\omega t}
 \end{aligned}
 \tag{46a}$$

or, restricting attention to one plate at a time and to the resonant condition so that  $G \approx \text{constant}$  and  $S_r \approx \text{constant}$ , this may be written as:

$$\begin{aligned}
 I_{1.e.} \ddot{\alpha} + (c-n_1U)\dot{\alpha} + [k + n_2U^2 - n_3X\alpha^2U^2 + 3n_3Xe^{i2\omega t}U^2] \alpha \\
 = n_4X(M)e^{i\omega t} U^2
 \end{aligned}
 \tag{46b}$$

Table 10. Vibration Characteristics of 1/4" plates at resonance.

Plate Pivot	Clamp #	$U_r$ fps	$f_r$ cps	$(\frac{f_r}{f_n})^{**}$	S	$S_r$	$(\frac{2a_0}{t})$	$(\frac{2a_{0t}}{t})$
1	2	3	4	5	6	7	8	9
#11 lead- ing edge	1	10.1	95.5	0.99	0.276	0.197	0.095	0.113
	4	7.9	81	1.00	0.275	0.214	0.155	0.184
	5	6.2	61	1.02	0.274	0.205	0.230	0.273
	7	(4.5)	(52)	----	0.270	-----	(.037)	(.044)
	free	6.9*	84*	----	0.280	-----	0.016	0.019
#11 1/4- chord	1	10.1	101	0.84	0.278	0.208	0.128	0.113
	4	9.0	93	0.90	0.274	0.216	0.250	0.222
	5	7.5	76	0.98	0.278	0.211	0.441	0.390
	7	5.5	56	1.10	0.268	0.212	0.403	0.356
#12 lead- ing edge	1	8.5	97	1.01	0.249	0.238	0.002	0.002
	4	7.4	82	1.01	0.249	0.231	0.002	0.002
	5	---	---	----	-----	-----	-----	-----
	7	---	---	----	-----	-----	-----	-----
	free	7.0*	82*	----	-----	-----	0.001	0.001
#12 1/4- chord	1	9.2	107	0.89	0.257	0.243	0.002	0.001
	4	8.3	100	0.97	0.256	0.250	0.004	0.004
	5	8.4	96	1.23	0.260	0.238	0.004	0.004
	7	7.4	87	1.71	0.260	0.245	0.004	0.004
#15 lead- ing edge	1	9.1	95.5	0.99	0.244	0.227	0.024	0.028
	4	7.8	83	1.02	0.250	0.222	0.033	0.039
	5	6.0	64	1.07	0.246	0.222	0.049	0.058
	7	---	---	----	-----	-----	-----	-----
	free	7.3*	79*	----	0.236	-----	0.032	0.038
#15 1/4- chord	1	9.3	103	0.85	0.274	0.231	0.014	0.012
	4	8.9	95	0.92	0.273	0.223	0.028	0.025
	5	7.8	85	1.09	0.280	0.227	0.040	0.035
	7	---	---	----	-----	-----	-----	-----
#16 lead- ing edge	1	16.8	96.5	1.00	0.141	0.120	0.118	0.140
	4	14.3	81	1.00	0.141	0.118	0.159	0.189
	5	11.0	61.5	1.02	0.134	0.117	0.294	0.350
	7	7.9	43	1.05	0.135	0.114	0.362	0.430
	free	12.5*	170*	----	0.142	-----	0.017	0.020
#16 1/4- chord	1	16.0	98	0.81	-----	0.128	0.104	0.093
	4	---	---	----	-----	-----	-----	-----
	5	14.5	80	1.02	-----	0.115	0.360	0.321
	7	9.6	56	1.12	-----	0.121	0.366	0.326

\* a value of free series for which  $U_{r5} < U < U_{r4}$ .

\*\* for determination of  $f_n$  values see Appendix C.

in which  $n_1 = \text{constant}$ , valid for rotation around the leading edge. The comparable equations for a plate pivoted around the  $l/4$ -chord are:

$$I_{l/4} \ddot{\alpha} + (c - n_1 U) \dot{\alpha} + [k - \frac{1}{3} X_1 b_{HGB} a^2 U^2 / S + X_1 b_{HGB} e^{i2\omega t} U^2 / S] \alpha = \frac{U^2}{S} X_1 b_{B_1 H} (M) e^{i\omega t} \quad [47a]$$

and:

$$I_{l/4} \ddot{\alpha} + (c - \frac{2}{3} n_1 U) \dot{\alpha} + [k - n_3 X_1 a^2 U^2 + 3n_3 X_1 e^{i2\omega t} U^2] \alpha = n_4 X_1 (M) e^{i\omega t} U^2 \quad [47b]$$

in which  $X_1 = X - \frac{1}{2}$ ;  $M = a_s + Ga_1 A_1^i - \frac{1}{3} Ga_1^3 A_1^3$ ;  $A_1^i \approx e^{-i\omega t}$

The maximum amplitudes of vibration, ( $A_1^i$ ), depend mainly on the damping leading to the approximate expressions:

$$\text{leading edge: } (c - n_1 U) \omega = n_4 MU^2 / A_1^i \quad [48a]$$

$$l/4\text{-chord: } (c - \frac{2}{3} n_1 U) \omega = n_4 MU^2 / A_1^i \quad [48b]$$

However, substitution of experimental values in order to verify Eqs. [48] and to determine  $a_1$ , led to inconsistent results and apparently shows that the simplification given by Eqs. [48] is impermissible for the non-linear equations [46] and [47]. Also, as in the linear case, the maximum amplitude depends critically on the damping when this is small. In the present case the exact value of the damping is unknown.

From Eqs. [46] and [47] also an approximate expression may be deduced for the resonant frequency  $f_r$ :

$$(f_r)_{l.e.} \approx \frac{1}{2\pi} \left[ \left( k + n_2 U^2 - n_3 X a^2 U^2 \right) / I_{l.e.} \right]^{1/2} \quad [49a]$$

$$(f_r)_{l/4} \approx \frac{1}{2\pi} \left[ \left( k - n_3 (X - \frac{1}{2}) a^2 U^2 \right) / I_{l/4} \right]^{1/2} \quad [49b]$$

Recalling that:  $f_n \approx \frac{1}{2\pi} \left[ \frac{k}{I} \right]^{1/2}$  and using from Table 10 the result that  $S_r = f_r \cdot t' / U_r \approx \text{constant}$  for each plate, there follows for the ratios  $f_r / f_n$  for a particular trailing edge:

$$(f_n/f_r)^2_{l.e.} = 1 + (n_2^1 - n_3^1 X \alpha^2_{l.e.})/I_{l.e.} \quad [50a]$$

$$(f_n/f_r)^2_{\frac{1}{4}} = 1 - \frac{7}{4} n_3^1 (X - \frac{1}{2}) \alpha^2_{\frac{1}{4}}/I_{l.e.} \quad [50b]$$

Since  $\bar{\alpha}^2$  is found to increase when  $k$  and  $U_r$  decrease and assuming that  $X \approx$  constant, it may be expected from Eq. [50] that  $f_r/f_n$  will increase when  $U_r$  decreases. With the exception of plate #15, column 8 of Table 10 shows that  $\alpha^2_{l.e.} < \alpha^2_{\frac{1}{4}}$  so that, according to Eq. [50],  $(f_r/f_n)_{\frac{1}{4}}$  should

increase with decreasing  $U_r$  at a faster rate than  $(f_r/f_n)_{l.e.}$

These expected trends are indeed borne out by the values for  $f_r/f_n$  in column 5 of Table 10, and confirm the formulated non-linearity in the equations of motion.

#### 4. Self-excitation of the Plate Vibration

The amplitude response curves for plate #16 have been compared qualitatively (see Figure 21) with the theoretical response curve for a single degree of freedom spring mass system with a damping of  $c/c_c = 0.05$  (i.e., approximately the viscous damping for the test plate - torsion spring system). This is the model to which the common explanation of vortex induced vibrations refers.

That theoretical response curve, given by a dashed line, would obtain if the exciting force were constant. In order to produce a theoretical response curve having the shape of the experimental curves it would be necessary for the forcing force to increase markedly near resonance.

At the same time the proximity of the natural frequency of the system will have resulted in increased amplitudes of motion. It appears that, depending on trailing edge geometry, increased lift forces are associated with a growth in vibrational amplitude or in other words: the motion may excite itself.

The element of self-excitation seems particularly clear in the amplitude response curves for plates #11 and #16 (Figures 18, 21 and 23). Also the step in the Strouhal graphs (Figures 12, 13 and 16) show that the wake structure is governed by the plate motion rather than the wake dynamics prevailing when the object is steady. The latter condition would have been reflected in a constancy of the Strouhal Number.

#### G. Reduced Amplitude Response Curves.

##### 1. Amplitude Response Curves as Function of Velocity

The amplitude response curves as given in Figures 18 through 21, and 23 are presented in a fashion which is significant from a practical point

of view as well as informative of the hydroelastic elements involved in the vibration.

In particular for plate #16 it was seen that, when  $\omega = \omega_n$ , severe vibration occurred over a very wide range of velocities. It appears that the frequency of vortex shedding may attach itself to the motion of the plates to a degree which depends on the trailing edge geometry. This fact is of obvious importance in the design for vibration control. It also indicates that the simple linear relation between the frequency of the forcing moment and the free stream velocity,  $U$ , expressed by the constancy of the Strouhal number,  $S$ , is not valid for larger motions.

Even if  $S$  remained constant the forcing function would, according to Eq. [22], depend on  $U^2$ . This further complicates the shape of the amplitude response curves.

## 2. Reduction of the Amplitude Response Curves

If the influence of the plate motion on the wake structure, expressed by Eq. [43], is indeed an important one it should be possible to show some similarity in the observed amplitude response curves for the various plates tested.

To this end the effect of deviations from the Strouhal relation (which are strongly dependent on trailing edge geometry) as well as the increase in the forcing moment (proportional to  $U^2$  according to Eq. [22]) were eliminated. After division of the amplitude values by a factor proportional to  $U^2/S$ , the amplitudes thus reduced were replotted as a function of frequency of plate vibration rather than velocity.

The reduced amplitude response curves are presented in Figures 30 through 33. It is seen that the mutually quite dissimilar amplitude curves given in Figures 18 through 21 and 23 can be reduced to a set of curves of similar shape.

## 3. Similarity of the Reduced Amplitude Response Curves

The similarity between the reduced amplitude curves resembles well the typical deviation from the response curve of a linear system indicated in Figure 10d. This can be taken as a confirmation that for the present vibrations the equation of motion will resemble the formulated relation, Eq. [43].

This does not mean that Eq. [43] is complete. A number of factors, such as the Reynolds number and the boundary layer thickness at the trailing edge,  $\delta_t$ , were not accounted for in the formulation. However, the resonant velocity for plate #16 ( $U_r = 14.3$  fps) happened to be almost twice the  $U_r$  ( $U_r = 7.6$  fps) which obtained for other plates with the same restraint (Clamp #4). This provides a relatively small change in  $R_g$ , and since  $\delta_t \propto U^{-1/2}$  (the boundary layer transition is estimated to occur at the trailing edge for  $U_r > 30$  fps) a still smaller variation in  $\delta_t$  thus

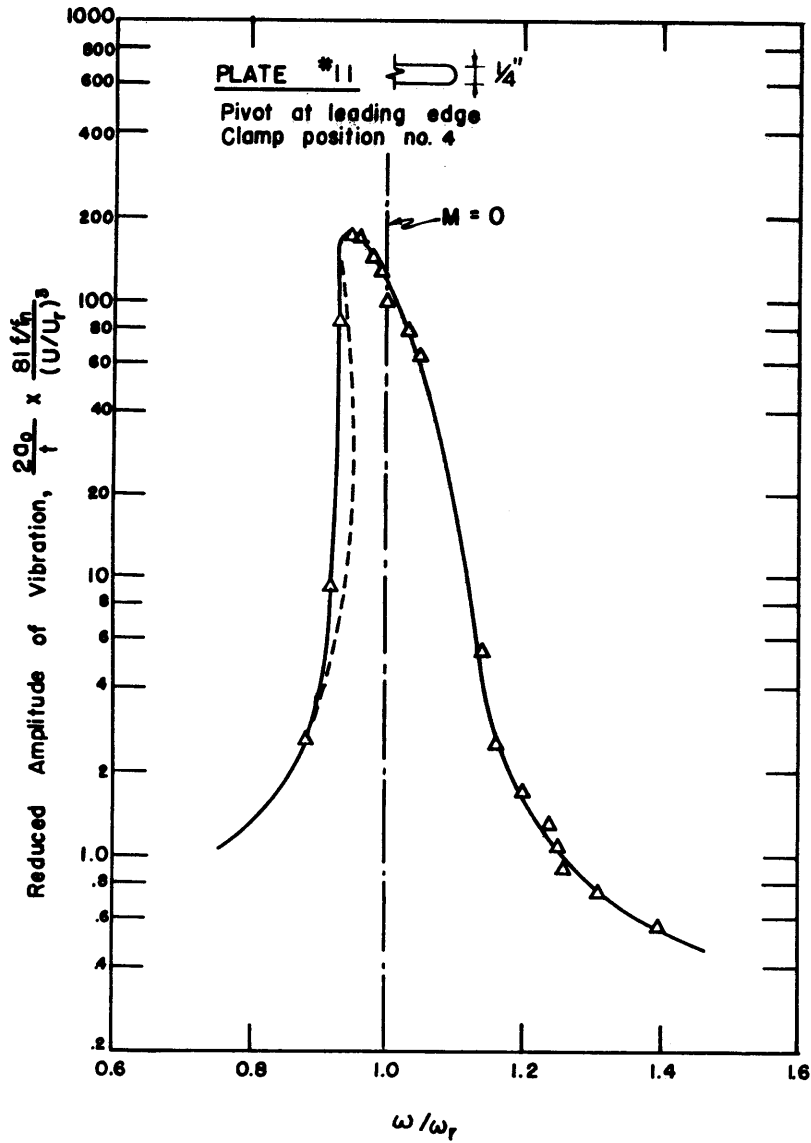


Figure 30. Reduced Amplitude Response Curve for Plate #11

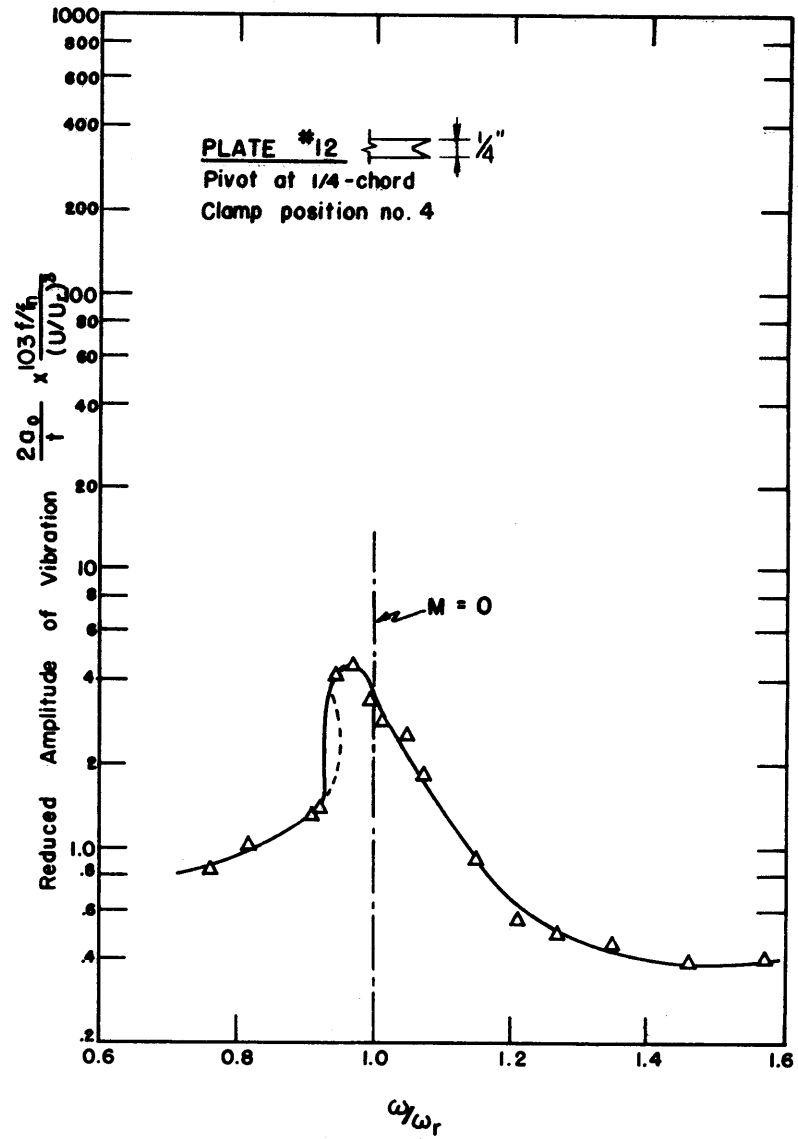


Figure 31. Reduced Amplitude Response Curve for Plate #12

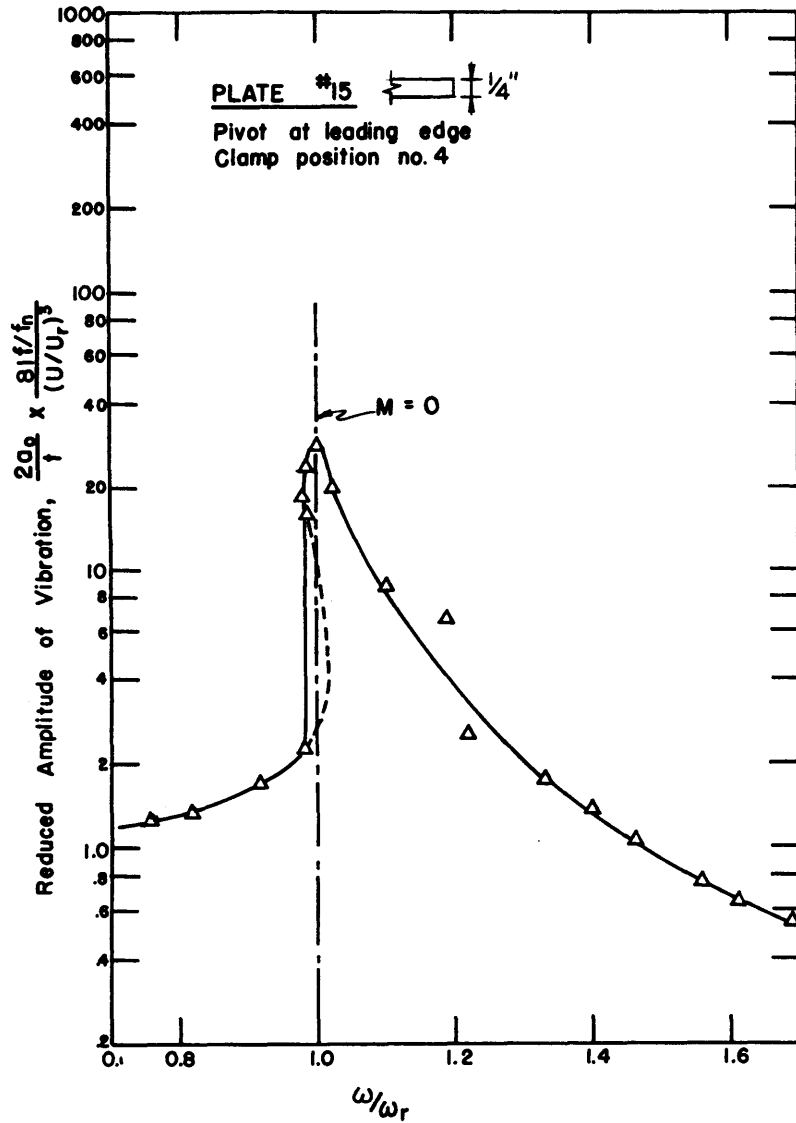


Figure 32. Reduced Amplitude Response Curve for Plate #15

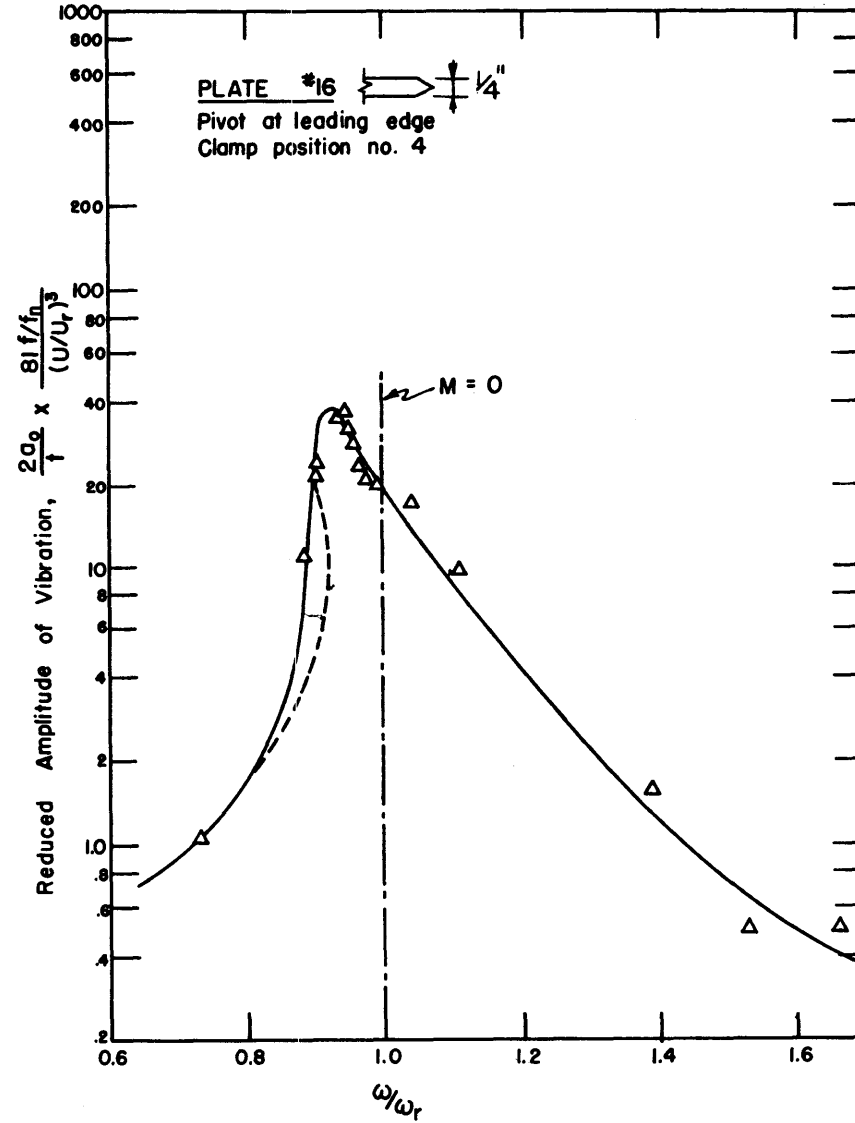


Figure 33. Reduced Amplitude Response Curve for Plate #16



no general conclusions can be drawn however it appears that these factors do not constitute a primary variable of the problem.

It may not be concluded, however, that boundary layer considerations would be of little importance. The contrary has been implied by the formulation in Table 1 which links vortex shedding to a "pulsating discharge of the boundary layer" into the wake. Fortunately it appears that unsteady boundary layer calculations are not essential to obtain a unified presentation of experimental results.

Also the reduced amplitude response curve for plate #12 which was pivoted at the  $1/4$ -chord point shows that the non-linearity indicated by the response curves is not primarily due to the circulatory lift force of potential origin, since the center of pressure of this lift force is at the  $1/4$ -chord.

This does leave the possibility that the apparent mass force is a function of vibrational amplitude due to (assumed) oscillations in the boundary layer flow.

## VI. CONCLUSIONS AND RECOMMENDATIONS

### A. Summary and Conclusions

The vibrational behavior of thin plates has been studied at zero mean angle of attack in water. The effects on this behavior of trailing edge geometry, geometric and elastic properties of the plate support, free stream velocity and ambient pressure intensity have been explored experimentally.

The usual model advanced in explanation of vortex induced vibrations involves the acceptance of a unique relationship between free stream velocity and vibrational frequency and reference to von Karman's analysis of the vortex street. It has been shown that this is a simplification which fails to direct attention toward basic facets of the problem.

An equation of motion has been written for the test plate - torsion spring system employed and qualitative analysis of this non-linear equation provides theoretical justification for many of the experimental results obtained.

The following conclusions may be drawn from these investigations:

1. The vibration phenomenon studied is associated with the periodic formation of vortices at the trailing edge of the plates.
2. Although the frequency of severe vortex induced vibrations is confined to a narrow range of frequencies near a natural frequency of the structural system, resonant amplitudes may persist over a wide range of free stream velocities.
3. Severe vortex induced vibrations are self-excited rather than forced vibrations.
4. These vortex induced vibrations are to be regarded as a hydroelastic phenomenon.
5. Severe vortex induced vibrations of blade shaped structural elements at small angles of attack are primarily a function of trailing edge geometry.
6. A theoretical understanding of vortex induced vibrations should be based upon the mechanics of vortex growth and discharge at the trailing edge, i.e., the dynamics of the "early" wake, rather than on the consideration of a periodic wake such as a vortex street.
7. An explanation for the large and seemingly inconsistent variation in the amplitude of plate vibration with change in trailing edge geometry is to be based upon the following factors:

- a. differences in the degree to which the separating shear layers annihilate each other;
  - b. differences in the degree to which two-dimensionality of the "early wake" is enhanced by transverse motions of the trailing edge.
8. The formulated equation of motion for the mechanical system employed is non-linear and indicates possible instabilities of the solution. These deduced behaviors are verified by analysis of the experimental data.
  9. The frequency of vortex formation during small test plate motions (i.e., "off-resonance") is unstable and hovers around a mean value indicated by the Strouhal number.
  10. Vibrations in a higher mode of the structural system may be more critical than those in the fundamental mode excited at a lower velocity.
  11. In the absence of visible cavitation the ambient pressure level has no apparent effect on vortex induced vibrations.

#### B. Recommendations for Practical Applications

1. In the design for vibration control the trailing edges of blade shaped objects should be well streamlined and faired out to a negligible thickness. In this case (at least at small angles of attack) the separating shear layers annihilate each other rather than give rise to a periodic formation of discrete vortices. The necessary minimum thickness may depend on the local boundary layer thickness.
2. In case well faired trailing edges are undesirable for structural reasons it is recommended that a groove be provided for in the trailing edge of blade shaped objects. This geometry exerts, during transverse plate motions, the least stabilizing influence on the inherently unstable free shear layers; two-dimensional wake conditions and hence a large net lift force are therefore less readily attained than with other non-streamlined trailing edge geometries.

#### C. Recommendations for Future Experiments

1. In some instances the reproducibility of test results as far as the amplitude of resonant vibration is concerned, was poor. This is attributed in part to variations in the mechanical damping present in the system. It is recommended that future experiments, aimed at a quantitative evaluation of the forces acting on vibrating plates, should provide for accurately predetermined values of the damping coefficient.
2. In order to investigate the presumed two- and three-dimensionality of the wake structure as a function of trailing edge geometry and vibrational amplitude, it is recommended that a correlation study be made at two points along the trailing edge, of the magnitude and phase of the velocity fluctuations just downstream of the early wake.

## VII. BIBLIOGRAPHY

1. Den Hartog, J.P.: "Recent Technical Manifestations of von Karman's Vortex Wake", Proc. Nat'l. Acad. Sci., Vol. 40, 155-157, 1954.
2. Dickey, W.L., and Woodruff, G.B.: "The Vibrations of Steel Stacks", ASCE Trans. Vol. 121, Paper No. 2831, 1055-1087, 1956.
3. Ozker, M.S. and Smith, J.O.: "Factors Influencing the Dynamic Behavior of Tall Stacks Under the Action of Wind", ASCE Paper No. 55-A-69, 1955.
4. Baird, R.C.: "Wind-Induced Vibration of a Pipe-Line Suspension Bridge, and its Cure", ASME Trans., Vol. 77, No. 6, August 1955.
5. Housner, G.W.: "Bending Vibrations of a Pipe Line Containing Flowing Fluid", J. Applied Mech., 19, 205-208, 1952.
6. Grimminger, G.: "The Effect of Rigid Guide Vanes on the Vibration and Drag of a Towed Circular Cylinder", David Taylor Model Basin Report 504, April 1945.
7. Price, P.: "Suppression of the Fluid-Induced Vibration of Circular Cylinders", Proc. ASCE, Paper 1030, July 1956.
8. Krall, G.: "Forced or Self-Excited Vibration of Wires", Proc. 7th Intern. Congr. Appl. Mech. 4, 221-225, 1948.
9. Penzien, J.: "Wind-Induced Vibration of Cylindrical Structures", Proc. ASCE, Paper 1141, January 1957.
10. Scruton, C.: "Wind-Excited Oscillations of Tall Stacks", The Engineer (London), Vol. 199, 806-808, 1955.
11. Work, C.E.: "Review of Marine Propeller Noise and Vibration Studies", U.S. Naval Ordnance Test Station and Propulsion Memo., 74, 1950.
12. Lankester, S. G. and Wallace, W.D.: "Some Investigations into Singing Propellers", N.E.C. Trans. Vol. 71, 291-318, April 1955.
13. Hunter, H.: "Singing Propellers", Trans. N.E.C. Inst. Eng. and Shipbuilders, 53, 189, 1936-37.
14. Conn, J.F.C.: "Marine Propeller Blade Vibration", Inst. of Eng. and Shipb. in Scot., 225-255, 1939.
15. Shannon, J.F. and Arnold, R.M.: "Statistical and Experimental Investigations on the Singing Propeller Problem", Trans. Inst. Eng. Shipb. Scot., Vol. 82, 256, 1939.
16. Davis, A.W.: "Characteristics of Silent Propellers", Inst. Eng. and Shipb. Scot., 83, 29-66, 1939.
17. Hughes, G.: "On Singing Propellers", Trans. Inst. Nav. Arch., Vol. 87, 1945.
18. Gutsche, F. von: "Geraus- und Tonerzeugung an Schiffschrauben", Schiff und Hafen, 3, 166-175, 1957.
19. Kito, F.: "in Zozenkyokai Zassen", 277, May 1948. See N.F.C. Inst. of Eng. and Shipb., 71, D 98, 1955.
20. Gongwer, G.A.: "A Study of Vanes Singing in Water", J. of Appl. Mech., Vol. 19, No. 4, 1952.

21. Krivtsov, Y.V. and Pernik, A.J.: "The Singing of Propellers", DTMB Translation 281, 1958.
22. Hughes, W.L.: "Propeller Blade Vibrations", N.E.C. Inst. Eng. and Shipb. Scot. 65, 273, 1949.
23. Burrell, L.C.: "Underwater Propeller Vibration Tests", N.E.C. Inst. Eng. and Shipb. Scot. 65, 301, 1949.
24. Hollingdale, S.B.: "Stability and Configuration of the Wakes Produced by Solid Bodies Moving through Fluids", Phil. Mag. 29, 209-257, 1940.
25. Strouhal, V.: "Über eine besondere Art der Tonerregung", Annalen der Physik, Vol. 5, 216, 1878.
26. Benard, H.: "Formation de centres de giration a l'arriere d'un obstacle an mouvement", Comp. Rend., Acad. Sci. (Paris) t. 147, 839-842, November 9, 1908.
27. Kovasznay, L.S.G.: "Hot Wire Investigation of the Wake behind Cylinders at low Reynolds Numbers", Proc. Roy. Soc. London, A. 198, 147, 1949.
28. Roshko, A.: "On the Development of Turbulent Wakes from Vortex Streets", NACA Report 1191, 1954.
29. Den Hartog, J.P.: "Vibration: A Survey of Industrial Applications", The Inst. of Mech. Eng., Forty-fourth Thomas Hawksley Lecture (Advance copy, November 1957).
30. Pagon, W.W.: "What Aerodynamics can Teach the Civil Engineer", Engineering News Record, March 15, 1934.
31. Dockstader, E.A. et al: "Resonant Vibration of Steel Stacks", ASCE, Separate No. 541, 1954.
32. Camiechel, C. and Teissie-Solier, M.: "Influence d'une perturbation sur le sillage en regime de Poiseuille d'un corps immerge", Comptes rendus 200, 704, 1935.
33. McGregor, D. M.: "An Experimental Investigation of the Oscillating Pressures on a Circular Cylinder in a Fluid Stream", University of Toronto, A.T.N. 14, 1957.
34. Gerrard, J.H.: "Measurement of the Fluctuating Pressure on the Surface of a Circular Cylinder", Aeronautical Research Council, 19, 844-F.M. 2637, 1958.
35. Richards, G.J.: "An Experimental Investigation of the Wake Behind an Elliptic Cylinder", Proc. Roy. Soc. London, Ser. A, Vol. 197, no. 1048, May 1949.
36. Fage, A. and Johansen, F.C.: "On the Flow of Air Behind an Inclined Flat Plate of Infinite Span", R. and M. No. 1104, British A.R.C., 1927.
37. Nøkkentved, C.: "Vibrations Produced by Wind", Publ. by Dansk Selskab for Bygningsstatic, Vol. XII, No. 3, Copenhagen, 1941.
38. Delany, N.K. and Sorensen, N.E.: "Low Speed Drag of Cylinders of Various Shapes", NACA, TN 3038, November 1953.
39. Shaw, R.A.: "An Explanation of Vortex Shedding on the Basis of Pulses Traveling at the Speed of Sound", Aeronautical Research Council 18, 455, F.M. 2406, 1956.

40. Fage, A. and Johansen, F.C.: "The Structure of Vortex Streets", R. and M. No. 1143, British A.R.C., 1927.
41. Fage, A.: "The Air Flow Around a Circular Cylinder in the Region Where the Boundary Layer Separates from the Surface", R. and M. No. 1179, British A.R.C., 1928.
42. Schiller, L. und Linke, W.: "Druck- und Reibungswiderstand des Zylinders bei Reynoldsschen Zahlen 5000 bis 40000", Zeits. für Flugtechn. und Motorl. 24-27, 1933.
43. Goldstein (editor): "Modern Developments in Fluid Mechanics", Oxford, Clarendon Press, 1938.
44. Petrikat, K.: "Oscillations of Weirs", Deutsche Wasser-Wirtschaft, 1941.
45. Makovsky, M.S.: "Vortex Induced Vibration Studies", DTMB Navy Dept., Report 1190, 1958.
46. Philips, O.M.: "The Intensity of Aeolian Tones", J. of Fluid Mech. Vol. 1, part 6, 607, 1956.
47. Lord Kelvin: "Vibrations of a Columnar Vortex", Phil. Mag. 10, 155-168, 1880.
48. Gutsche, F. von: "Singende Schiffsschrauben", Shiffbau, 110, 1937.
49. Helmholtz, H.: "Über discontinuierliche Flüssigkeitsbewegungen", Monatsber. Berlin, Akad., 215-228, 1868.
50. Kirchhoff, G.: "Zur Theorie freier Flüssigkeitsstrahlen", J. Reine Angew. Math. 70, 289-298, 1869.
51. Karman, Th. von: "Über den Mechanismus des Widerstandes den ein bewegter Körper in einer Flüssigkeit erfährt", Gott. Nachr. 547-556, 1912.
52. Karman, Th. von; and Rubach, M.: "Über den Mechanismus des Flüssigkeits- und Luftwiderstandes", Phys. Zeit. 13, 49-59, 1912.
53. Prandtl, L. and Tietjens, D.G.: "Applied Hydro- and Aero-Elasticity", Dover Press, 1957.
54. Schmieden, C.: "Zur Theorie der Karmanschen Wirbelstrasse", Ing. Archiv. 7, 215-221, 1936.
55. Birkhoff, G.: "Formation of Vortex Streets", J. Applied Physics, 24, 98-103, 1953.
56. Heisenberg, W.: "Die absoluten Dimensionen der Karmanschen Wirbelbewegung", Phys. Zeit., 23, 363-366; comments by Prandtl p. 366, 1922.
57. Roshko, A.: "A New Hodograph for Free-streamline Theory", NACA T.N. 3168, 1954.
58. Roshko, A.: "On the Drag and Shedding Frequency of Two-dimensional Bluff Bodies", NACA T.N. 3169, 1954.
59. Jeffreys, J.: "The Wake in Fluid Flow past a Body", Proc. Roy. Soc. 128, 383, 1930.
60. Rosenhead, L.: "The Formation of Vortices from a Surface of Discontinuity", Proc. Roy. Soc. A, 134, 171-192, 1931.

61. Richardson, E.G.: "Flow and Sound Field near a Towed Cylinder", Appl. Sci. Res., A-7, 341-350, 1958.
62. Pankhurst, R.C. and Thwaites, B.: "Experiments on the Flow past a Porous Circular Cylinder fitted with a Thwaites Flap", Aer. Res. Council R.M. 2787, 1953.
63. Heskestad, G. and Olberts, D.R.: "Influence of Trailing Edge Geometry on Hydraulic-Turbine-Blade Vibration from Vortex Excitation", ASME, Paper No. 59-Hyd-7, May 1959.
64. Meier-Windhurst, A.: "Flatterschwingungen von Zylindern im gleichmazingen Flüssigkeitsstrom", Mitteil. Hydr. Inst., Techn. Hochschule, München, No. 9, 1939.
65. Chuan, R.L. and Magnus, R.J.: "Vortex Shedding as related to the Self-excited Torsional Oscillations of an Airfoil", NACA T.N. 2429, 1951.
66. Toebes, G.H., Perkins, F.E. and Eagleson, P.S.: "Design of a Closed Jet, Open Circuit Water Tunnel for the Study of Wake Mechanics", M.I.T., T.N. 3, April 1958.
67. Theodorsen, T.: "General Theory of Aerodynamic Stability and the Mechanism of Flutter", NACA Rept. 496, 1935.
68. Stoker, J.J.: "Nonlinear Vibrations in Mechanical and Electrical Systems", Interscience Publishers Inc. N.Y., 1950.
69. Lamb, H.: "Hydrodynamics", art. 71, 6th Edition, Dover Publications.
70. Bisplinghoff, R.L., Ashley, H. and Halfman, R.L.: "Aero-Elasticity", Addison-Wesley, Reading, Mass. 1955.

## APPENDIX A

### Hydraulic Characteristics of the Water Tunnel

#### 1. Calibration of the Contraction as a Velocity Meter

The pressure differential between the upstream and downstream end of the water tunnel contraction which exists under operating conditions, has been utilized for the continuous measurement of the mean velocity of flow in the test section. For this purpose the leads of two piezometer rings around both ends of the contraction have been connected through a manifold to manometers mounted on an instrument panel near the tunnel. In order to insure sufficient accuracy for the wide range of pressure differentials to be measured both a "water-mercury" and a "water-blue fluid" manometer were employed. The "blue fluid" is a blue colored Meriam No. D-8325 indicating fluid which has a specific gravity of 1.75.

A volumetrically calibrated 18" x 10" venturi meter, located in the header loop upstream of the tunnel, was selected as the standard of comparison for the calibration of the water tunnel contraction. In addition a previously calibrated Prandtl tube was inserted through the test section wall so that its tip was 6 inches downstream of the test section entrance. Simultaneous manometer readings allow calibration of the venturi meter and contraction in terms of the free-stream test section velocity as indicated by the Prandtl tube. This calibration is presented in Fig. A-1.

Figure A-1 also shows a curve for the contraction found from a computation based on the venturi meter discharge, the accurately known geometric dimensions of that tunnel component and an assumption of uniform velocity distribution. The extent of the disagreement between these computed and experimental values is an indication of the importance of viscous velocity profile modification in the test section.

In order to check variation of this viscous effect with Reynolds number, Figure A-2 has been prepared. No systematic trend is obvious in this plot, which furthermore is seen to yield for the contraction calibration the relationship:

$$U_0 = 1.018 \sqrt{2g\Delta h} \quad [A-1]$$

in which  $\Delta h$  is the deflection of the contraction manometer in feet of water and  $U_0$  is the average velocity in the test section.

The boundary layer displacement thickness in the test section at the location where the test plates are mounted is estimated to be 0.03" for  $U_0 = 10$  fps. By taking this effect into account the coefficient in Equation [A-1] becomes  $C = 1.019$ . In view of the experimental scatter in Figure 6 no such change of the coefficient seems warranted. Presuming uniformity of the flow,  $U_0$  in Equation [A-1] can thus be assumed to represent the maximum or free stream velocity in the test section at the location of the test plate mounting.



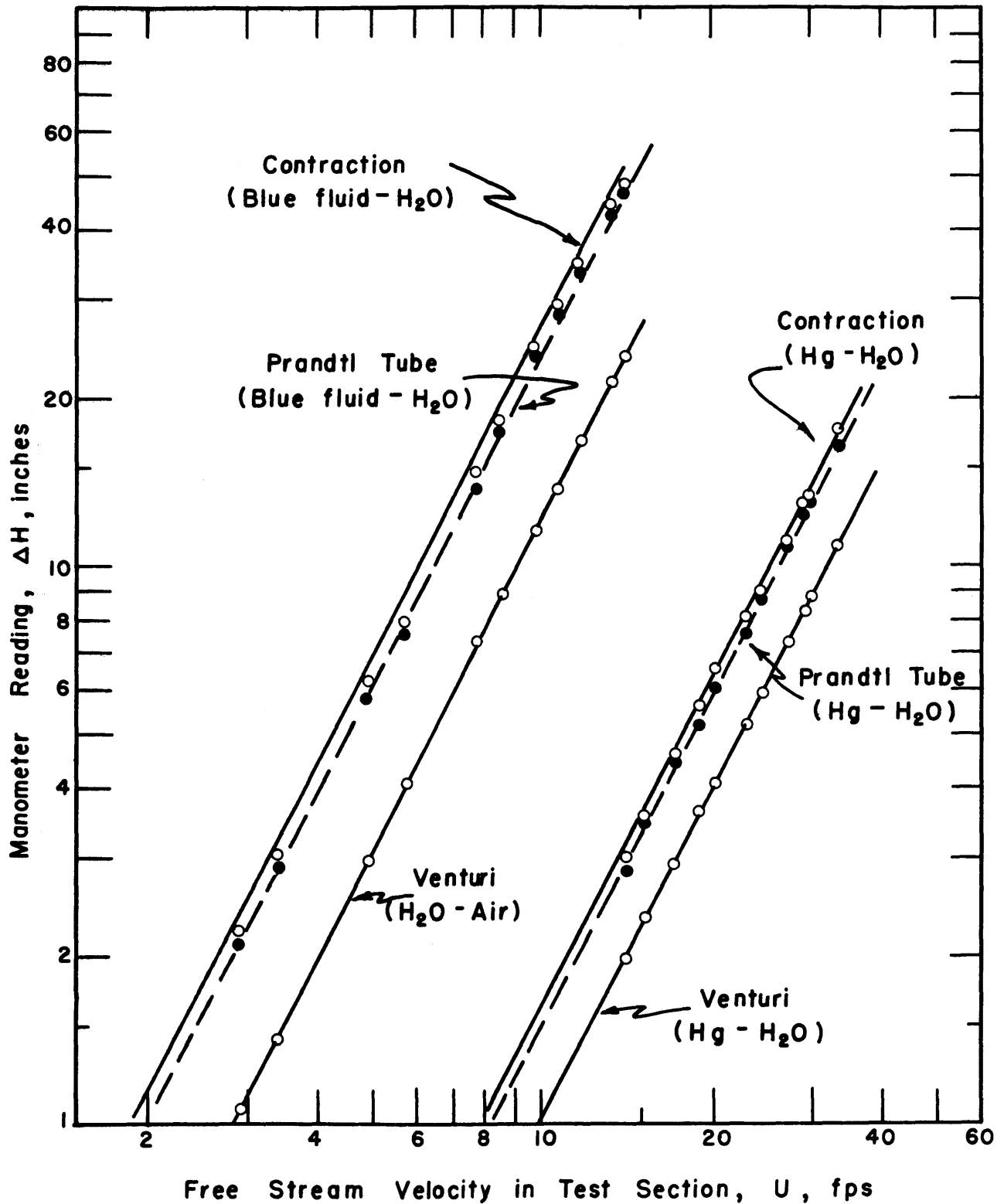


Figure A-1. Calibration Curves of Water Tunnel Contraction

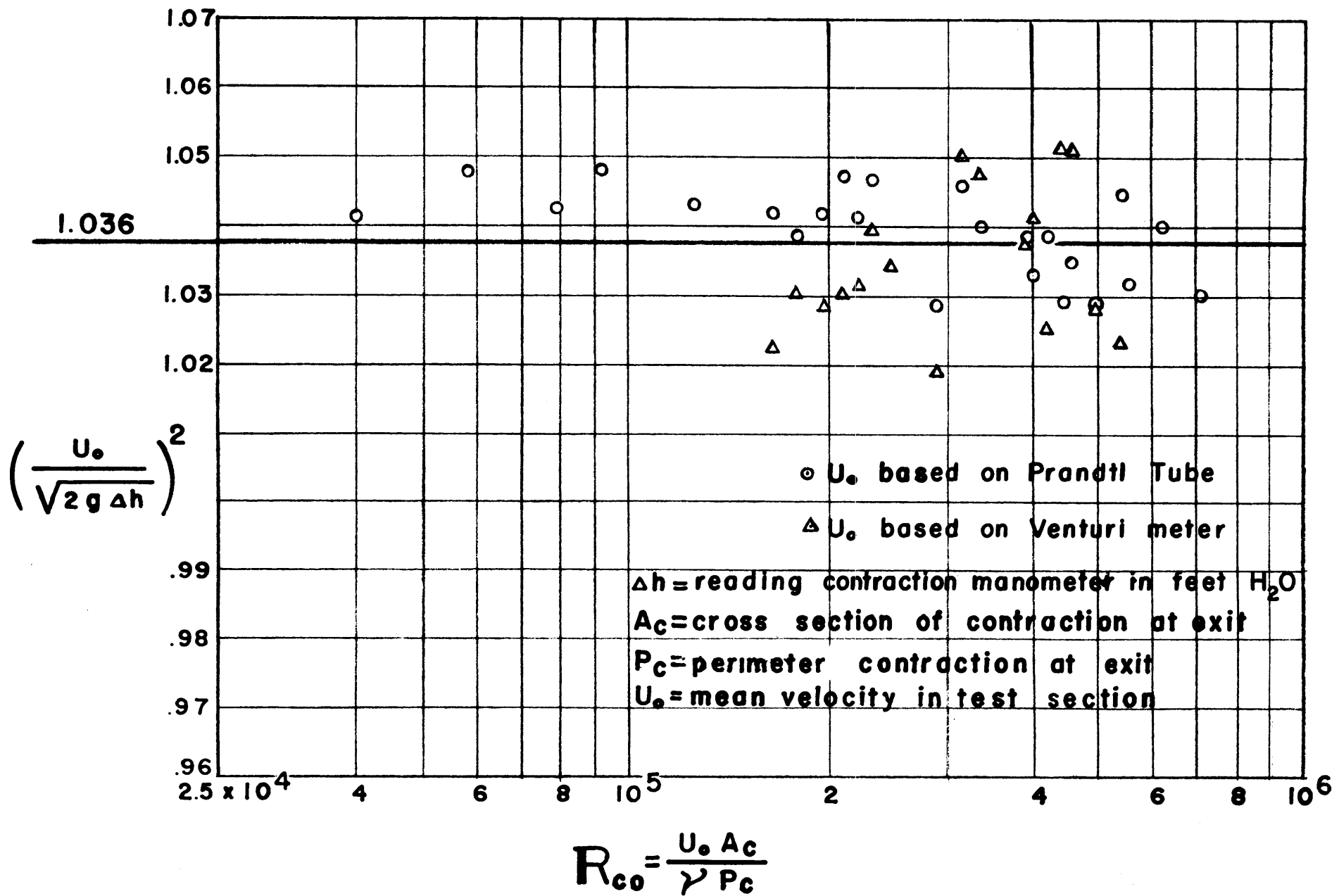


Figure A-2. Contraction Calibration Constant

## 2. Uniformity of Test Section Flow

Uniformity of the test section flow, which is a function of both the employed damping screens and the contraction design is a water tunnel characteristic of obvious importance. To investigate the tunnel performance in this respect the local mean velocities in a horizontal section of the test section have been carefully measured. To this end a pitot static tube with small tip dimensions and a traversing mechanism were constructed. The stem of the tube slides in a groove in the leading edge of a streamlined strut which spans the test section horizontally. The strut may be inserted through packing glands at any of the 9 pair of wall ports provided in the test section.

Velocity profiles in the mid-horizontal plane at each of two test section locations for average velocities of 3, 7, 18, 26 and 35 ft. per sec. are presented in Figures A-3 and A-4. The plots show, over a wide range of velocities, excellent uniformity of flow outside the boundary layer as well as the increase in boundary layer thickness in the downstream direction. The pitot static tube was subsequently calibrated against the contraction manometer from which was obtained

$$u = 1.00 \sqrt{2g\Delta h} \quad [A-2]$$

in which  $\Delta h$  is measured in ft. of water column and  $u$  is the local mean velocity in ft. per sec. at the location of the tip.

## 3. Ambient Pressures in the Water Tunnel

The operating pressure in the tunnel depends on the amount of flow and the opening of the foot valve at the downstream end of the structure. Operating pressures were measured by means of a pressure gage connected to the first elbow (see Figure 2). At that location an indication is obtained of excessive pressures which could damage the tunnel. This "elbow pressure" is one of the variables appearing in Figure A-5 in which the solid lines present the relation between pressure, foot valve opening and test section velocity based on a large number of systematic measurements. The graph depicts the range of tunnel operating characteristics: elbow pressures above 18 psig are unsafe structurally. For pressures below -4 psig the flow approaches zero whereas the maximum velocity in the (empty) test section is limited to 50 fps by the onset of cavitation in the diffuser.

Cavitation may occur on objects in the test section at free stream velocities well below 50 fps. For example, cavitation started on the pitot static tube at a cavitation index,  $\sigma$ , of about 2. The cavitation index is given by:

$$\sigma = \frac{P_0 - P_v}{\frac{1}{2}\rho U_0^2} \quad [A-3]$$

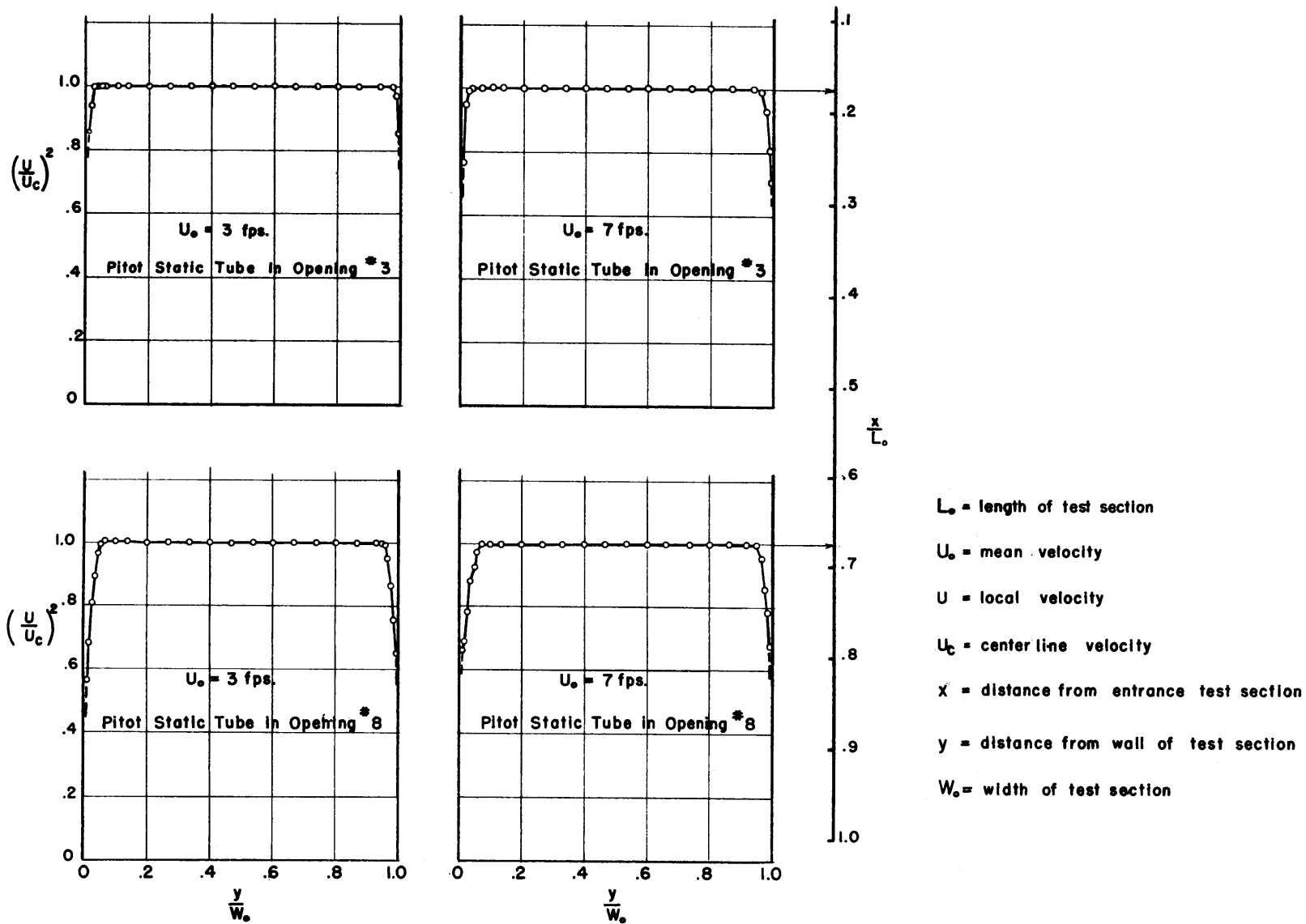


Figure A-3. Velocity Profiles in Horizontal Plane of Test Section

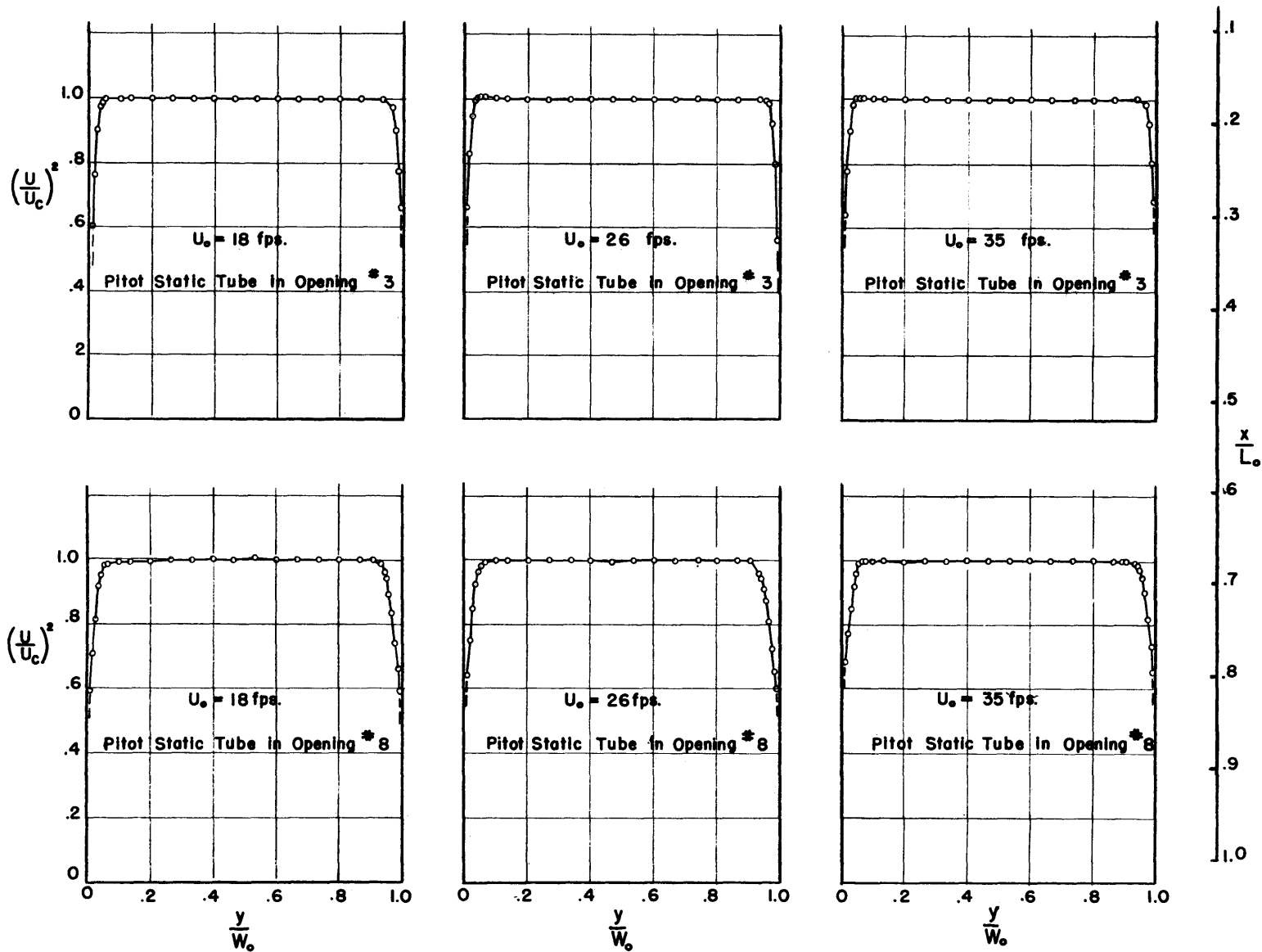


Figure A-4 Velocity Profiles in Horizontal Plane of Test Section

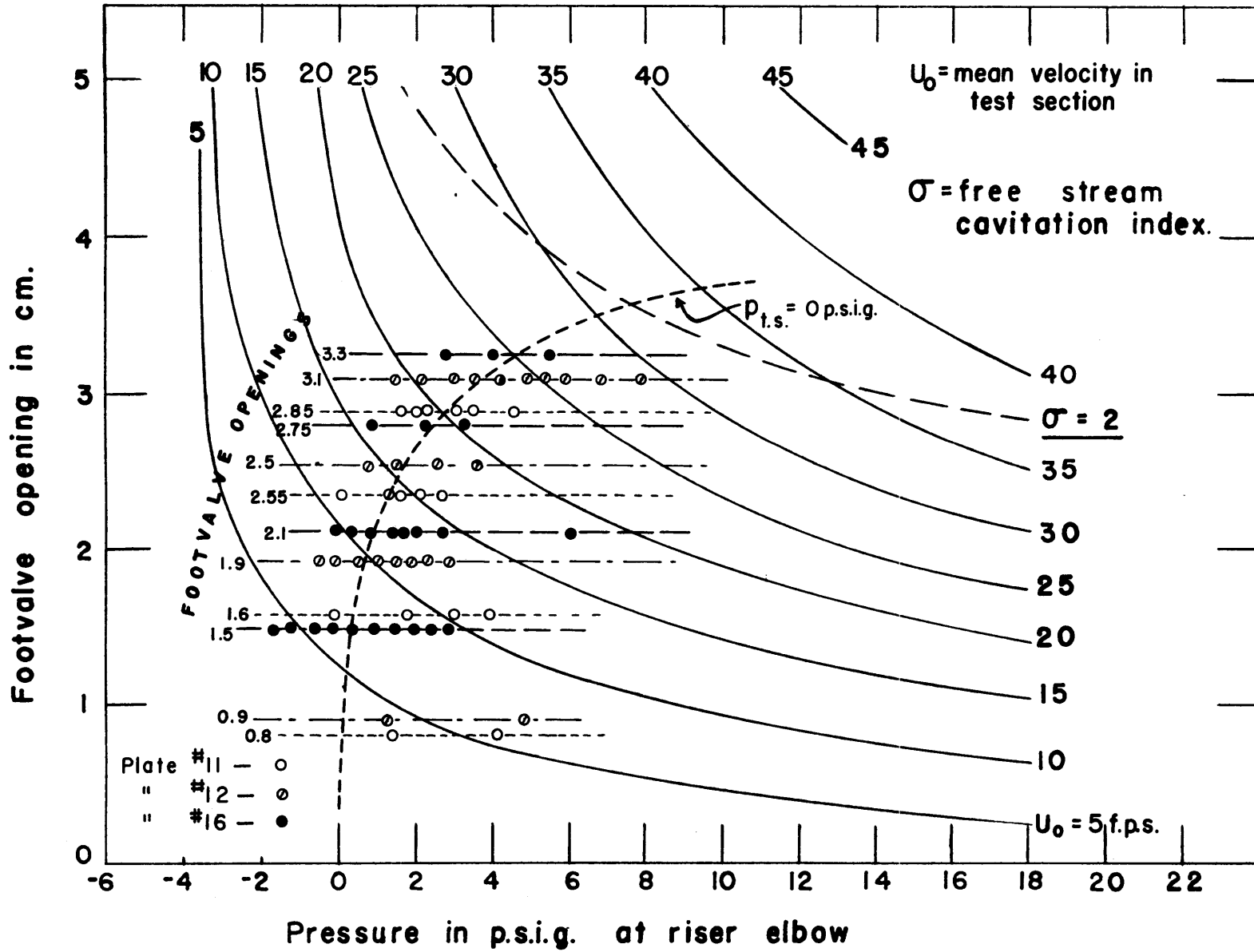


Figure A-5. Operating Characteristics of Water Tunnel

in which  $p_0$  = ambient pressure intensity in the test section in psia.

$p_v$  = vapor pressure of water at 70°F in psia.

$U_0$  = mean test section velocity in fps.

The test section pressure,  $p_{ts}$ , was measured directly by means of a pressure gage.

As an approximate practical limit of operation the curve  $\sigma = 2$ , is shown with a dashed line in Figure 9, and indicates a practical maximum velocity of from 35 to 40 fps.

Besides causing cavitation, test section pressures may release dissolved air and overstress the seals around the test plate spindles. This could alter the vibrational behavior of the test plates. Therefore the usual operating conditions were selected such that the ambient pressure in the test section,  $p_{ts}$ , was never far removed from  $p_{ts} = 0$  psig. This has been shown also in Figure 9 where the dotted line presents the  $p_{ts} = 0$  psig condition and the plotted data points are those of a typical test series for 1/4"-thick test plates.

It should be remembered that the behavior indicated in Fig. A-5 is dependent upon the losses in the screens which lie between the riser elbow and the test section. These tests were done with clean screens.

#### 4. Water Tunnel Vibrations

For small openings of the foot valve noticeable vibrations occur in the water tunnel structure, with predominant frequencies varying between 60 and 80 cps. The vibrations appear forced by the flow conditions near the foot valve but the actual mechanism is not yet clear. Anchoring of the lower portion of the tailrace to the reservoir walls by means of bracing beams proved only moderately effective in preventing the vibration. Subsequent use of a sensitive accelerometer proved that the floor slab has a natural frequency of about 60 cps.

Besides the effect of possible pressure pulses in the flow on the output of a turbulence pressure gage, the vibration will impart some transverse motion to the test section. The spindles around which the test plates pivoted were in direct contact with the test section. The center of mass of the test plate assembly, however, was not located in the axis of rotation. Therefore rotational motion of the test plates induced by tunnel vibration is a possibility. The likelihood of this effect is discussed in Section V.

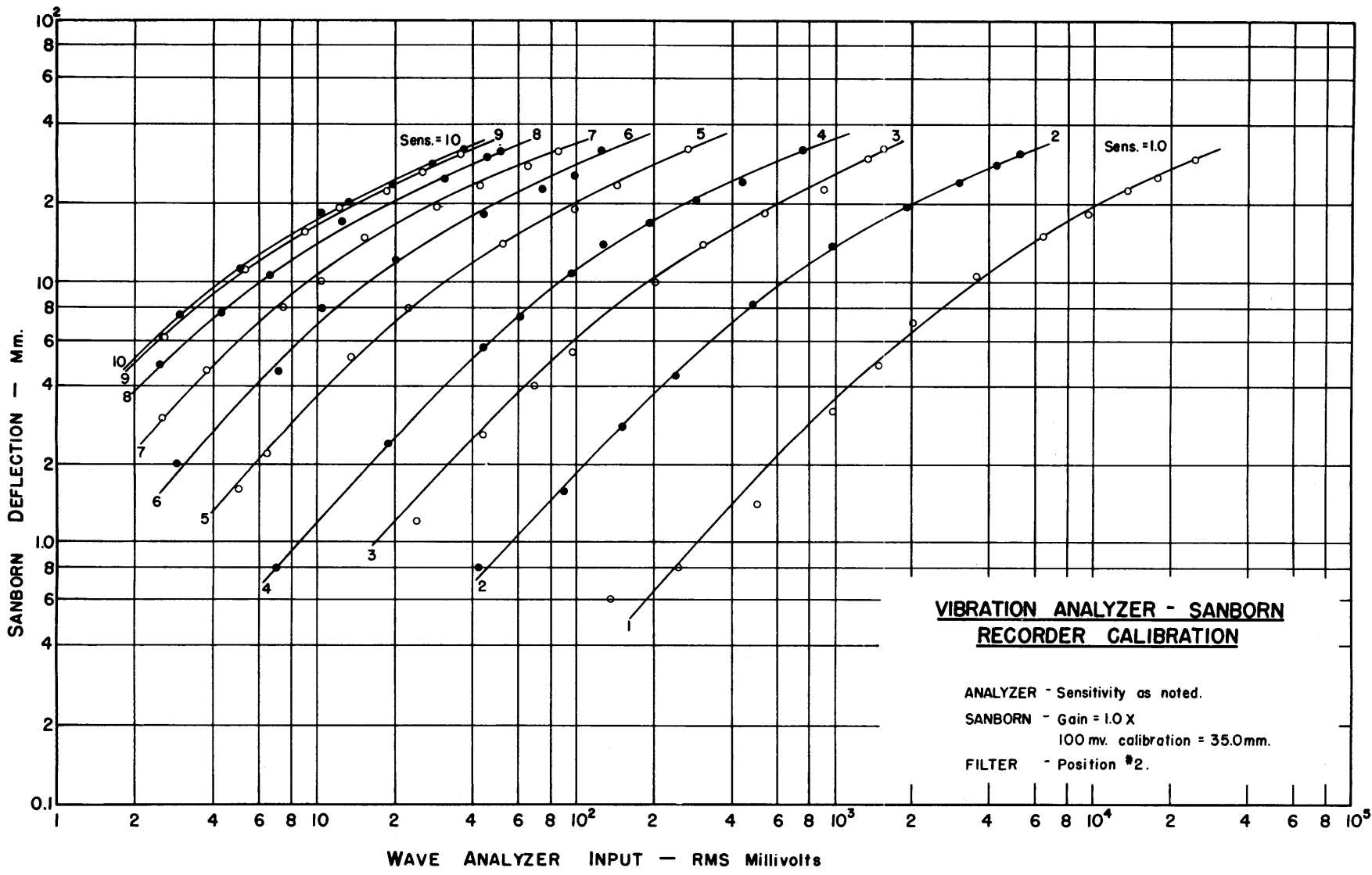


Figure B-1. Wave Analyzer Calibration Curves



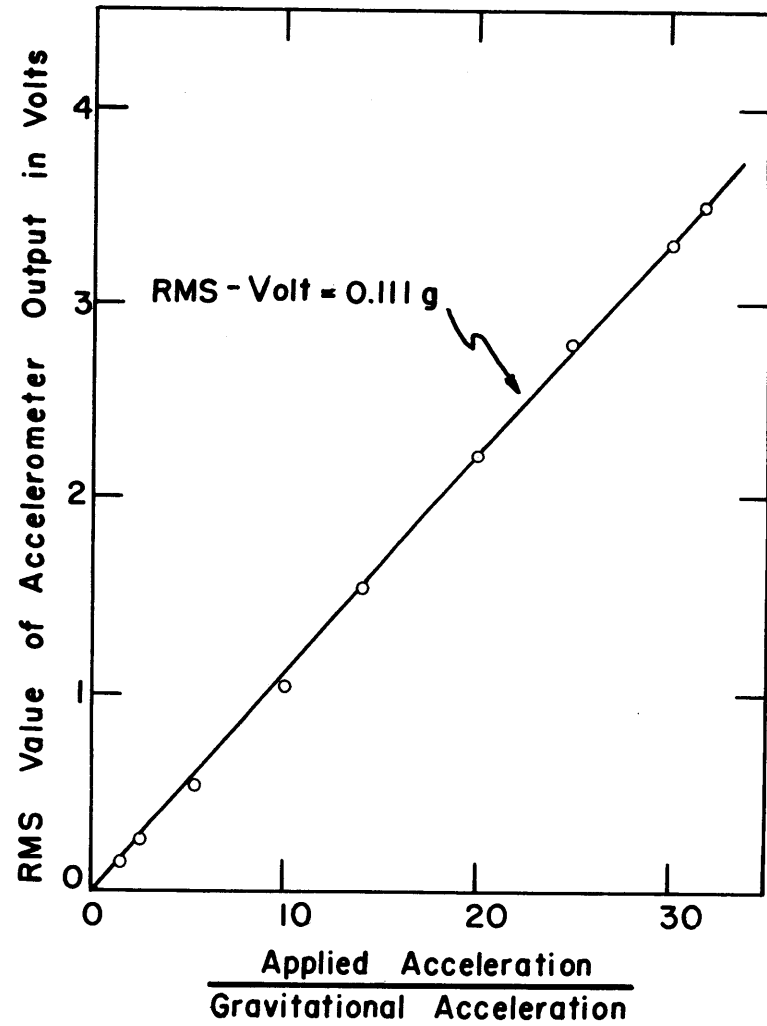
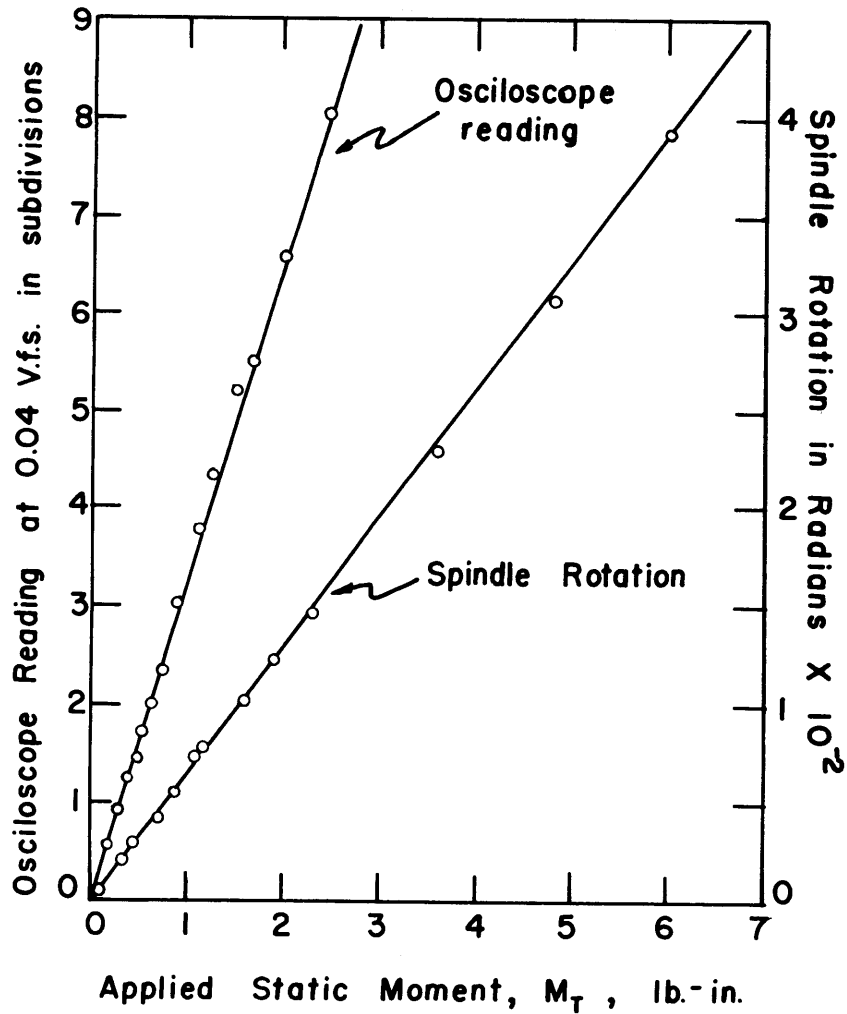


Figure B-2. Calibration of Leaf Spring and Accelerometer

## APPENDIX C

### Natural Frequency and Apparent Mass Determination

#### 1. 1/8" Thick Test Plates

Apparent mass forces cannot be distinguished from the hydrodynamic forces acting on the vibrating plates; yet an accurate knowledge of their magnitude is useful in a formulation of a mechanism for the test plate vibrations.

For an infinitely long flat plate of chord  $2b$ , translating in the direction of its normal, the apparent mass per unit length is (see Ref. 69):

$$m'_{\infty} = \pi \rho b^2 \quad [C-1]$$

Substitution of equation [C-1] into the expression for the mass moment of inertia of a flat plate which pivots around the leading edge gives:

$$I'_{\infty} = m'_{\infty} \cdot \frac{b^2}{3} + m'_{\infty} \cdot (b)^2 \quad [C-2]$$

where  $I'_{\infty}$  = polar apparent mass moment of inertia per unit length of plate.

For a plate of length  $l$  an empirical coefficient,  $C'$ , has to be introduced to account for the effect of the finite aspect ratio. Eq. [C-2] then becomes:

$$I' = \frac{4}{3} \cdot C' m'_{\infty} b^2 \quad [C-3]$$

Using equations [C-1] and [C-2] the apparent mass for a 1/8" test plate plus the immersed parts of the spindles not possessing axial symmetry was estimated at  $I' = C' \times 37.9 \times 10^4$  lbs-in-sec<sup>2</sup>.

The constant  $C'$  has been determined from a set of natural frequency determinations, obtained by deflecting the test plate and recording the ensuing vibration. As indicated in Table C-1 these determinations were made for different free lengths of the restraining leaf spring, for two moments of inertia and for the test plate suspended first in air and then in water.

For the test plate - leaf spring system the natural frequency is approximated by

$$\omega_n = \left(\frac{k}{I}\right)^{1/2} \quad [C-4]$$

where:  $\omega_n$  = natural circular frequency in radians per second;  
 $k$  = stiffness of the leaf spring in lbs-in/rad;  
 $I$  = total mass moment of inertia in lbs-in-sec<sup>2</sup>.

The stiffness  $k$  is a function of the free length of the leaf spring.  
The inertia  $I$  is composed of:

$I_p$  = moment of inertia of 1/8" test plate

$I_s$  = moment of inertia of both spindles

$I_m$  = moment of inertia of additional mass employed to alter the total  $I$

$I'$  = apparent mass moment of inertia.

The columns 5 through 8 in Table C-1 contain ratios of the measured values of  $\omega_n$ . From these ratios the spring stiffness,  $k$ , has been eliminated so that they represent also the square roots of moment of inertia ratios. For the ratios of each column the square of the average value was determined. These numbers then represent the ratios of the moments of inertia associated with the conditions of column 1 through 4. For example:  $2.25 =$

$$\left(\frac{\text{column 1}}{\text{column 2}}\right)^2 = \frac{I_2}{I_1} = \frac{I_m + I_p + I_s}{I_p + I_s} .$$

Thus Equation [C-4] and Table C-1 determine the following relations:

$$I_m + I_p + I_s = 2.25 (I_p + I_s)$$

$$I' + I_p + I_s = 4.96 (I_p + I_s)$$

$$I_m + I' + I_p + I_s = 1.24 (I' + I_p + I_s)$$

[C-5]

$$I' + I_m + I_p + I_s = 2.73 (I_m + I_p + I_s)$$

$I_p$ ,  $I_s$  and  $I_m$  can be estimated from geometric dimensions. The computed values for  $I_s + I_p = 8.65 \times 10^{-4}$  lbs-in-sec<sup>2</sup>, substituting this into the first of the above relations gives:  $I_m = 1.25 \times 8.65 = 10.8 \times 10^{-4}$  lbs-in-sec<sup>2</sup>, which agrees well with the computed value  $I_m = 11.4 \times 10^{-4}$  lbs-in-sec<sup>2</sup>. Substitution of the three known values  $I_p$ ,  $I_s$  and  $I_m$  into eq. [C-5] yields:

$$I' = 3.96 \times 1.65 = 34.2 \times 10^{-4} \text{ lbs-in-sec}^2,$$

$$I' = 4.16 \times 8.72 = 36.2 \times 10^{-4} \text{ lbs-in-sec}^2,$$

$$I' = 1.73 \times 19.45 = 33.8 \times 10^{-4} \text{ lbs-in-sec}^2.$$

Average value  $I' = 34.7 \times 10^{-4}$  lbs-in-sec<sup>2</sup>. It thus follows that  $C' = 34.7/37.9 = 0.91$ .

## 2. 1/4" Thick Test Plates Pivoted at the Leading Edge

From the natural frequency and the stiffness determinations made for the spindle, acting as a torsion spring, the apparent mass moment for a

1/4" thick test plate is readily computed. Using the spring characteristics collected in Table C-2 the moments of inertia are determined from eq. [C-4] and presented in column 4 and 5 of the Table. By subtracting the values in column 4 from those in column 5, the apparent mass moment is obtained.

The computed total mass moment of inertia for the spindles, test plate and accelerometer is  $I_{total} = 26.0 \times 10^{-4}$  lbs-in-sec<sup>2</sup>, which is in good agreement with the measured average value in column 5. The computed apparent mass moment is, from Eq. [C-2]:

$$I' = C' \times 34.9 \times 10^{-4} \text{ lbs-in-sec}^2$$

where, as in the case of the 1/8" plates,  $C'$  is an experimental factor to account for the influence of the finite aspect ratio. From the three last values in column 6, Table C-2, it follows that  $C' \approx 1.0$ . This high value is due to the end plates (not present on the 1/8" plates) which prevent occurrence of the "end-effects" associated with the finite aspect ratio.

By means of a lever and a set of weights rotational moments of known magnitudes were applied to the spindle at the location of the accelerometer. Simultaneously the deflection of an arm clamped to the spindle just below the lever was measured. The stiffnesses  $k$  in Table C-2 determined from these measurements are acceptable as long as the torsional stiffness of the spindle and plate portion between lever and the actual test plate is much larger than the stiffness of the spindle between lever and clamp. When this condition is not fulfilled, the measured  $k$ -value is too large. This is reflected in the obvious discrepancies in column 5, Table C-2.

If  $I = 61.9 \times 10^{-4}$  lbs-in-sec<sup>2</sup> is adopted as the moment of inertia including the apparent mass effect, and this inertia is considered located at the joint of spindle and test plate, the effective  $k$ -value for the spindle clamped at #1 and #4 is found to be:

$$k_1 = \frac{61.9}{159.0} \times 5.75 \times 10^3 = 2.24 \times 10^3 \text{ lb.in/rad}$$

$$k_4 = \frac{61.9}{90.0} \times 2.34 \times 10^3 = 1.61 \times 10^3 \text{ lb.in/rad.}$$

### 3. 1/4" Thick Test Plates Pivoted at 1/4-Chord

For cases in which the plate pivoted around the 1/4-chord (i.e., 1/2" downstream of the trailing edge) the natural frequencies are higher than those reported above. For pivoting around the leading edge:

$$I_p = \frac{1}{3} m' b^2 + m' (b)^2 = \frac{4}{3} m b^2; \text{ around the 1/4-chord:}$$

$$I_p = \frac{1}{3} m' b^2 + m' \left(\frac{b}{2}\right)^2 = \frac{7}{12} m b^2.$$

The reduction in mass moment of inertia therefore is:

$$\left(\frac{4}{3} - \frac{7}{12}\right) / \frac{4}{3} = 9/16$$

so that in that case:

$$I_{\text{total}} + I' = 9/16 (15.9 + 34.8) + 0.7 + 1.8 + 7.6 = 38.3 \text{ lbs-in-sec}^2$$

from which may be obtained:

- Clamp #1 -  $f_n = 121 \text{ cps}$
- Clamp #4 -  $f_n = 103 \text{ cps}$
- Clamp #5 -  $f_n = 78 \text{ cps}$
- Clamp #7 -  $f_n = 51 \text{ cps.}$

1/8" test plate	Frequencies in cps				Ratios of the values			
Media	Air	Air	Water	Water	in column 1 through 4			
Additional mass attached	No	Yes	No	Yes	1:2	1:3	3:4	2:4
Spring Support Position No.	Columns							
	1	2	3	4	5	6	7	8
#1	62.0	40.5	28.0	25.5	1.53	2.22	1.10	1.59
#3	57.5	38.0	25.5	23.0	1.51	2.26	1.11	1.65
#5	51.0	34.0	24.0	20.5	1.50	2.14	1.17	1.66
#7	45.0	31.0	20.5	18.5	1.46	2.25	1.11	1.68
Average					1.50	2.22	1.12	1.65
(Average) <sup>2</sup>					2.25	4.96	1.24	2.73

Table C-1. Determination of Moment of Inertia Ratios

Test Plate #11	Natural Frequencies in cps		Spring Constant k in $10^3 \times \frac{\text{lbs-in}}{\text{radian}}$	Moment of Inertia in $10^{-4} \text{ lbs-in-sec}^2$		Apparent Mass Moment of Inertia in $10^{-4} \times \text{lbs-in-sec}^2$
	Air	Water		Air	Water	
Clamp at Spindle Position No.	Columns					
	1	2	3	4	5	6
#1	-	96	5.75	-	159.0	-
#4	135	82	2.34	28.0	90.0	64.0
#5	95	64	0.93	26.0	65.3	39.3
#7	60	42	0.39	27.4	58.5	31.1
#8	52	35	0.30	28.0	62.0	34.0
Average of #5-#7-#8				27.1	61.9	34.8
Corrected values for:						
#1	-	96	2.24	-	61.9	-
#4	-	82	1.61	-	61.9	34.8
Computed values:	$I_{\text{total}} = I_{\text{plate}} + I_{\text{hub}} + I_{\text{spindle}} + I_{\text{accelerometer}}$ $= (15.9 + 0.7 + 1.8 + 7.6) \times 10^{-4} \text{ lbs-in-sec}^2$ $= 26.0 \times 10^{-4} \text{ lbs-in-sec}^2$ $I' = C' \times 34.9 \times 10^{-4} \text{ lbs-in-sec}^2$ $\therefore C' = 34.8/34.9 = 1.0$					

Table C-2. Determination of Apparent Mass Moment of Inertia

## APPENDIX D

### Conversion Factor Transducer Output - Amplitude of Vibration

From the calibration curve for the accelerometer, given in Figure B-2, follows:

$$\begin{aligned} 111 \text{ mV - RMS} &= 32.17 \times 12 \text{ in/sec}^2 = 386 \text{ in/sec}^2 \\ \therefore 1000 \text{ mV} &= 3.5 \times 10^3 \text{ in/sec}^2 \end{aligned} \quad \text{[D-1]}$$

For a harmonic motion given by:

$$a = a_0 \sin \omega t$$

where  $a_0$  = single amplitude expressed in inches, the RMS-value is:

$$\sqrt{(a)^2} = a_0 \omega \sqrt{\sin^2 \omega t} = \frac{1}{2} 2\sqrt{a_0 \omega^2} = 28 a_0 f^2 \frac{\text{in}}{\text{sec}^2} \quad \text{[D-2]}$$

From Eqs. [D-1] and [D-2] follows that the relation between an RMS-voltmeter reading of  $x$  mV and the double amplitude of motion,  $2a_0$ , at the location of the accelerometer is:

$$2a_0 = \frac{3.5 x}{14 f^2} \text{ mV} = 0.25 x/f^2 \text{ mV} \quad \text{[D-3]}$$

Referring this to the plate thickness,  $t = 0.25''$ , there is obtained:

$$\frac{2a_0}{t} = \frac{x}{f^2} \frac{\text{mV}}{\text{in}} \quad \text{[D-4]}$$

This dimensionless amplitude  $2a_0/t$ , which was readily obtained by dividing the Voltmeter reading (in mV) over the square of the predominant frequency component (in cps), has been employed in the preparation of the Amplitude Response Curves (Figures 18 through 21 and 23).

The accelerometer and the trailing edge of the test plate are located at 27/16 inch respectively 2 inch from the axis of rotation. The double amplitude of vibration at the trailing edge,  $2a_{ot}$ , in terms of the plate thickness  $t'$  is therefore:

$$\frac{2a_{ot}}{t'} = \frac{32}{27} \cdot \frac{x}{f^2} \approx 1.2 \left( \frac{2a_0}{t} \right) \quad \text{[D-5]}$$

It is to be noted, however, that the amplitude response curves are not too exact quantitatively. The Voltmeter signal employed in their preparation incorporates the effect of higher harmonics. For the mainly qualitative discussion of the amplitude response curves an attempt to eliminate these effects was considered unwarranted.

## APPENDIX E

### Comparison of Some Voltmeter Readings and Micrometer Measurements

For checking purposes some direct measurements were made of the amplitude of vibration of the accelerometer. The amplitudes at resonant conditions for the plate #11, rotating around the leading edge, were estimated by means of a micrometer:

U fps	Clamp No.	Voltmeter RMS-mV	Frequency f in cps	Micrometer inch
1m	2	3	4	5
8.5	4	1.020	82	.040
11.2	5	1.100	62	.070
13.0	5	1.000	68	.065

Table E-1. Micrometer Measurements

Using equation D-2 there follows:

$\frac{1}{4} \times \text{Voltmeter}$ $\frac{1}{4} \times \text{RMS-mV}$	$(\text{Frequency})^2$ $f^2 \text{ in cps}^2$	$2a_0 \text{ in inch}$ $\text{RMS-mV}/4f^2$	$\frac{2a_0 \times 100 \%}{\text{Micrometer}}$
1	2	3	4
0.255	673	0.038	95 %
0.275	385	0.072	103 %
0.250	463	0.054	83 %

Table E-2. Comparison of Micrometer and Voltmeter Measurements.

In view of the difficulties in measuring the vibrational amplitude by means of a micrometer, the agreement is quite satisfactory.



TECHNICAL REPORTS\*  
Hydrodynamics Laboratory  
Department of Civil and Sanitary Engineering  
Massachusetts Institute of Technology

NO.	AUTHORS	TITLE	SPONSOR	DATE
1	A.T. Ippen, D.R. Harleman	Studies on the Validity of the Hydraulic Analogy to Supersonic Flow, Parts I and II	U.S. Air Force, USAF TR 5985	May, 1950
2	J.W. Daily, K.C. Deemer, A.L. Keller	The Unsteady Flow Water Tunnel at the Massachusetts Institute of Technology	Office of Naval Research	May, 1951
3	A.T. Ippen, R.S. Yoseph, B.N. Posthill	The Continuous Measurement of Oxygen Concentration in Water during Aeration Processes	U. S. Public Health Service	Mar., 1951
4	A.T. Ippen, D.R. Harleman	Studies on the Validity of the Hydraulic Analogy to Supersonic Flow, Part III	U.S. Air Force, USAF TR 5985	Oct., 1950
5	A.T. Gifford, R.E. Nece, R.E. DuBois	Water Tests of Eight-Inch Check and Stop Valves	U.S. Atomic Energy Commission	Aug., 1953
6	D.R. Harleman, H.E. Crossley	Studies on the Validity of the Hydraulic Analogy to Supersonic Flow, Part IV	U.S. Air Force, USAF TR 5985	Feb., 1952
7	A.T. Ippen, L.G. Campbell, C.E. Carver, Jr.	Determination of Oxygen Absorption in Aeration Processes	U.S. Public Health Service	May, 1952
8	J.W. Daily, S.C. Stephan	The Solitary Wave--Its Celerity, Profile, Internal Velocities and Amplitude Attenuation	Office of Naval Research	July, 1952
9	J.W. Daily, K.C. Deemer	Measurements of Fluid Friction with Steady and Unsteady Motion	Office of Naval Research	July, 1952
10	J.W. Daily, W.L. Hankey	Resistance Coefficients for Accelerated Flow Through Orifices	Office of Naval Research	Oct., 1953
11	H.E. Crossley, D.R. Harleman	Studies on the Validity of the Hydraulic Analogy to Supersonic Flow, Part V - Towed Model Investigation of Transonic Flow	U.S. Air Force, USAF TR 5985	Dec., 1952
12	D.R. Harleman, O.A. Boedtke	Water Table Experiments on Transient Shock Wave Diffraction, Part I, Operation, Instrumentation and Preliminary Experiments	U.S. Air Force	Aug., 1953
13	D.R. Harleman, O.A. Boedtke, S. Wolf	Water Table Experiments on Transient Shock Wave Diffraction, Part II, Experimental Results and Evaluation	U.S. Air Force	Oct., 1954
14	A.T. Ippen, C.E. Carver, Jr.	Oxygen Absorption and Turbulence Characteristics in Bubble Aeration	U.S. Public Health Service	Apr., 1955
15	A.T. Ippen, G. Kulin	Shoaling and Breaking of the Solitary Wave	Office of Naval Research	Apr., 1955
16	A.T. Ippen, G. Kulin, Mir A. Raza	Damping Characteristics of the Solitary Wave	Office of Naval Research	Apr., 1955
17	D.R. Harleman, R.S. Gooch, A.A. Vulgaropoulos	Hydraulic Model Performance of Spillway and Outlet Works of Peligre Dam	Brown and Root, Inc.	Apr., 1955
18	A.T. Ippen, P.S. Eagleson	A Study of Sediment Sorting by Waves Shoaling on a Plane Beach	Beach Erosion Board	May, 1955
19	D.R. Harleman, W.C. Shapiro	Experimental and Analytical Studies of Wave Forces on Basic Components of Offshore Structures, Part I: Results for Vertical Cylinders	Humble Oil Company	May, 1955
20	A.T. Ippen, R.S. Tankin, F. Raichlen	Turbulence Measurements in Free Surface Flow with an Impact Tube-Pressure Transducer Combination	Office of Naval Research and the David Taylor Model Basin	July, 1955
21	J.W. Daily, V.E. Johnson	Turbulence and Boundary Layer Effects on the Inception of Cavitation from Gas Nuclei	Office of Naval Research	July, 1955
22	J.W. Daily, J.M. Jordaan	Effects of Unsteadiness on Resistance and Energy Dissipation	Office of Naval Research	Dec., 1956
23	A.T. Ippen, M.M. Mitchell	The Damping of the Solitary Wave from Boundary Shear Measurements	Office of Naval Research	June, 1957
24	D.R. Harleman, W.C. Shapiro, T.A. Marlow, II	Experimental and Analytical Studies of Wave Forces on Offshore Drilling Structures. Part II: Buoyancy Components for Floating Platforms	Humble Oil Company	June, 1957
25	P.S. Eagleson, T.A. Marlow, C.T. I ke, F.J. Turpin	Hydraulic Model Study of Protective Works for Fleet Berthing Facilities in Coddington Cove, Narragansett Bay, R. I.	First Naval District, Boston, Mass.	June, 1957
26	P.S. Eagleson, R.G. Dean, L.A. Peralta	The Mechanics of the Motion of Discrete Spherical Bottom Sediment Particles Due to Shoaling Waves	Beach Erosion Board	Oct., 1957
27	J.W. Daily, R.E. Nece	Roughness and Chamber Dimension Effects on Induced Flow and Frictional Resistance of Enclosed Rotating Disks	Office of Ordnance Research	May, 1958
28	D.R. Harleman, W.C. Shapiro	Investigation on the Dynamics of Moored Structures in Waves	Humble Oil and Refining Co.	July, 1958
29	F. Ursell, R.G. Dean, Y.S. Yu	Forced Small-Amplitude Water Waves: A Comparison of Theory and Experiment	Office of Naval Research	July, 1958
30	J.W. Daily, G. Bugliarello	The Effects of Fibers on Velocity Distribution, Turbulence and Flow Resistance of Dilute Suspensions	Technical Association of the Pulp and Paper Industry	Oct., 1958
31	D.R. Harleman, J.M. Jordaan, J.D. Lin	Diffusion of Two Fluids of Different Density in a Homogeneous Turbulent Field	Nat.Inst. of Health, Dept. of Health, Educ. and Welfare	Feb., 1959
32	P.S. Eagleson	The Damping of Oscillatory Waves by Laminar Boundary Layers	Beach Erosion Board, U.S. Dept. of the Army, Corps of Engrs.	Apr., 1959
33	D.R. Harleman, R.S. Broughton, C.J. Huvial, H.W. Partenscky	Model Study of a Flood Control Pumping Station at the Charles River Dam	Metro. Dist. Commission, Commonwealth of Massachusetts	June, 1959
34	J.W. Daily, J.D. Lin, R.S. Broughton	The Distribution of Mean Static Pressure in Turbulent Boundary Layers in Relation to Inception of Cavitation	Office of Naval Research	June, 1959
35	J.W. Daily, G. Bugliarello, W.W. Troutman	Measurement and Analysis of Turbulent Flow of Wood Pulp Fiber Suspensions	Tech. Assoc. of the Pulp and Paper Industry	Sept., 1959

\* Technical Reports and Technical Notes, if available, may be obtained from the Hydrodynamics Laboratory at a charge of \$1.50 per copy.

STAFF PUBLICATIONS  
Hydrodynamics Laboratory  
Department of Civil and Sanitary Engineering  
Massachusetts Institute of Technology

NO.	AUTHORS	TITLE	PUBLISHED	DATE
1	A.T. Ippen	The New Hydrodynamics Laboratory	Technology Review, M.I.T.	June, 1951
2	A.T. Ippen, and Staff of Hydrodynamics Laboratory	Hydrodynamics in Modern Technology, A symposium held at the Dedication of the Hydrodynamics Laboratory	Hydrodynamics Laboratory, MIT	Apr., 1952
3	A.T. Ippen	The Influence of Viscosity on Centrifugal Pump Performance	Trans. A.S.M.E.	Nov., 1946
4	J.W. Daily	Cavitation Characteristics and Infinite Aspect Ratio Characteristics of Hydrofoil Section	Trans. A.S.M.E.	Apr., 1949
5	A.T. Ippen	Mechanics of Supercritical Flow, Symposium on High-Velocity Flow in Open Channels	Trans. A.S.C.E., Vol. 116	1951
6	A.T. Ippen, J.W. Dawson	Design of Channel Contractions, Symposium on High-Velocity Flow in Open Channels	Trans. A.S.C.E., Vol. 116	1951
7	A.T. Ippen	Channel Transitions and Controls,	Chapter VIII, Engineering Hydraulics (ed. by H.Rouse), John Wiley and Sons	1950
8	J.W. Daily	Hydraulic Machinery	Chapter XIII, Engineering Hydraulics (ed. by H.Rouse), John Wiley and Sons	1950
9	A.T. Ippen, D.R. Harleman	Steady State Characteristics of Subsurface Flow, Symposium on Gravity Waves	National Bureau of Standards NBS Circular 521	June, 1951
10	A.T. Ippen, D.R. Harleman	Certain Quantitative Results of the Hydraulic Analogy to Supersonic Flow	Proc., Second Midwestern Conference on Fluid Mechanics, Ohio State University	Mar., 1952
11	H.M. Paynter	Methods and Results from M.I.T. Studies in Unsteady Flow	Jr., Bos. Soc. of Civil Engrs.	Apr., 1952
12	J.W. Daily, S.C. Stephan	Characteristics of the Solitary Wave	Trans. A.S.C.E., Vol. 118	1953
13	H.M. Paynter	Electrical Analogies and Electrical Computers: Surge and Water Hammer Problems	Trans. A.S.C.E., Vol. 118	1953
14	J.W. Daily, K.C. Deemer	The Unsteady Flow Water Tunnel at the Massachusetts Institute of Technology	Trans. A.S.M.E., Vol. 76, No. 1	Jan., 1954
15	A.T. Ippen, C.E. Carver	Continuous Measurement of Dissolved Oxygen with Dropping Mercury and Rotating Platinum Electrodes, Conference on Instrumentation in Water, Sewage and Industrial Waste Treatment, Manhattan College, May, 1953.	Instruments and Automation, Vol. 27	Jan., 1954
16	A.T. Ippen, R.P. Verma	The Motion of Discrete Particles Along the Bed of a Turbulent Stream	Proc., Minn. International Hydraulics Convention Trans. A.S.C.E.	1955
17	J.W. Daily, S.C. Stephan	The Solitary Wave -- Its Celerity, Profile, Internal Velocities and Amplitude Attenuation in a Horizontal Smooth Channel	Proc., Third Conference on Coastal Engineering, Cambridge, Massachusetts	Oct., 1952
18	A.T. Ippen, D.R. Harleman	Maintenance of a Navigable Channel through a Breakthrough Area	Proc., Fourth Conference on Coastal Engineering, Chicago, Illinois	Oct., 1953
19	A.T. Ippen, C.E. Carver	Basic Factors of Oxygen Transfer in Aeration Systems	Sewage and Industrial Wastes, Vol. 26, No. 7	July, 1954
20	D.R. Harleman, A.T. Ippen	The Range of Application of the Hydraulic Analogy in Transonic and Supersonic Aerodynamics	Anniversary Volume for M.D. Riabouchinsky, Pub. Scientifiques et Tech. du Ministere de l'Air, Paris, France	May, 1954
21	A.T. Ippen, D.R. Harleman	Verification of Theory for Oblique Standing Waves, A.S.C.E. Proc. Separate No. 526, Vol. 80, Oct., 1954	Trans., A.S.C.E.	1956
22	J.W. Daily, A.T. Ippen	Some Instruments and Facilities of the M.I.T. Hydrodynamics Laboratory	Proc., Joint Admiralty and U.S. Navy Meeting on Hydroballistics, Teddington, England	Sept., 1954
23	D.R. Harleman	Effect of Baffle Piers on Stilling Basin Performance	Jr. Bos. Soc. of Civil Engrs.	Apr., 1955
24	A.T. Ippen, G. Kulin	The Shoaling and Breaking of the Solitary Wave	Proc., Fifth Conference on Coastal Engineering, Grenoble, France	Sept., 1954
25	R.E. Nece, R.E. DuBois	Hydraulic Performance of Check and Control Valves	Jr. Bos. Soc. of Civil Engrs.	July, 1955
26	C.R. Carver	Absorption of Oxygen in Bubble Aeration	Proc., Biological Treatment of Sewage and Industrial Wastes Conference, Manhattan College, N.Y., Reinhold Publ. Corp., N.Y.	Apr., 1955
27	A.T. Ippen, P.S. Eagleson	A Study of Sediment Sorting by Waves Shoaling on a Plane Beach	Proc., I.A.H.R. Meeting, Delft, Netherlands	Sept., 1955
28	J.W. Daily, W.L. Hankey, R.W. Olive, J.M. Jordaen	Resistance Coefficients for Accelerated and Decelerated Flows through Smooth Tubes and Orifices	Trans. A.S.M.E.	July, 1956
29	A.T. Ippen	Hydrodynamic Models of Pressure Conduits	Proc., International Congress on Models in Technology, Venice	Oct., 1955
30	J.W. Daily, V.E. Johnson	Turbulence and Boundary Layer Effects on Cavitation Inception from Gas Nuclei	Proc., Symposium on Cavitation in Hydrodynamics, National Physical Laboratory, Teddington, England	Sept., 1955
31	A.T. Ippen, P.S. Eagleson	A Study of Sediment Sorting by Waves Shoaling on a Plane Beach	Beach Erosion Board Tech. Memorandum No. 63	Sept., 1955

STAFF PUBLICATIONS  
(Contd)

NO.	AUTHORS	TITLE	PUBLISHED	DATE
32	G.R. Williams	Hydrology	Chapter IV of <u>Engineering Hydraulics</u> (edited by H.Rouse), John Wiley and Sons	1950
33	J.M. Jordaan	Some Aspects of the Design and Stability Analysis of Spillways on Alluvium	Trans., South African Inst. of Civil Engineers, Vol.6, No.2	Feb., 1956
34	A.T. Ippen	Hydrodynamics: A Review of von Karman's Contributions	Special Issue of the <u>Journal of Aeronautical Sciences</u> in honor of Th. von Karman	May, 1956
35	J.W. Daily, V.E. Johnson	Turbulence and Boundary Layer Effects on Cavitation Inception from Gas Nuclei	Trans, A.S.M.E., Vol.78, No.8	Nov., 1956
36	A.T. Ippen, G. Kulin	The Effect of Boundary Resistance on Solitary Waves, (L'effet produit sur les ondes solitaires par le frottement a la paroi)	<u>La Houille Blanche</u> , No.3	July, Aug., 1957
37	J.G. Housely, D.C. Taylor	Application of the Solitary Wave Theory to Shoaling Oscillatory Waves	Trans. Amer.Geophys.Union	Feb., 1957
38	P.S. Eagleson	Properties of Shoaling Waves, by Theory and Experiment	Trans., Amer.Geophysical Union	Oct., 1956
39	D.R. Harleman, R.S. Gooch, A.T. Ippen	Submerged Sluice Gate Control of Density Currents	Proc. A.S.C.E. Hydr.Division	Apr., 1958
40	A.T. Ippen, F. Raichlen	Turbulence in Civil Engineering Measurements in Free Surface Streams (with an Impact Tube-Pressure Cell Combination)	Symposium on Turbulence in Civil Engineering, Proc. A.S.C.E., Hydro.Division	Oct., 1957
41	A.T. Ippen, J.W. Daily, G. Bugliarello	Pertinent Factors in Flow Research on Dilute Fiber Suspensions	TAPPI Mag. Vol.40, No.6	June, 1957
42	D.R. Harleman	Density Currents Studied in Glass-Walled Flume	<u>Civil Engineering</u> ,	Feb., 1954
43	P.S. Eagleson	Hydraulic Model Study of Protective Works for Fleet Berths in Narragansett Bay	Trans. Bos.Soc.of Civil Engrs, Vol.46, No.1	Jan., 1959
44	P.S. Eagleson, L.A. Peralta, R.G. Dean	Motion of Discrete Bottom Sediment Particles due to Shoaling Waves	Beach Erosion Board, Tech. Memorandum #104	Feb., 1958
45	J.W. Daily, R.E. Nece	Chamber Dimension Effects on Induced Flow and Frictional Resistance of Enclosed Rotating Disks	A.S.M.E. Paper No.59-Hyd-9	Apr., 1959
46	D.R. Harleman	Discussion on Turbulent Characteristics of the Hydraulic Jump, by Hunter Rouse, et al., (A.S.C.E., Proc. Paper 1528, February, 1958)	Jr..of Hydraulics Division, A.S.C.E.	Nov., 1958

TECHNICAL NOTES\*

NO.	AUTHORS	TITLE	SPONSOR	DATE
1	R.E. Nece	Water Test Results for an Experimental "Ten-Inch" Swing Check Valve	Westinghouse Electric Corp.	July, 1956
2	J.W. Daily, G. Bugliarello	The Characteristics of Flow with Dilute Fiber Suspensions. A Progress Report of Work under TAPPI Project 93	Tech.Assoc.of the Pulp and Paper Industry	Dec., 1957
3	G.H. Toebes, F.E. Perkins, P.S. Eagleson	Design of a Closed Jet, Open Circuit Water Tunnel for the Study of Wake Mechanics	David Taylor Model Basin	Apr., 1958
4	J.W. Daily, A. Tsuchiya	Flow of Nylon Fiber Suspensions. A Progress Report on a Phase of Work under TAPPI Project 147	Tech.Assoc.of the Pulp and Paper Industry	Feb., 1959
5	F.E. Perkins, P.S. Eagleson	The Development of a Total Head Tube for High Frequency Pressure Fluctuations in Water	David Taylor Model Basin	July, 1959
6	R.E. Nece, C.A. Givler	Measurement of Boundary Shear Stresses in an Open Channel Curve with a Surface Pitot Tube	ARS, U.S. Dept.of Agriculture	Aug., 1959

\* Technical Reports and Technical Notes, if available, may be obtained from the Hydrodynamics Laboratory at a charge of \$1.50 per copy.

APPROVED DISTRIBUTION LIST FOR  
UNCLASSIFIED TECHNICAL REPORTS ISSUED UNDER

CONTRACT Nonr-1841(21)

Government Agencies

Chief of Naval Research Department of the Navy Washington 25, D. C. Attn: Code 438	(3)	Director Naval Research Laboratory Washington 25, D. C. Attn: Code 2021	(1)
Commanding Officer Office of Naval Research Branch Office 495 Summer Street Boston, Massachusetts	(1)	Documents Service Center Armed Services Technical Information Agency Arlington Hall Station Arlington 12, Virginia	(5)
Commanding Officer Office of Naval Research Branch Office The John Crerar Library Bldg. 86 East Randolph Street Chicago 1, Illinois	(1)	Chief, Bureau of Aeronautics Department of the Navy Washington 25, D. C. Attn: Research Division	(1)
Commanding Officer Office of Naval Research Branch Office 346 Broadway New York 13, New York	(1)	Chief, Bureau of Ordnance Department of the Navy Washington 25, D. C. Attn: Research and Development Division	(1)
Commanding Officer Office of Naval Research Branch Office 1030 East Green Street Pasadena 1, California	(1)	Office of Ordnance Research Department of the Army Washington 25, D. C.	(1)
Commanding Officer Office of Naval Research Branch Office 1000 Geary Street San Francisco 9, Calif.	(1)	Commander Air Research and Development Command Andrews Air Force Base Washington 25, D. C. Attn: Fluid Mechanics Division	(1)
Commanding Officer Office of Naval Research Navy #100, Fleet Post Office New York, New York	(1)	Director of Research National Aeronautics and Space Administration 1512 H Street, N. W. Washington 25, D. C.	(1)

Director Langley Research Center National Aeronautics and Space Administration Langley Field, Virginia	(1)	Director Woods Hole Oceanographic Institute Woods Hole, Massachusetts	(1)
Director National Bureau of Standards Washington 25, D. C. Attn: Fluid Mechanics Section Library	(1) (1)	Commanding Officer and Director U.S.N. Underwater Sound Laboratory Fort Trumbull New London, Connecticut	(1)
Commander Naval Ordnance Test Station 3202 E. Foothill Blvd. Pasadena 8, California	(1)	Chief, Bureau of Ships Department of the Navy Washington 25, D. C. Attn: Research Division Code 420 (Preliminary Design) Technical Information Section	(1) (1) (3)
Commanding Officer and Director David Taylor Model Basin Washington 7, D. C. Attn: Code 513	(65)	<u>Institutions</u>	
Chief, Bureau of Yards and Docks Department of the Navy Washington 25, D. C. Attn: Research Division	(1)	Stevens Institute of Technology Davidson Laboratory 711 Hudson Street Hoboken, New Jersey	(1)
Hydrographer U. S. Navy Hydrographic Office Washington 25, D. C.	(1)	California Institute of Technology Division of Engineering Pasadena 4, California	(1)
Director U.S. Waterways Experiment Station Box 631 Vicksburg, Mississippi	(1)	Brown University Graduate Division of Applied Mathematics Providence 12, Rhode Island	(1)
Office of the Chief of Engineers Department of the Army Engineering Division, Civil Works Washington 25, D. C.	(1)	Stanford University Applied Mathematics and Statistics Laboratory Stanford, California	(1)
Beach Erosion Board U.S. Army Corps of Engineers 5201 Little Falls Road Washington 16, D. C.	(1)	Massachusetts Institute of Technology Department of Naval Architecture Cambridge 39, Massachusetts	(1)
Commissioner Bureau of Reclamation Denver Federal Center Denver, Colorado	(1)	Ordnance Research Laboratory The Pennsylvania State University University Park, Pennsylvania	(1)

Applied Mechanics Reviews  
Southwest Research Institute  
8500 Culebra Road  
San Antonio 6, Texas (1)

Institute of Fluid Mechanics  
University of Maryland  
College Park, Maryland (1)

Institute of Aerophysics  
University of Toronto  
Toronto, Canada (1)

Library  
Institute of Aeronautical Sciences, Inc.  
2 East 64th Street  
New York 21, N. Y. (1)